KEPLER Deliverable Report

Final report on Deliverable D3.3

Deliverable name	Final report on research gaps of space-based Arctic monitoring			
Scheduled delivery	**month:**	18	**date:**	June 2020
Actual delivery	**month:**	18	**date:**	June 2020
Report type	Final report			
Lead author	Carolina Gabarró, ICM/CSIC			

Contributing authors

Laurent Bertino (NERSC), Astrid Bracher (AWI), Thomas Diehl (JRC), Wolfgang Dierking (AWI), Carolina Gabarro (ICM/CSIC), Verónica González-Gambau (ICM/CSIC), Nick Hughes (MetNo), Thomas Lavergne (MetNo), Eirik Malnes (NORCE), Marko Scholze (ULUND).

Other contributing authors: Leif Toudal Pedersen (EoLAB), Steinar Eastwood (MetNo), Signe Aaboe (MetNo), Rune Storvold (NORCE), Jordi Isern (ICM/CSIC), Marcos Portabella (ICM/CSIC), Miriam Pablos (ICM/CSIC), Teresa Madurell (ICM/CSIC).

Context of deliverable within Work Package

Draft version of delivery of WP3 task 3. This document consists of:

- Executive Summary and Acronyms list
- Section 1 (part 1) contains a review per parameters of the technologies used and retrieval algorithms, characteristics of the parameter, validation methods, errors and uncertainty and known limitations gaps.
- Section 2. Current and in-development satellite products, 3. List of parameters from future missions, 4. Feasibility of synergies, section 5 Analysis on the assimilation of parameters into models, and section 6 is Conclusions and recommendation.
- Finally the references of all the text.

Co-funded by the Horizon 2020 programme of the European Union

Index

Co-funded by the Horizon 2020 programme of the European Union

List of Tables and Figures

Co-funded by the Horizon 2020 programme of the European Union

Important note: In this report, we have analysed sea ice, land and ocean parameters. Greenland and Antarctica ice sheets and glaciers, as well as atmospheric parameters, are not covered in the inventory below.

Co-funded by the Horizon 2020 programme of the European Union

ACRONYMS

ACRONYMS WP3	
AVHRR	Advanced Very High Resolution Radiometer
AMSR-E	Advanced Microwave Scanning Radiometer
CIMR	Copernicus Imaging Microwave radiometer
Chl	Chlorophyll
CHIME	Copernicus Hyperspectral Imaging Mission
CMEMS	Copernicus Marine Environment Monitoring Services
CLMS	Copernicus Land Monitoring Services
CO2M	Copernicus Anthropogenic Carbon Dioxide Monitoring
CRISTAL	Copernicus Polar Ice and Snow Topography Altimeter
DA	Data Assimilation
ECV	Essential Climate Variables
ECMWF	European Centre for Medium-Range Weather Forecasts
FORUM	Far-infrared Outgoing Radiation Understanding and Monitoring
IR	Infra-Red
JAXA	Japan Aerospace Exploration Agency
HPCM	High Priority Copernicus Missions
LSTM	Copernicus Land Surface Temperature Monitoring
METOP	ESA's Meteorological Operational (METOP)
MODIS	Moderate Resolution Imaging Spectroradiometer

Co-funded by the Horizon 2020 programme of the European Union

PFT	Plankton Functional Types
PMR	Passive Microwave Radiometers
RA	Radar altimeter
RCM	Radarsat Constellation MIssion
ROSE-L	Radar Observing System for Europe at L-band
SAR	Synthetic Aperture Radar
SMOS	Soil Moisture and Ocean Salinity
SSMIS	Special Sensor Microwave Imager Sounder
SSM/I	Special Sensor Microwave Imager
SMMR	Scanning Multichannel Microwave Radiometer
TRMM	Tropical Rainfall Measuring Mission
PALSAR	Phased Array Type L-band Synthetic Aperture Radar

Executive Summary

The main **objectives** of the WP3 are: 1) to identify the potential for retrieving additional variables from EO data linked to the state of the Polar Regions that are required for assimilation into models and forecasts of meteorological and environmental processes and their variations and 2) to assess the capabilities of future satellite missions (with special focus on the Copernicus Expansion Missions) for environmental monitoring and for providing data for integration/assimilation into modelling/forecast products, considering different *In situ* and airborne field measurement scenarios.

To achieve these objectives we have prepared a comprehensive review of the current status of remotely sensed parameters acquired over Polar Regions and compared them with the products

Co-funded by the Horizon 2020 programme of the European Union

provided by the Copernicus service to identify current data gaps. Besides, an assessment of future satellite missions (in particular the HPCMs) has been performed, in terms of their benefit for environmental monitoring and their integration/assimilation in modelling/forecast products. We have also identified possible synergies between parameters obtained from different satellite missions to enhance the information content of specific data products considering the end-users requirements. Finally, we have identified the limitations of the currently assimilated variables as well as the potential of new variables that are relevant for assimilation into models for simulations and forecasts of conditions in the Polar Regions. Moreover, a concept for a move forward on data assimilation is presented.

Important note: *In this report we have analysed sea ice, land and ocean parameters. Greenland and Antarctica ice sheets and glaciers as well as atmospheric parameters are not covered in the inventory below.*

In **Section 1** we have reviewed the state of the art of sea ice, land, and ocean parameters acquired with current remote sensing missions. We have provided a review of the technologies used to measure each parameter, its resolution (temporal and spatial), the latency, the uncertainty of the available products, and also the validation techniques. We have also assessed the main known limitations and gaps for each parameter retrieval.

The inventoried parameters for land are: snow cover fraction, snow water equivalent, snowmelt, snow depth, snow avalanches, snow albedo, lake ice, permafrost and soil moisture; for sea ice: concentration, thickness, drift and deformation, ice type, ice edge position, snow on sea ice, surface albedo, characteristics of melt pond fraction, and ice surface temperature. The ocean parameters analysed are: ocean surface biogeochemical compounds and light, sea surface temperature, sea surface salinity, sea surface height, surface currents, and surface stress (winds).

- Summary of **the identified gaps and recommendations for improving the monitoring of the Polar Regions, based on Remote sensing observations** in Table ES. 2.

In **Section 2 data gaps on the products distributed by Copernicus have been identified.** Several parameters are not delivered by Copernicus or they distribute the models outputs only, while the parameters can be measured with remote sensing techniques. We identify the remote sensing parameters which Copernicus is not currently serving while datasets with acceptable maturity are available from different providers, such as universities and research institutes. These **parameters** are listed below:

- **Sea ice parameters:** Sea ice age, melt pond areal fraction, sea ice albedo, the areal

Co-funded by the Horizon 2020 programme of the European Union

fraction of leads.

- **Land parameters:** Lake ice thickness and duration, snowmelt, snow depth, snow avalanche monitoring, inland water chlorophyll and turbidity, permafrost properties (combined with models).
- **Ocean parameters**: Surface currents, surface stress (wind), wave spectra, ocean albedo.

➢ **Recommendation for Copernicus:** to **include the above 14 remotely sensed parameters** in the **future evolution of Copernicus Services.**

In **Section 3** we compiled the **list of those parameters which can be acquired/estimated with future missions** (already planned or under discussion). This section is specially focused on the EU HPCM missions (CIMR, CRISTAL, ROSE-L, CO2M, CHIME, LSTM). The expected quality of the parameters and the advantages of the future instruments, with regards to the current missions, are summarized here. Besides, other missions are also assessed correspondingly.

This review **emphasizes the great potential that the 3 future HPCM polar missions** (CIMR, CRISTAL and ROSE-L) have for the monitoring of the Polar Regions with better resolution and accuracy with respect to the current missions. The main objectives of these missions are:

- **CIMR,** with a passive microwave sensor at 1.41, 6.9, 10.7, 18.7, 36.5 GHz as payload:
  - Land: snow extent, snow water equivalent, lake ice extent and thickness.
  - Sea-ice: sea ice concentration, sea ice thickness for thin ice, snow-depth on ice, sea ice drift, ice type/age, ice surface temperature.
  - Ocean: sea surface temperature, sea surface salinity and surface winds.

- **CRISTAL,** with a synthetic aperture radar (SAR) altimeter operating at Ku-band (13.5 GHz) and Ka-band (35.75 GHz) as a payload:
  - Land: land surface elevation and permafrost.
  - Sea-ice: thick sea ice thickness with better accuracy (>1m), snow-depth on ice, icebergs detection and height.
  - Ocean: Sea level
- **ROSE-L**, which carries a synthetic aperture radar (SAR) working at L-band (1.275 GHz):
  - Land: snow water equivalent, snow avalanche occurrence, lake ice extent and thickness, permafrost extent and properties.
  - Sea-ice: high-resolution sea ice concentration and ice edge position, sea ice drift and deformation, iceberg occurrence and areal density, ice type.

Co-funded by the Horizon 2020 programme of the European Union

- **The main conclusion is that the future HPCM missions have a great potential for improving the monitoring of the Polar Regions, especially with the three polar missions: CIMR, CRISTAL and ROSE-L.**

In **Section 4** we evaluate the **current and potential synergies** to improve the quality and resolution of remote sensing data products for the Polar Regions.

Synergies are achievable by combining data from satellite instruments operated at different frequencies/wavelengths, in passive or/and active modes, with different spatio-temporal resolutions, different penetration depths into the ground, which means to have different sensitivities to the geophysical parameters.

Some of the results are listed below:

- Eight potential synergies of different types of sensors are presented for land, eight more for ocean and ice and two for biogeochemistry parameters, most of them already demonstrated in the scientific literature. From those **potential 18 synergies, only 4 will be operational in Copernicus by the end of phase 1,** the rest are experimental.
- The type of **user** (intermediate users or end-users land /ocean **who can benefit** from the new product) is specified, as well as the **impact** for the users (high, middle, low) of producing these enhanced products. Most of the proposed parameters are appropriate for **intermediate users and in a later stage will have an important impact** for end-users.
- Larger number of similar observations (similar instruments onboard different missions) would improve the measurement uncertainty as well as the temporal resolution.

Table ES. 1 shows a matrix of potential synergies that could be put into operation with current and future capabilities. The synergies mentioned are already tested experimentally.

Table ES. 1: Matrix of potential synergies that could be put on operation with current and future HPCM satellites. The synergies mentioned are already tested experimentally. The green boxes are synergies for land applications, light grey for ice and sea applications. Text in red

Co-funded by the Horizon 2020 programme of the European Union

means an operational product in Copernicus phase 1 (2021). Parameters with high impact for intermediate and end-users are marked with bold.

Sensors	**PMR** **(e.g. CIMR)**	**RA** **(e.g. CRISTAL)**	**IR** **(e.g.LSTM)**	**Optical** **(e.g. CHIME)**	**SAR** **(e.g. ROSE-L)**
PMR		lake ice thickness		**Soil moisture** **downscaling**	Snow Water Equivalent **Soil moisture**
RA	**SIT[1], ice type,** snow depth			Phytoplankton groups	
IR	**SIT, ice surface temperature,** **sea surface temp**	**SIT, ice type**			
Optical	**SIC, ice type**	**ice type** MPF		**Phytoplankton groups, phytoplankton dynamics**	snow extent snow wetness **snow avalanche** lake ice extent
SAR	**SIC, SIDrift**	sea ice deformation evolution **iceberg properties,** snow depths on sea ice	**ice type**	**SIC, ice type**	

This section puts special effort on synergies achievable with the three polar HPCM missions (**CIMR, CRISTAL, ROSE-L**), and emphasizes the need for combined data acquisition strategies that enable **overlapping data acquisition within sufficiently short time intervals**.

Co-funded by the Horizon 2020 programme of the European Union

- **Recommendation for Copernicus: to promote the production and distribute the products resulting from the synergies described in** Table ES. 1**, especially the ones with a higher impact for the user** (marked in bold). The tables also specify the community who will benefit from the synergy and the degree of impact.

The gap analysis of the remote sensing parameters (section 1), the analysis of new parameters derived by the planned future missions (section 3) and the feasible synergies (section 4) have allowed us to perform a list of **recommendations to improve the Copernicus services for Polar monitoring**. The recommendations are summarized in Table ES. 2, organized by: general, land, sea-ice and ocean applications recommendations, and by the time required to achieve the objective, as well as the impact to the users.

Table ES. 2: Gaps and recommendations to improve the monitoring of Polar Regions. Timeline to achieve the goal, its impact and user beneficiary.

Objectives for the improvement of RS data of Copernicus for the Polar regions		
Objectives	**Time period** **Impact** **Users**	**Enhancements needed and recommendations for achieving them**
Time period: short term (<5 years, Copernicus next phase), mid-term (current and future technology <10 years, HPCM missions), long term (future technology >10 years, Sentinel-NG's) **Impact :** level of impact to achieve the challenge (high, mid and low) **Users**: marine end-users (as WP1 T1), land end users (as WP1 T2), intermediate users (as WP1 T3)		
General		
Increase in situ observations	mid term high impact intermediate users	*In situ* measurements in polar regions are very scarce in Copernicus and in general. This is a clear gap, since this *In situ* data is needed to improve and validate parameter retrievals and products derived from the remote sensing data. **Recommendations:** Acquisition and archiving of a more extensive *In situ* dataset, with a more active role in managing it played by the Copernicus *In situ* Component. This would allow provision of a more robust quality assessment of satellite

Co-funded by the Horizon 2020 programme of the European Union

		products and improve the geophysical retrieval algorithms.
Reduce polar observation hole	mid term mid impact intermediate users	New polar missions should consider the extent of their polar observation hole in the design phase, and reduce it as much as possible within the constraints of the mission's objectives. This is particularly important for visible/infrared imagers, for which twilight acquisition mode should be part of the core mission requirements. **Recommendations:** Carefully consider the twilight acquisition, and more generally polar data coverage, when designing future missions, e.g. the Sentinel-NG missions.
Enable low timeliness of Copernicus polar missions data flow	short term high impact intermediate and end users	Sea ice is constantly on the move, avalanches can happen at any time, Search and Rescue operations require timely sea-ice imagery and forecasts. The requirements from the end-users for low timeliness in the access to imagery, derived products, and forecasts prompt for low latency in data downlink and processing. **Recommendations:** ensure near-real-time (<1h) or better for critical operational missions (e.g. ROSE-L, CIMR) in the Arctic region, e.g. through pass-through downlink, several receiving stations, on-site processing.
Land monitoring		
Snow cover	short term high impact intermediate users	Existing snow cover services (CCI Snow, Copernicus Snow) focus all on latitudes below the Arctic circle where light conditions and favourable cloud cover allows consistent products and services using medium resolution optical radiometers (MODIS/Sentinel-3). To monitor Arctic environments considerable efforts need to be done to take into account results from alternative sensors (passive and active microwaves) and perhaps also use signals in the infrared end of the spectrum from radiometers. A complete and consistent Arctic snow cover product will probably involve using all types of data available, in addition to multi-temporal interpolation techniques. **Recommendations:** Demonstrate multi-sensor snow services for Arctic regions (above Arctic circle) and integrate them in existing PanEuropean/global services for completeness of ECV.

Co-funded by the Horizon 2020 programme of the European Union

Snow avalanche monitoring	short term high impact land end users	Snow avalanches can be detected using SAR. This has been demonstrated in Northern Norway and for specific Arctic regions, and should be applicable for mountain areas too. Snow avalanche monitoring can be an important input to snow avalanche services, and improve the accuracy of avalanche warning. Extended activity within this field could be valuable in sparsely populated areas where limited observations are available. **Recommendations:** Extend near-real-time avalanche monitoring across, at the least, European mountains based on S1.
Soil moisture	short term mid to high impact intermediate & land end users	Current operational algorithms for soil moisture (PWR or SAR for higher resolutions) retrieval do not take properly into account freezing/thawing in Arctic regions. This parameter is used on fire risk indexes. **Recommendations:** Additional sensors or retrieved products, such as snow extent products from optical sensors (or higher-order products using SAR/PMR/models), could be used to remove erroneous detections. CIMR and ROSE-L will provide SM products.
Lake ice	short term mid impact intermediate & land end users	Lake ice products based on MODIS data exist only for a limited area in Scandinavia (Copernicus) and do only cover mid-winter/ice break up periods. The freeze-up periods are not covered. **Recommendations:** Future services should be based on combinations of SAR and optical instruments (maybe also with Sentinel 2 and 3) to assure data also during polar night conditions. This will also allow for observations of lake ice conditions in the Arctic.
Snow water equivalent/Snow depth	long term high impact intermediate & land end users	Coarse-resolution SWE products at high latitudes exist. They are not applicable in mountain areas. ROSE-L could be a potential solution for this problem using the interferometric phase. Cal/Val sites with a good characterization of snow parameters (SWE, depth, density, grain size, wetness, layering, etc.) are important to build up in the Arctic mountains to verify the proposed approach.

Co-funded by the Horizon 2020 programme of the European Union

		Recommendations: Enhanced efforts to measure SWE in Arctic and mountain regions are highly needed. Build up of competencies alongside the development of ROSE-L.
Permafrost	long term high impact intermediate & land end users	More advanced development is needed to have a good assessment of permafrost. Only sparse *In situ* evaluations of the permafrost fraction are available, strongly complicating validation for this parameter. The quality of the active layer thickness predictions depends strongly on the quality of the prescribed ground stratigraphy. **Recommendations:** Uptake products from the ESA Permafrost CCI project, where data from RS and reanalyses are combined with the CryoGrid model to derive permafrost parameters. Additional estimates of the permafrost extent could be provided in some cases based on the detection of land surface movements. CRISTAL and ROSE-L will provide these retrievals. The new European Ground Motion service, currently being implemented as a new Copernicus Service Element, should be extended to cover the circumpolar Arctic area.
Sea-Ice monitoring		
Snow depth on sea-ice	mid term high impact intermediate users	Not measured remotely with proper accuracy. This parameter is very important on its own, and to properly measure sea ice thickness from altimetry, among others. **Recommendations:** Assess possible synergies, new HPCMs (CIMR, CRISTAL and ROSE-L) will contribute to improve the retrieval of this parameter.

Co-funded by the Horizon 2020 programme of the European Union

Near real time high resolution ice analysis	mid term high impact intermediate & marine end users	High resolution (sub kilometers) ice analysis is today done manually based on SAR images, and it is necessary to automatize it to handle ever-increasing volumes of data and to meet the demand for increased detail (ice rheology). Progress is also limited by the fact that radar altimetry and passive microwave radiometry satellites for sea ice thickness have a period of operation outside of summer months, which is when data of sea ice conditions are most important. **Recommendation:** Enhanced automation of high resolution (sub km) ice chart production to handle increased satellite data volumes and provide additional detail. Further research to improve sea ice parameter retrievals in summer.
Improved sea ice concentration for forecasting	mid term high impact intermediate users	Ice concentration retrievals rely on semi-operational or outdated passive microwave radiometer satellite missions (AMSR2 and SSMIS). With increased forecast model resolution, coverage and increased accuracy, SIC data is required at the ice edge and in the coastal zones. **Recommendation:** Fully operational missions with long-term continuity are needed. Synergy with SAR and/or optical must be further explored.
Multi-sensor sea-ice drift analyses.	mid term mid impact intermediate users	There is to date no satellite product (operational or research-based) that combines accurately radiometry-based and SAR-based sea-ice drift data. This would, however, fill a key observation gap (complete daily coverage, with higher spatial resolution and accuracy where SAR is available), particularly in the Antarctic where SAR coverage is sparse. The same yields for mosaicking of several SAR-based sea-ice drift products (e.g. Sentinel 1 A-B-Cs, the RCMs, etc.). Propagation of the uncertainties into the Level-4 analysed sea-ice drift product must be treated as well. **Recommendation:** Develop and implement operational multi-sensor sea-ice drift analyses, e.g. in CMEMS.
Summer Sea ice concentration	medium & long term high impact	During melting periods the accuracy of PMR-based SIC estimates considerably decrease. In the presence of melt-ponds, PMR can only sense the ice surface fraction. PMR algorithm must be refined to achieve better observation of the ice surface fraction.

Co-funded by the Horizon 2020 programme of the European Union

	intermediate users	In parallel forecast models must be developed to ingest the Ice Surface Fraction **Recommendation:** Improve accuracy and generate melt-pond-fraction data products from visible/infrared imagers (such as OLCI-Sentinel3, Sentinel-2, MODIS, MERIS, VIIRS, ...). Investigate if modern SAR sensors (Sentinel-1) can accurately measure MPF at a basin scale. In parallel, further develop melt-pond parameterization in forecast models to exploit the ice surface fraction products routinely.
Sea ice thickness	long term high impact intermediate & marine end-users	High temporal resolution ice thickness products covering the whole range of thickness are missing. A higher spatial resolution sea ice thickness product (sub km) is also missing. Coverage for the melt season is also lacking. Snow depth measurement with enough precision is crucial for deriving SIT with good accuracy. **Recommendation:** Supplement microwave remote sensed data sources with optical satellite and *In situ* data during summer. Further research into snow retrievals over sea ice.
Ocean monitoring		
Surface ocean biogeochemical compounds (also for inland waters)	mid term high impact intermediate users	Parameters on ocean productivity, biogeochemical fluxes and radiation. The main limitations are due to the low temporal coverage, sea ice cover, unfavourable light and rough weather conditions. Higher spatial resolution (of order 10–100 m) data to retrieve parameters from bays and estuaries at the polar coasts and in inland waters are necessary. Missions providing such data are focused on land applications (e.g., Sentinel 2 or Landsat 8) which only cover the Arctic coasts below 74°N and not the Antarctic continent. Products on phytoplankton functional types are currently released but limited to S3 and need higher spatial scale which would help to improve predictions for water quality, HABs, fishery, coastal management by themselves but also indirectly by improving the quality of Chl products. **Recommendations:** Merging satellite data can improve this tremendously. *In situ* data are sparse for validation and the implementation and further development of autonomous *In situ* bio-optical measurements need to be promoted. Promote

Co-funded by the Horizon 2020 programme of the European Union

		CHIME also for pan polar applications.
Sea surface salinity	mid term mid impact intermediate users	This parameter is provided by L-band microwave radiometers only. It is very important for the assessment of freshwater fluxes changes. Its accuracy is limited, mainly due to the sparse *In situ* data available. **Recommendations:** Promote CIMR mission since it also carries onboard an L-band radiometer. More *In situ* measurements are required to enhance satellite salinity products.
Wind speed	long term mid impact intermediate users	An improvement on the accuracy of wind speed observations over ice and ocean is needed since the wind controls the surface ocean circulation and hence freshwater transport rates and pathways. **Recommendations:** To add Doppler capability to future scatterometers, allows for simultaneous measurements of surface winds and currents and improves directional accuracy.

In **Section 5** we analyse the **status quo in data assimilation,** showing that many observations are routinely assimilated, some with success, some with potential for improvement, and several not being assimilated at all for various reasons.

The parameters that are assimilated into CMEMS models (some of them with important constraints) are assessed in the document and itemized below, classified by its degree of limitations:

- Parameters assimilated with **severe limitations**: SST (from IR), SIT, Ice Drift, Chl
- Parameters assimilated with a **medium level of limitations**: SIC
- Parameters with quality of assimilation not sufficiently documented: SSH, SST (from PMR)

There is to our knowledge no assimilation of satellite land data as part of the Copernicus Land nor Climate Change Services as of today.

The **remotely sensed parameters that are not being assimilated and are recommended for data assimilation** are summarized below, organized by the time required to achieve each goal. The specific problems faced by each parameter are explained in the report.

- **Short term:** sea surface salinity.
- **Mid-term:** snow cover, permafrost extent, sea ice drift, wave height, ocean colour Chl, ocean

Co-funded by the Horizon 2020 programme of the European Union

colour PFT.

- **Long term:** soil moisture, river level, sea ice surface temperature, melt pond areal fraction.

Besides, the **assimilation of satellite information at lower processing levels** has been investigated. We explore how services would benefit from going beyond the current status-quo (assimilation of daily/weekly/monthly averaged gridded satellite products) and start assimilating individual swaths (and/or scenes) of satellite-derived product in swath projection, and even directly raw satellite data.

The **recommendations** to be considered when **new data assimilation approaches** are assessed are stated below organized by the time required to achieve the goals:

- In the **mid term**:
  - Working towards the development of higher-resolution regional ocean/ice forecasting systems: test, refine, and adopt data assimilation of sea-ice parameters at **Level-2** (in a swath or along the track). This is a necessary preparatory step for the optimal ingestion of Level-2 data products from the HPCM CIMR and CRISTAL.
  - Foster the collaboration and enable further dialogue between the modelling and Earth Observation communities, to get the benefit of the expertise in both communities.
- **In the long term**:
  - Continue the development of fully-fledged yet efficient microwave emission models for sea-ice and snow. Community models -such as SMRT- should be preferred, ideally coupled and reconciled with radiative transfer models for the atmosphere and ocean surface.

Co-funded by the Horizon 2020 programme of the European Union

Section 1: State of the Art of Polar Remote Sensing Parameters

1.1 Land Parameters:

1.1.1.Snow cover

1.1 Snow Cover Fraction

1.1.1. Technologies used and retrieval methods

The main technology used for snow cover fraction estimation is medium resolution spectrometers such as AQUA/TERRA MODIS, Envisat MERIS/AATSR, AVHRR and in the last years VIIRS and Sentinel-3. More or less consistent climate records can then be established from 1980 - today. Most of the techniques are based on utilizing the NDSI=(Radiance Visible ch- Radiance Near IR CH)/(Radiance VIs + Radiance NIR). The NDSI is then typically scaled linearly to a snow cover fraction (Salomonson and Appel, 2004) between 0-100%. The typical resolutions based on these instruments are 250 -1000m.

Emerging from the launch of Landsat-8 and Sentinel-2 higher resolution snow fraction estimates seems to be possible with resolutions down to 10-30m. This can be of high value for local and regional monitoring.

1.1.2 Characteristics of the parameter

- Temporal Resolution: Daily
- Spatial Resolution 250-500m
- Latency: Typically, a few hours after acquisition.

1.1.3 Validation

Medium resolution products such as MODIS and S3 are validated using simultaneous high-resolution products from S2 or Landsat-8. Under ideal conditions the accuracies are typically in the range 90-95% (Metsämäki et al., 2012).

1.1.4 Error sources/Accuracy/uncertainty

Clouds - Optical instruments can not measure snow fraction under clouds. Partial cloud cover and shadows from clouds can also affect the quality of the product.

Co-funded by the Horizon 2020 programme of the European Union

Patchy snow: Sub-pixel scaled patch snow cover can often be challenging to measure accurately.

Forested area: Dense forests often completely absorb the signatures from snow on the ground.

Shadows from slopes: Steep mountainous terrain leads to shadows at north slopes, and incorrect estimates of the snow cover fraction if the terrain is not properly corrected for.

1.1.5 Known limitations and gaps

Polar night is challenging. Due to consistency many services do not start before March and end in October. In particular, the estimates of the first snowfall in the autumn is uncertain due to a combination of cloudy conditions and if the first snowfalls are late, occurring after the sun is very low and the services stop.

1.2. Snow Water Equivalent

Snow water equivalent (SWE) is an ECV. SWE is the density multiplied by the depth of the snow and indicates the amount of liquid water that a snow-mass in a unit area ($1m^2$) will translate into.

1.2.1. Technologies used and retrieval methods

SWE can be measured using passive microwave instruments such as SSM/I and AMSR-E. PMR techniques to measure SWE utilizes the fact that radio waves at different frequencies have different extinction coefficients (damping) by the snow. By utilizing the measurements at e.g. the 18 and 37GHz a simple retrieval model assumes that SWE= constant * $[T_B(37)-T_B(18)]$ where is T_B the brightness temperature measured by the satellite.

In several projects (e.g. GlobSnow and CCI Snow) the Finnish Meteorological office (Pulliainen, 2006) together with collaborators have developed a global service that utilizes PWM together with data from the meteorological weather station network to provide global estimates of SWE (http://www.globsnow.info/).

Co-funded by the Horizon 2020 programme of the European Union

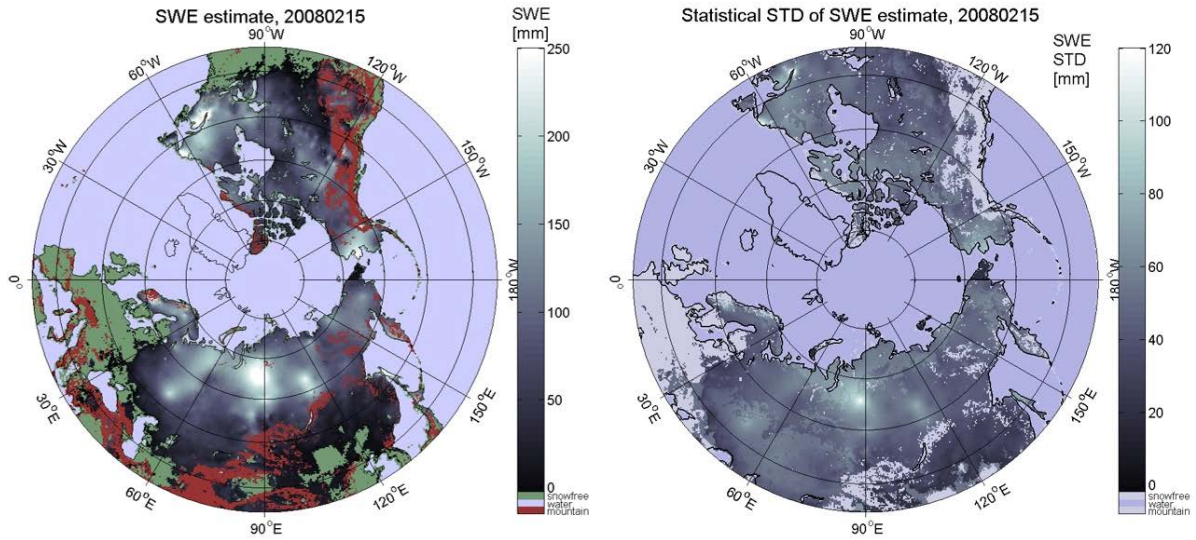

Fig 1. Example of the GlobSnow SWE product for 15 February 2008.

1.2.2 Characteristics of the parameter

- Temporal Resolution Daily
- Spatial Resolution 25km
- Latency NRT

1.2.3 Validation

Validation is done using *In situ* measurements from meteorological stations (usually from snow depth and assuming density) or other transects. There is a big uncertainty in obtaining representative measurements of SWE over a large 25x25km pixel, and the technique does hence only work for flat terrain where the snow depth is fairly constant.

1.2.4 Error sources/Accuracy/uncertainty

PMR does not work in mountains and complex terrain. Impurities at the sub-pixel scale such as lakes or coastlines can also affect the result.

Melting snow can be a problem since radio waves do not penetrate to ground, and may lead to large errors although the algorithms usually try to detect and mask out areas affected.

Co-funded by the Horizon 2020 programme
of the European Union

The theory is based on some assumptions about the snow grain size. This can lead to over or underestimations in certain conditions.

1.2.5 Known limitations and gaps

The main problem with PMR techniques is its inability to measure SWE in mountains. GCOS requires a spatial resolution of 1 km. Possible improvements have been targeted by several authors, and with a few possible technologies. The main satellite-based possibilities lie in either using radar backscatter changes over variable snow water equivalents using high-frequency SAR (X and Ku-band) or using the change in the interferometric phase under variable SWE.

The first method was targeted in the ESA Earth Explorer 7 candidate CoReH2O (Rott et al., 2010). This sensor concept was unfortunately not chosen by ESA in the final selection, but will probably be suggested in other contexts. The sensor applied both X and Ku-band and two polarizations (VV,VH) thus providing four measurement channels used to retrieve SWE. The suggested retrieval algorithm was based on a radial transfer model where SWE and snow grain size are the most sensitive parameters.

An alternative to relate changes in backscatter to changing SWE, is to directly measure the changes in interferometric phase Φ from one acquisition to a repeated satellite pass (typically 6 -35 days later). SWE can be shown to be directly proportional to the phase change. ($\Delta SWE = k*\Delta\Phi$). This approach was already suggested using C-band SAR with ERS-tandem by Guneriussen et al. (2001). Unfortunately, later research showed that C-band is very sensitive to decorrelation and phase wrapping effects, and in practice the technique is not very applicable for mountainous snow when large snowfalls can happen hours. L-band SAR interferometry (Rott et al., 2003) has been suggested as a remedy for avoiding the problems with C-band decorrelation effects. At present there are several planned launches (NISAR and ROSE-L) using L-band SAR. SAOCOM-CS or ALOS-2 are also options, but there is little data available.

1.3. Snow Melt

Co-funded by the Horizon 2020 programme of the European Union

Can be monitored using C-band SAR at good spatial resolution (50-100m), weekly temporal resolution is somewhat poor but might be improved with full utilization of the Radarsat Constellation Mission (RCM).

1.3.1. Technologies used and retrieval methods

Wet snow can be detected using passive instruments at coarse (25km) resolution. This can be regarded as a bi-product of the Snow Water Equivalent services. Higher resolution sensors such as scatterometers can also be used (5 km), but in mountainous terrain C-band SAR seems to be the best option. The main technique for measuring the presence of wet snow is by change detection against a dry snow reference or preferably an average over as many dry snow scenes as possible. Nagler and Rott (2000) suggested this method for ERS-1.

1.3.2 Characteristics of the parameter

- Temporal Resolution: 2-7 times per week depending on latitude.
- Spatial Resolution: 50-100m allows good speckle filtering
- Latency: NRT is achievable

1.3.3 Validation

Validation of wet snow maps against simultaneous optical snow classifications indicates that the accuracy of the algorithms is around 90% for most scenarios using Sentinel-1 (Nagler et al., 2016). In cases where not all snow can be assumed wet, it is much harder to assess the accuracies as only *In situ* data can be used for comparison. Some studies are underway but it appears that there are great challenges in finding *In situ* datasets indicating snowmelt status and presence of snow for representative areas (i.e. outside cities where contamination of the SAR signal is probable) .

1.3.4 Error sources/Accuracy/uncertainty

The main error sources for SAR derived melting snow maps are the variability in radar backscatter signatures for various land cover types (forest, farmland, glaciers, etc.) leading to needs for adaptations in the classification algorithms.

1.3.5 Known limitations and gaps

In addition to flagging the status of melting snow it would also be desirable with more precise quantification of the liquid water content in melting snow. LWC can be an important parameter for both hydrologists and avalanche forecasters. Present algorithm developments

Co-funded by the Horizon 2020 programme of the European Union

have focussed on the classification scope, but since there is also a sensitivity in radar backscatter to variable LWC, new studies should also take this into consideration.

1.4. Snow-depth

Snow depth (SD) is related to snow water equivalent (SWE) since SWE=SD*□, where □ is the mass density of snow. At large scales snow depth is controlled by climate processes and varies typically from low densities (0.1g/cm^3) in early winter to high densities (0.3g/cm^3) late in the winter after several compression and melting events (Borman et al., 2013). At local scales in e.g. mountains wind drift and topography play an important role (Nolin, 2010).

1.4.1. Technologies used and retrieval methods

Snow depth can potentially be measured by space-borne LIDARS. Airborne LIDAR experiments (Paintner et al., 2016) and ground-based terrain scanning laser measurements (TLS) show high accuracies within a few cm. Similar results have not been reported from spaceborne LIDARS (ICESat & ICESat-2).

A more viable approach for wide-scale retrieval seems to be to derive SD from SWE retrievals using microwave instruments (passive microwave for coarse-scale and active radar for high resolution, see section 1.2). By making assumptions about the density one can provide SD. These assumptions can be based on snow process models (e.g. Crocus or SnowPack) forced by meteorological inputs and can provide estimates of density. Synergistic use of EO data and snow process models can also be an approach to improve estimates (Xiao et al, 2018; Kim et al., 2019). In a study in China (Qiao et al., 2018) the Globsnow dataset was used to estimate snow depth assuming a constant density of 0.24 g/cm^3.

Lievens et al. (2019) reports a high correlation between the cross-pol ratio □^{VH}/□^{VV} and snow depths on a 1km scale for Sentinel-1. Using an empirical change detection approach, they found correlations in the range 0.6-0-8 when compared with *In situ* measurements of snow depth worldwide in mountainous areas. The authors can, however, not explain the correlation theoretically with volume scatter theory. They even claim that the method works when the snow is wet, although theoretically volume scatter from the snowpack should then be absorbed completely in the top layer of the snow. This result is hence still controversial, although being able to retrieve SD with Sentinel-1 is a very attractive capability.

Co-funded by the Horizon 2020 programme of the European Union

1.4.2 Characteristics of the parameter

- Temporal Resolution: Daily
- Spatial Resolution: 25km
- Latency: NRT

1.4.3 Validation

Snow depth measurements can be validated against the *In situ* measurements. These exist on many meteorological stations. The problem is, however, often that the point measurements from a station are hard to relate to an average over a large pixel (e.g. 25km x 25km as for passive microwave instruments). In this case one should ideally use distributed measurements of snow depth (snow stretches or other sampling strategies to capture the variability in SD over the pixel).

1.4.4 Error sources/Accuracy/uncertainty

Passive microwave radiometers (PMR) and other means for measuring SWE/SD have several error sources. For coarse resolution PMR retrieval the sub-pixel problem is challenging. Sub-pixel contamination of sea, lakes, glaciers and forests may have severe effects on the retrieval accuracy.

1.4.5 Known limitations and gaps

Passive microwave methods for retrieving SWE, and thus snow depth have saturation effects for deep snow (~1m) due to the use of high-frequency bands in PWM (18-36GHz). PMR derived SWE and hence SD is usually masked in mountainous terrain and glaciers due to high variability.

1.5. Snow avalanches

1.5.1. Technologies used and retrieval methods

The technology used for snow avalanche (hereafter called avalanche) detection depends on the spatiotemporal scale of a monitoring or detection purpose. For regional avalanche forecasting, daily knowledge of spatiotemporal avalanche activity is critical. The main technology used for such a monitoring task is high resolution, radar satellite data. Studies

Co-funded by the Horizon 2020 programme of the European Union

have shown the potential of C-band Radarsat-2 data and in recent years, C-band Sentinel-1 data (e.g. Eckerstorfer et al., 2017; Vickers et al., 2016). Especially the Sentinel-1 constellation, which covers the majority of snow-covered mountain areas worldwide, has the highest potential in consistent and reliable avalanche activity monitoring over large regions. For the quantification of single high magnitude avalanche periods, very high-resolution optical data is the preferred sensor (Bühler et al., 2019). Although highly expensive, the very high spatial resolution allows for detailed mapping of avalanche activity during cloud-free conditions.

For avalanche hazard mapping or avalanche activity monitoring in communities, in ski resorts or on single slopes, terrestrial sensors are the favored choice of technology (Eckerstorfer et al., 2016). Both optical time-lapse cameras and terrestrial LiDAR scanners have been successfully deployed for continuous slope-scale avalanche activity monitoring. Optical and radar satellite sensors can be used for slope-scale monitoring as well, however, the application of these sensors is highly dependent on the acquisition repeat frequency. Continuous monitoring with seconds to minutes sampling rates are obviously not possible.

1.5.2. Current state of automatic detection

The application of algorithms for automatic avalanche detection was first tested in very high-resolution optical airborne images (Bühler et al., 2009) and optical satellite images (Lato et al., 2012). These algorithms were based on object-oriented image interpretation which employed segmentation and classification methods to detect avalanches. Achieved accuracies ranged over 90 % with errors of commission as low as 5 %. However, in recent years, no follow-up studies explored automatic avalanche detection in optical satellite images any further. On the contrary, the most recent study deployed expert interpretation of very high-resolution Spot 6 images (Bühler et al., 2019).

Using radar satellite images, the development occurred the other way around. First, proofs-of-concept studies were carried out with expert interpretation of SAR images (Eckerstorfer and Malnes, 2015), before the first study on automatic classification and segmentation of SAR images appeared (Vickers et al., 2016). With the vast amount of Sentinel-1 data freely available, this automatic avalanche detection algorithm was developed further and integrated into a near-real-time processing system that is currently used by the Norwegian Avalanche Centre in daily, public avalanche forecasting (Eckerstorfer et al., 2019). At the same time, a handful of studies emerged very recently, testing the use of neural networks for avalanche segmentation in SAR images (Bianchi et al., 2019; Kummervold et al., 2018; Sinha et al., 2019; Waldeland et al., 2018).

Co-funded by the Horizon 2020 programme of the European Union

1.5.3. Retrievable parameters

Using either optical or radar satellite imagery for avalanche detection, the following parameters are retrievable:

Reference	**(Eckerstorfer et al., 2019)**	**(Bühler et al., 2019)**
Sensor	SAR	Optical
Satellite	Sentinel-1	Spot6/7
Resolution	20 m	1.5 PAN
Min. avalanche size	501-10000 m^2	10-500 m^2
Avalanche type	No	Yes
Wet / Dry snow	Yes	Yes
Starting zone	No	Yes
Continues detection	Yes	No
Temporal resolution	Daily at high latitudes	Daily
Latency	Typically, a few hours after acquisition	Typically, a few hours after acquisition
Costs	Free	Several 1000 USD per image

1.5.4. Validation

Satellite-borne SAR avalanche detection:

Eckerstorfer et al. (2019) validated their automatic avalanche detection system in Sentinel-1 images by comparing the automatic detections with the expert interpretation of SAR images as well as to a database of field-observed avalanches. Compared to the field-observed avalanches (N=243), manual interpretation achieved a probability of detection of 77.3 %, while automatic detection achieved a POD of 57 %. The POD of 77.3 % for manual interpretation is likely the maximum detection probability using satellite-borne SAR data for avalanche detection. Considering manual interpretation as the golden standard, the accuracy for automatic detection is 79 %. This means that 79 % of the manually found avalanches were detected automatically, of which large to very large avalanches (> 10000 m3) were detected

Co-funded by the Horizon 2020 programme of the European Union

with an accuracy of over 90 %. Moreover, automatic detection works better on wet snow avalanches due to the more backscatter energy being reflected back to the sensor.
However, Bianchi et al. (2019) recently showed that using a fully convolutional neural network for avalanche segmentation significantly outperforms the algorithm used by Eckerstorfer et al. (2019). Compared to manual identification of 99 avalanches in a Sentinel-1 image, the FCN achieved an accuracy of 66.6 % compared to 38.1 % by the conventional algorithm.

Satellite-borne optical avalanche detection:

Bühler et al. (2019) digitized validation images from helicopter reconnaissance to validate manual avalanche detections in Spot 6/7 images. The overall achieved accuracy was 73 % with an omission and commission error of 16 % and 11 % respectively. In illuminated areas, the accuracy was at 80 % compared to an accuracy of 64 % in shaded areas. Especially the omission error was high in shaded areas (25 %).

1.5.5. Error sources/uncertainty/limitations

Satellite-borne SAR avalanche detection:

Using SAR for avalanche detection is challenging since both avalanches and their surroundings consist of snow. Moreover, it cannot be deduced from the SAR images, if there is dry snow or no snow on the ground. There are parts of mountain landscapes that exhibit relative backscatter change over a couple of days and resemble avalanches in their shape. Talus slopes, avalanche fans or debris flow tracks are examples of geomorphological features that can lead to false alarms. Glaciers exhibit also highly dynamic backscatter change and are thus another source of error. There is thus a general level of uncertainty in using SAR for avalanche detection. As an error source mitigation measure, all areas that are not considered avalanche runout areas (e.g. areas where avalanches are most likely to stop) are masked out.
The high variability of backscatter from snow-covered landscapes makes simple backscatter thresholding that separates avalanches from non-avalanches dynamic as well. Of special importance is the evolution of snow wetness in time when temporal backscatter change between two SAR image acquisitions are used for avalanche detection. If the snow transforms from wet to dry snow, a net increase in backscatter takes place, blurring the backscatter difference between avalanches and surrounding undisturbed snow. In such cases, false alarm rates are high.
Since satellite-borne SAR sensors are side looking instruments, radar shadow and layover areas occur that make detection impossible in affected regions. This is especially concerning

Co-funded by the Horizon 2020 programme of the European Union

when only one geometry (ascending or descending) is available, and certain slope aspects cannot be monitored.

The problem of SAR data availability is a geographical one when it comes to Sentinel-1 data. The European satellites focus mainly on European landmasses and adjacent waters, as well as selected hotspots worldwide. Mountain regions in North America for example are covered to a minor degree with 12 days repeat cycle. The planned Sentinel-1 acquisition scenario can be downloaded from here: https://sentinel.esa.int/web/sentinel/missions/ sentinel-1/observation-scenario.

Other SAR data that can be used for avalanche detection provided for example by Radarsat-2 or TerraSAR-X are behind paywalls, however, they have the advantage of pre-ordered acquisition timing, at least when the satellites are available at the desired acquisition time.

Both Radarsat-2 and TerraSAR-X provide very high-resolution SAR data (1-3 m spatial resolution), compared to high-resolution data provided by Sentinel-1 (20 m). This allows for the detection of smaller avalanches that are not detectable in Sentinel-1 images (Eckerstorfer and Malnes, 2015).

Satellite-borne optical avalanche detection:

Thus far, only very high-resolution optical satellite data has been used for avalanche detection. Both QuickBird and Spot 6/7 data have sub-meter spatial resolution in their panchromatic channels. Compared to ground truth, automatic avalanche detection in QuickBird data achieved higher accuracy than in SAR data. Nevertheless, these detection algorithms were not transferred to freely available Sentinel-2 data. The most recent study by Buehler et al. (2019) used Spot 6/7 data to manually detect avalanches, achieving high accuracy compared to ground-truthing. Optical satellite data is in best-case scenarios highly suitable for avalanche detection as all parts of an avalanche, from its starting zone to its deposit can be clearly visible. However, cloud cover is a serious problem, especially for the rapid detection of avalanche activity after high magnitude events, as well as for consistent monitoring throughout an entire winter. One is highly dependent on ground visibility to be able to detect avalanches. Thus darkness, for example during the Polar Night or the short mid-latitude winter nights as well as shaded areas pose problems for using optical satellite data.

It seems, moreover, that visual interpretation of avalanches requires very high-resolution optical data. Eckerstorfer et al. (2016) showed nevertheless the potential of avalanche detection in Landsat-8 data in its panchromatic channel. Large wet avalanches were perfectly manually detectable.

Co-funded by the Horizon 2020 programme of the European Union

1.5. Albedo

Surface Albedo is defined as an ECV by the WMO. The Surface Albedo is defined as the ratio between the hemispherical reflected radiation and the hemispherical incoming radiation. Normally this is integrated over the solar radiation range (0.32 - 2.8um) and sometimes referred to as broadband albedo.

1.5.1. Technologies used and retrieval methods

Snow broadband albedo is retrieved from satellites, airborne measurements and ground-based measurements. Each measurement method has different challenges making it difficult to compare and cross-validate the products.

Satellite sensors do not measure broadband irradiance directly and due to the measurement geometry of imaging satellites, the albedo is retrieved through modelling where the measured upwelling spectral radiance is converted to upwelling irradiance and corrected for BRDF (bidirectional Reflectance Distribution Function) effects and atmospheric contributions and Top of Atmosphere (TOA) downwelling irradiance corrected to downwelling surface irradiance. On land, one of the major challenges is to correct for terrain slopes and shading as BRDF (Bidirectional Reflectance Distribution Function) is anisotropic and depends on snow surface type and structure, and one has to correct for the sun-surface-sensor geometry. This implies the albedo will vary with the angular distribution of the incoming radiation and slope. There are multiple approaches to retrieving albedo from satellite data an overview is given in (He et.al, 2014).

Regular satellite-based broadband albedo time series go back to 1979 based on the Advanced Very High Resolution Radiometer (AVHRR) on the NOAA POES satellites. Since 2000 the MODIS instruments on the NASA Terra and Aqua satellites, and from 2015 the MSI on the Sentinel-2 satellites have been used to produce global albedo products. The albedo product based OLCI instrument on the Sentinel-3 satellites launched in 2016 and 2018 have lower spatial resolution than the multispectral instrument (MSI) on board Sentinel-2 but have 4 times larger swath width, hence more frequent cover. Intercomparison between MODIS and OLCI in Kokhanovsky et. al, 2019 indicates that the ILCI product has slightly higher accuracy (within about 1% absolute albedo value). The Copernicus program and the Sentinel satellites will ensure high quality high spatial and temporal resolution high Arctic albedo products needed to produce consistent long time series of this ECV.

Co-funded by the Horizon 2020 programme of the European Union

Airborne albedo measurements are done either by multispectral imaging band instruments, often simulating satellite bands, or by hyperspectral imagers. The latter has the advantage of avoiding the need for modelling the spectrum before integrating over wavelengths to calculate the broadband albedo. Hyperspectral imagers commonly do not cover the SWIR range, hence requires modelling to get the full broadband, though imaging SWIR instruments are now available. Aircraft could also be instrumented with up and down looking broadband pyranometers with hemispheric fields of view to directly measure broadband albedo. The disadvantage of these sensors is that the aircraft have to fly very low and the footprint is large, instrument response time is long and sensors need to be level. Which means that spatial resolution will be very poor.

Ground-based albedo measurements are usually done with down looking sensors mounted on a boom from a tower and upward-looking hemispheric instruments often on solar trackers to split direct solar and diffuse components of the downwelling irradiance. Most measurement sites have a combination of hyperspectral, multispectral and broadband sensors.

1.5.2 Characteristics of the parameter

- Temporal Resolution - from 12 hrs, daily, 8 and 16-day mosaiced products common.
- Spatial Resolution -
  - AVHRR from 1.1 km, swath width 2500 km
  - MODIS from 250 m, swath width 2330 km
  - Sentinel-2 MSI from 20 m, swath width 290 km
  - Sentinel-3 OLCI from 300m, swath width 1270 km
- Latency

1.5.3 Validation

There are multiple validation studies of snow surface albedo products. These are done in a combination of intercomparison between different satellite sensors and towards ground validation instrumentations. In particular long-term monitoring sites such as the DOE ARM sites (www.arm.gov) and the WCRP baseline Surface Radiation Network (BSRN) sites. A validation study on the Sentinel 2 MSI albedo can be found in Li et. al, 2018. A snow albedo validation study for MODIS is i.e. found in Williamson et. al, 2016. A snow product validation and product evaluation for the Sentinel 3 OLCI instrument is found in Kokhanovsky et. al, 2019.

Co-funded by the Horizon 2020 programme of the European Union

1.5.4 Error sources/Accuracy/uncertainty

Suggested absolute averaged accuracy requirement of surface albedo products for climate models is approximately 0.02–0.05 (Henderson-Sellers and Wilson, 1983; Sellers et. al, 1995). The main sources of error lie in the conversion from spectral remote sensing reflectance to broadband albedo, failure of cloud discrimination, thin cirrus clouds in the particular and accurate calibration of the sensors. The satellite products from MODIS, MSI and OLCI are shown to have absolute accuracy within 0.02 (Kokhanovsky et. al, 2019). Validation study used sites up to 80 deg. N and for SZA less than 70 deg, hence valid for the high Arctic Region.

1.5.5 Known limitations and gaps

To correctly model satellite and airborne albedo based on point remote sensing reflectance measurements, corrections for sun, ground and sensor geometry must be done. This requires knowledge of the surface BRDF. The BRDF will depend on the snow surface properties and errors tend to be larger the lower the solar elevation is and the further from nadir the observation direction. BRDF functions used in the retrieval of surface albedo have been developed through modelling and semi-empirical methods. Based on multiple passes over a 16 day period, daily BRDF products have been developed based on MODIS and VIIRS (Liu et. al, 2017). These BRDF data are used in albedo retrieval from the Sentinel-2 MSI
Black-sky and white-sky albedo (Li et. al, 2018).

With regard to the early satellite albedo products retrieved from the AVHRR instruments on the NOAA POES satellites there are challenges discriminating between snow and clouds in the Arctic Region, caused by inconsistent temperature differences between the cloud top and snow cover due to frequently strong temperature inversions. This was mitigated with a new SWIR Channel (3A 1.58–1.64um) on the NOAA-15 and later satellites (Khlopenkov and Trishchenko, 2007). Due to small spectral response deviations on the same channels on the different AVHRR instruments (Trishchenko et al. 2002; Trishchenko, 2006) it is challenging to construct long time series from these data.

1.1.*2. Lake ice* (ice extent, ice thickness, snow depth, ice duration, river ice)

Lake ice occurs at high latitude lakes and in high mountain lakes during wintertime. Typical ice seasons are from December to May. Lake ice extent, ice duration and river ice can be

Co-funded by the Horizon 2020 programme of the European Union

observed with both optical and radar sensors, but the spatial resolution of the sensor must match the size of the lake/river. Ice thickness and snow depth are challenging parameters that no sensor/product can deliver with satisfactory accuracy/coverage presently. Dugay et al. (2015) gives a review of the development in the field.

2.1. Technologies used and retrieval methods

Lake ice extent can be monitored at an appropriate scale using optical or SAR sensors. Optical sensors (MODIS) have been used for operational monitoring of lake ice (CCL Lakes, Copernicus Global Land Product). The fact that lake ice forms at high latitudes makes it, however, hard to detect the ice formation period (Dec-Jan). Also cloud cover can impede the detection of lake ice during the ice breakup period and lead to uncertainties. Future lake ice monitoring services should focus on combining optical and SAR data to improve the accuracy. Wang et al (2018) has demonstrated highly accurate lake ice classification using RS2 in Canada. Scatterometers can also be used to assess the presence of ice on lakes using ASCAT (Bergstedt et al., 2018) and Quikscat (Howell et al., 2009).

Lake ice duration can be derived from the time series of lake ice extent products given that the extent products can be delivered during the ice formation and ice break up periods. For Arctic lakes this demands that SAR sensors are involved.

River ice has similar features as lake ice (Duguay et al., 2015) but the demands for high spatial resolution imply that only S1 and S2 or sensors with similar high spatial resolution can be used. Several experiments and demonstrations have shown the feasibility of monitoring river ice break up periods (e.g. demonstrations in EU FP7 CryoLand for Tana and Torne rivers). A river ice monitoring service could be devised using S1 and S2 for Northern Europe with special attention to ice jams and resulting flooding.

Lake ice thickness can be derived using passive microwave data for some large lakes. Kang et al. (2014) have shown that AMSR-E brightness temperature at 18GHz has a linear dependence with the ice thickness (measured on *In situ* stations). Du et al. (2017) used AMSR-E/2 to provide thickness/phenology for 71 selected large lakes with 5km resolution for the period 2002-2015 with good results.

The presence of snow on lake ice can be monitored with optical instruments. MODIS/S3 and Landsat8/S2 are suitable instruments as the contrast between clear ice and snow-covered ice

Co-funded by the Horizon 2020 programme of the European Union

is good. Snow-covered lake ice is an operational product within the Copernicus Global Land Service for northern Europe. To determine the snow depth on lake ice is, however, a much more challenging task. Given that the water level and the ice thickness is known, it is probably possible to estimate the snow depth from lidar and/or SAR altimeters.

Retrieval of lake ice thickness and snow depth on lake ice is in general a very challenging task for satellite remote sensing. In a general scenario where lakes of arbitrary size need to be considered, only high-resolution SAR perhaps in tandem with radar and lidar altimeters could provide the needed information. Radar backscatter models for lake ice need to consider parametrization of the whole system (ice roughness, slush ice with variable liquid water content, snow depth, snow grain size, layering, etc.). This is in practice a multi-dimensional retrieval problem with many challenges.

2.2 Characteristics of the parameter

In the table below, we indicate lake ice products that could be derived based on existing sensors.

Parameter	**Sensor**	**Temp res**	**Spatial res.**	**Latency**
Lake ice extent	MODIS	Daily*	250m	< 1 day
Lake ice extent	S3	Daily*	300m	< 1 day
Lake ice extent	S2	2 days*	10m	< 1 day
Lake ice extent	S1	1-6**	250m	< 1 day
Lake ice duration	S1/S2	Daily	10m	Annually
River ice extent	S1/S2	Daily	10m	< 1 day
Lake ice thickness	PMR	Daily***	~5-20 km	< 1 day
Snow depth	TBD			

**) Limited by cloud cover*

***) Limited by SAR coverage*

****) Limited to large lakes*

Co-funded by the Horizon 2020 programme of the European Union

Snow cover on lake ice is observable in optical data, due to a good contrast between bare lake ice and snow-covered lake ice, and is a separate class in the Copernicus Global Land Service - Lake ice product provided by SYKE based on MODIS/250m. The product covers, however, only northern Europe.

2.3 Validation

The Copernicus Global Land Service - Lake ice product provided by SYKE is based on MODIS/250m from March 2017 to the present. The product covers northern Europe. It has 3 classes (open water, snow-covered ice, partial/snow-free clear ice). The quality has been validated against *In situ* observations of a few lakes in Finland and the difference between *In situ* and satellite-derived ice disappearance date is around +3 days and median of the dataset being +2 days, the standard deviation being 5.2 days.

SAR remote sensing of lake ice has been validated using manual ice charts with an overall accuracy of 90% (Wang et al, 2018).

2.4 Error sources/Accuracy/uncertainty

The various lake/river ice products have a variety of sources that may lead to errors.

Optical lake ice monitoring: The main sources of error would be poor cloud masking, mixed-pixel contamination of land in lake pixels and light conditions in the dark parts of the winter.

SAR lake extent monitoring: Poor contrast between water and thin ice. Challenges in separating surface water and lake ice during various wind conditions. For large lakes it can be a problem that many SAR swaths only cover parts of the lake. Also, the variability in backscatter for various stages of melting snow on lake ice may confuse the classification algorithms.

Scatterometers: Scatterometers have typical 2-5 km spatial resolution and will hence have challenges for small to medium-sized lakes with mixed land/water pixels. Other sources of errors are similar to SAR, e.g. separability between thin ice and water, separability between melting snow and wind-roughened water. In addition, partial ice cover can be hard to resolve at these scales.

Co-funded by the Horizon 2020 programme of the European Union

Passive microwave instruments: PMR instruments like SSM/I, AMSR-E have very coarse resolution 10-20km and can probably only be used on the very largest lakes. Mixed pixels are in general a big source of errors (water/ice, ice/land). Thin ice, and various stages of melting of snow and ice can also harm the error budget in an ice thickness retrieval algorithm.

Altimeters: Laser altimeters (ICESat-1/2) can capture the top of the snow on a lake. By combining this information with simultaneous (or nearly simultaneous) information from the first return (freeboard) over the same lake using a radar altimeter could potentially be used to derive ice thickness and snow depth, but still there are error sources related to the permittivity of snow/ice leading to uncertainties in the estimation of freeboard. The water level is also a source of error since many lakes experience variability in the water level due to seasonal cycles and/or climate changes. Under optimal conditions (Beckers et al., 2017) SAR altimeters (CS2) can separate the return from the ice-lake interface and the snow-ice interface and thus determine the ice thickness.

2.5 Known limitations and gaps

Lake ice monitoring has not reached the same level of attention as sea ice monitoring. Some services have been launched (CCI Lakes and Copernicus Global Land Product) based on optical instruments The main gap in operational lake ice monitoring seems to be that SAR or coarser sensors have not been included, and thus there are many problems with the ice products during cloud cover or polar darkness.

1.1.3. Permafrost

Knowledge of permafrost distribution and dynamics is relevant both for operational activities (transport, construction) and for understanding its interactions with ecosystems and climate change. The main permafrost variables (Bartsch et al., 2014)

- **ground temperature profile** (required parameter by GCOS for the permafrost ECV)
- **active layer thickness** (required parameter by GCOS for the permafrost ECV)
- **permafrost extent/fraction**

cannot be directly observed from space. However, in some cases, they can be estimated based on **proxies** (land cover, ground deformation, water storage, lake extent) or determined from a **combination of modeling and satellite data** products of ground temperature, soil moisture, vegetation cover, and snow cover.

Co-funded by the Horizon 2020 programme of the European Union

Several methods based on these two basic approaches (or combinations of both) have been described in the literature (Trofaier et al., 2017). The proxy approach is generally not operational and has several limitations. Proxy-permafrost relationships established from field measurements are usually only valid locally. Other known issues are errors related to changing surface conditions due to snow, soil moisture, and vegetation, and to the heterogeneity of ground-surface conditions, as described in Trofaier et al. (2017).

Currently, there is no consistent and frequently updated global map of the parameters permafrost temperature and active layer thickness, as required by GCOS (GCOS-200) based on Earth Observation (EO) records, so that permafrost change detection is only possible at localized sites with *In situ* observations. ESA's Permafrost_CCI service (http://cci.esa.int/Permafrost) will for the first time provide such information for different epochs, attempting to meet user requirements as well as possible.

3.0.1. Technologies used and retrieval methods (for all three permafrost variables):

Several methods to generate permafrost ECVs based on combining modeling with EO have been developed and evaluated both within the **ESA Permafrost_CCI** and also the **ESA GlobPermafrost** (https://www.globpermafrost.info/cms) project. These methods are (Bartsch et al., 2019):

A) ***ESA GlobPermafrost:*** *Equilibrium permafrost modeling driven by land surface temperature (LST) time series.* In ESA's GlobPermafrost project, a simple TTOP equilibrium permafrost model was used to transfer freezing and thawing degree days from remotely sensed LST (from the MODIS sensor), remotely sensed land cover for ESA CCI landcover and snow information to produce a global 1 km map of ground temperatures and permafrost fraction (Obu et al., 2019). The employed equilibrium model is simple and computationally efficient, but it has two distinct disadvantages in the context of the Permafrost_cci: first, it can only deliver an average ground temperature for periods on the order of a decade, so it is not suitable for change detection. Second, it cannot deliver active layer thickness. However, the general agreement of the resulting map with existing permafrost maps suggests that the employed input data sets are in general suited for permafrost models. Furthermore, the scheme demonstrated that ensemble methods (i.e. modeling many different realizations for a pixel

Co-funded by the Horizon 2020 programme of the European Union

using slightly perturbed input data) can deliver meaningful values for permafrost fraction within 1 km pixels.

B) Transient permafrost modeling driven by LST time series from EO, without ensemble representation. Recently, Westermann et al., (2017) demonstrated a transient approach based on the CryoGrid 2 model (Westermann et al., 2013) to infer ground temperature and active layer thickness on a regional scale for the Lena River Delta in Northeast Siberia, based on similar input data as employed by the ESA GlobPermafrost project (described above). Here, it is crucial to prescribing the spatial variability of ground thermal properties in terms of a typical ground stratigraphy. In the presented 1 km approach, subgrid variability is not taken into account, so permafrost fractions can only be computed in a binary (yes/no) way.

C) ESA Permafrost_cci: Method (B) can be further improved by combining it with the global input data sets and the *ensemble approach* established in ESA GlobPermafrost.

In Bartsch et al. (2019) it is demonstrated that method (C) is best suited to consistently characterize all three permafrost variables. Variable features are provided below (from Bartsch et al., 2019) based on using the method (C) for the generation of permafrost ECVs.

3.1 Ground temperature

3.1.1 Characteristics of the parameter

Temporal resolution: 8 days
Spatial resolution: 1 km
Vertical extent: 15 m
Vertical resolution: 50 cm (exponential)

3.1.2 Validation

Validation has been accomplished with a collection of *In situ* ground temperatures in boreholes, comprising 359 boreholes in the GTN-P (Global Terrestrial Network for Permafrost, Biskaborn et al., 2015), 392 in the TSP (Thermal State of Permafrost) network (International

Co-funded by the Horizon 2020 programme of the European Union

Permafrost Association, 2010), and 169 MAGT measurements from different publications in China (overview in Obu et al., 2019).

3.1.3 Error sources/Accuracy/uncertainty

A comparison with 920 borehole sites, using the years 2003-2012 for comparison at a depth 2m was selected since it is well below the active layer for most borehole sites, but at the same time close to the "top of permafrost temperature" (TTOP) inferred in ESA GlobPermafrost. The comparison shows no significant overall bias and a Root Mean Square Error (RMSE) of 1.85 to 1.95 K, depending on the employed ground stratigraphies.
Precision: 0.1 K

3.1.4 Known limitations and gaps

Neither time of acquisition nor the depth of the temperature measurement are standardized in the validation borehole data, thus strongly limiting the value of a comparison with algorithm output at a specific depth and time.

3.2 Active Layer Thickness

3.2.1 Characteristics of the parameter

Temporal resolution: 8 days
Spatial resolution: 1 km

3.2.2 Validation

For active layer thickness, *In situ* data by the CALM program downloaded from https://www2.gwu.edu/~calm/data/north.html is employed. At this stage, only exemplary comparisons are provided by the Permafrost_CCI project.

3.2.3 Error sources/Accuracy/uncertainty

In summary, the CCI+ permafrost algorithm appears capable of reproducing measured active layer thickness at CALM sites, if suitable ground stratigraphies can be made available. This is an important point, since ground stratigraphy products are likely improved in the future, so that the performance regarding active layer thickness will gradually improve. Published global studies with global focus have reached an RMSE with respect to *In situ* measurements of 0.53 m (Aalto et al., 2018, using machine learning without EO data) and a correlation coefficient

Co-funded by the Horizon 2020 programme of the European Union

(R2) of 0.7 (based on 303 individual sites), or a correlation coefficient of 0.76 (Park et al., 2016; no comparable RMSE provided).
Precision: 10 cm

3.2.4 Known limitations and gaps

In transient permafrost modeling, as with CryoGrid CCI, the modelled active layer thickness is almost completely controlled by the applied ground stratigraphy. Therefore, a spatially distributed product of ground stratigraphies is required as input to CryoGrid CCI in order to achieve a satisfactory performance for the active layer thickness. At present, such a product does not exist globally, so generic stratigraphies compiled for six landcover classes employed in ESA GlobPermafrost have been employed to compile preliminary benchmarks with respect to the active layer thickness.

3.3 Permafrost extent/fraction

3.3.1 Characteristics of the parameter

Temporal resolution: 8 days
Spatial resolution: 1 km

3.3.2 Validation

For permafrost fraction, only a few *In situ* data sets are available, as already pointed out by previous studies (Chadburn et al., 2017). Here, in particular existing maps can serve as a benchmark, but also spatially distributed measurements of ground surface or near-surface ground temperatures with arrays of temperature loggers (e.g. Gisnås et al., 2014).

3.3.3 Error sources/Accuracy/uncertainty

A significant advantage of the Permafrost_cci algorithm (C) compared to the algorithm (B) is that also ground surface temperatures can be employed for validation, and not only temperatures measured in deeper layers. This makes it possible to directly employ temperature distributions provided by spatially distributed temperature logger arrays, which have been installed at several locations in the past five years. For individual cases it can be shown that the model ensemble is generally in the right temperature range, it is cold-biased by about 1°C (highest density of the ensemble members around -3°C instead of -2°C) and it does not represent the “warmer” locations” between -1.5 and 0°C. Despite the small bias, the comparison clearly shows the strengths of the ensemble approach taken in Permafrost_cci,

Co-funded by the Horizon 2020 programme of the European Union

in that the scheme indeed represents a range of temperatures within a pixel instead of a single temperature as e.g. in method (B).

3.3.4 Known limitations and gaps

Only sparse *In situ* evaluations of permafrost fraction are available, strongly complicating validation for this parameter (see Chadburn et al., 2017).

1.1.4. Soil Moisture

Soil moisture (SM) is one of the most important variables in land surface hydrology. It regulates the energy exchange at the land surface/atmosphere interface through the latent and sensible heat fluxes, and controls the water exchange providing key information about evaporation, transpiration, infiltration and runoff. Furthermore, SM was recognized as the Essential Climate Variable (ECV) in 2010 (GCOS, 2010). With global warming, extreme weather conditions and wildfires in regions as Siberia, Alaska and Scandinavia become more frequent. It is important to mention that a better knowledge of SM can give us an insight into wildfire probability and propagation, being a relevant variable in fire risk indices. Therefore, this variable has a high impact on end-users for wildfires prevention and extinction.

4.1. Technologies used and retrieval methods

Main technologies to remotely measure global SM are based on the use of passive (radiometers) or active (scatterometers or radars) microwave sensors. A microwave radiometer is sensitive to SM with high accuracy and temporal resolution (few days), however, the measured brightness temperature (TB) has a coarse spatial resolution (tens of km), which is primarily limited by the antenna size. By contrast, a microwave Synthetic Aperture Radar (SAR) provides backscatter measurements at high spatial resolution (tens of meters to km), but it has a limited accuracy to SM sensing due to its high sensitivity to surface roughness and vegetation scattering and a low temporal resolution (some days and even weeks).

Different microwave frequency bands were used to measure SM from L-band (1-2 GHz) to K-band (18-36 GHz). Currently, the L-band is considered the optimal band to retrieve SM. Signals at L-band are significantly less affected by rain and atmospheric effects than those at higher microwave frequencies, being the atmosphere nearly transparent (Crane, 1971). The radiation emitted by the Earth's surface at L-band can also pass through sparse up to

Co-funded by the Horizon 2020 programme of the European Union

moderate canopies, which corresponds to 70% of non-frozen land areas on Earth, excluding dense forest. In addition, the soil penetration depth at L-band (around 5 cm) is higher than the higher microwave bands. Notwithstanding, the soil penetration depth also depends on the SM content, being higher in dry than in wet soils (Owe and Van de Griend, 1998). In 2020, two active satellites are carrying an L-band radiometer: Soil Moisture and Ocean Salinity (SMOS) from ESA and Soil Moisture Active Passive (SMAP) from NASA.

Several passive and active microwave sensors have been used to measure SM, since the late '70s. In the next section a table resume of the satellite, type of the sensors and the frequency used are reported.

During the last decade, two strategies were investigated to improve the spatial resolution of SM by the combination with ancillary data at higher resolution: i) synergy of passive microwave + optical and thermal infrared (TIR) data and ii) synergy of passive + active microwave data. The resulting resolution ranges between 100 m and 10 km. A brief explanation of these two synergies is included in the Synergy section 4.

4.2. Characteristics of the parameter

The following table summarizes the main characteristics of the SM variable measured by different technologies.

Type	Sensor	Band	Frequency (GHz)	Spatial resolution	Temporal resolution	Latency
Passive sensors	SMMR	C	6.6	150 km	2 days	daily
	SSM/I & SSMIS	K	19.35	43 x 69 km	0.5 days	daily
	TMI	X	10.65	38 km	2 days	daily
	AMSR-E	C	6.925	75 x 43 km	2 days	daily
	WinSAT	C	6.8	39 x 71 km	8 days	daily
	AMSR-2	C	6.925	35 x 62 km 10 km	2 days	daily

Co-funded by the Horizon 2020 programme of the European Union

	SMOS	L	1.413	35-70 km	3 days	daily 3h
	Aquarius	L	1.413	76 x 94 km 84 x 120 km 96 x 156 km	7 days	daily
	SMAP	L	1.413	39 x 47 km ~9 km	3 days	daily
Active sensors	SCAT	C	5.3	50 km	3 days	daily
	RADARSAT 1 & 2	C	5.3	10-100 m	24 days	
	ASAR	C	5.33	30 m-1 km	7 days	3 days 3h
	PALSAR	L	1.27	10-100 m	46 days	
	ASCAT	C	5.25	25-50 km	2 days	daily 3h
	Sentinel 1 A & B	C	5.4	5-40 m	6 days	
	SMAP	L	1.26	1-3 km	3 days	daily

4.3. Validation

The classical strategy to validate remotely sensed SM is the temporal comparison of selected pixels over the study area against collocated and concurrent *In situ* observations provided by a network or acquired during a field campaign (i.e., point scale measurements that are overlapped by the pixel and are obtained at the same day or the time-overpass of the remote sensor) (Entekhabi et al., 2010). In general, when the network is sparsed the comparison is performed for each measurement (pixel vs. station), while in dense networks it is done for the study area (pixel vs. area), after upscaling *In situ* data. A variety of upscaling methods were used, including the simple average, inverse distance weighting average, kriging, Voronoi and other geostatistical interpolations (Wang et al., 2015). The triple collocation (TC)

Co-funded by the Horizon 2020 programme of the European Union

technique was also used to validate SM, employing 3 independent datasets and assuming that their errors are uncorrelated (Gruber et al., 2016).

4.4. Error sources/Accuracy/Uncertainty

Uncertainties affecting TB and backscatter measurements are translated to the SM variable through their retrieval models.

SMOS data is provided mainly by three processing data centers: Centre d'Etudes Spatiales de la Biosphère (CESBIO), the Barcelona Expert Center (BEC) and INRA (Institut National de la Recherche Agronomique) with the so called SMOS-IC algorithm.

The SMOS data uncertainties:

- Nominal accuracy: 0.04 m^3/m^3 at a spatial resolution of 35-50 km and a revisit time of 1-3 days, (Kerr et al., 2012).
- CESBIO SMOS L3 SM: correlation with validation data is 0.6-0.8 and the STD 0.05-0.1 m^3/m^3 for L3 and 0.04-0.08 m^3/m^3 for L2 (Al Bitar et al., 2017).
- BEC SMOS L3 SM: Correlation with *In situ* data of 0.8-0.9 and errors of 0.04 m^3/m^3 computed with Triple Collocation technique (González-Zamora et al., 2015).
- SMOS-IC from INRA L3 SM has a better agreement with ECMWF SM than for CESBIO L3 SM (Fernández-Moran et al., 2017).
- A dry bias was found in all SMOS products.

The SMAP data uncertainty:

- Nominal accuracy: 0.04 m^3/m^3 at 10 km resolution and 3-day average.
- The passive only SM product at 36 km obtained correlations with validation site of about 0.6-1 and STD of 0.02-0.06 m^3/m^3,
- The active/passive SM at 9 km showed correlations of 0.4-1 and errors of about 0.02-0.08 m^3/m^3 (Colliander et al., 2017).

In RADARSAT 2, a target accuracy of 5% is achieved at a sub-18m final spatial resolution (Agriculture and Agri-Food Canada, 2016). Using ASAR, the STD was 4.0 and 5.8% for the image and wide modes, respectively (Loew et al., 2006). In ASCAT, the expected STD of the soil water index is about 2.5%, which corresponds to about 0.03-0.07 m^3/m^3, depending on soil type (EUMETSAT, 2017).

4.5. Known limitations and gaps

Co-funded by the Horizon 2020 programme of the European Union

An important error source in SMOS and SMAP SM is the presence of Radio Frequency Interference (RFI) (Oliva et al., 2016; Mohammed et al., 2016). RFIs produce an increase of TB and, consequently, a drier SM is obtained. In an interferometric radiometer or a SAR, RFIs do not only affect a particular point but also degrade the entire image due to an effect of blurry. In addition, the characterization of some input parameters, especially those related to vegetation and surface roughness, has a relevant impact on the resulting SM accuracy. This causes higher SM errors in estimates over densely vegetated than over bare soils.

An issue to consider when validating remotely sensed SM is the different representative spatial scale (area-average of the sensor footprint) with respect to *In situ* observations (point-scale). In this regard, the upscaling techniques applied to *In situ* data try to avoid this mismatch, as previously commented. Another thing to take into account is the limitation of the penetration depth using space-borne sensors. In the best case (i.e., using L-band) the penetration depth is 0-5 cm. However, knowledge of the SM at the root zone, defined down to 1 m below the soil surface, had a growing interest, particularly for agriculture. To overcome this limitation, different land-surface or hydrological models were developed to estimate root zone SM (Wagner, 1999; Muñoz-Sabater et al., 2007; Draper et al., 2011). The spatial resolution of the SM measured by radiometry (tens of kms) is another limitation. Several synergies were developed to obtain disaggregated SM at 100 m-10 km, as previously commented. Nevertheless, the combination of passive microwave + optical and TIR data results in SM maps affected by cloud cover.

Co-funded by the Horizon 2020 programme of the European Union

1.2 Sea Ice Parameters:

1.2.1. Sea ice concentration

1.1 Technologies used and retrieval methods

The most prevalent measurement of SIC is via multi-frequency passive microwave radiometers (e.g. AMSR2, SSMIS, MWRI), typically recording the Earth leaving radiation at microwave window channels (e.g. C-band: ~6.9 GHz, Ku: ~19 GHz, Ka: ~37 GHz, W: ~90GHz). These frequency channels do not require solar light, and are not blocked by clouds. They thus offer the all-weather capability and work during the polar night. For a given space-borne passive microwave radiometer, channels with higher microwave frequency (and shorter wavelength) have a better spatial resolution (e.g. AMSR2 89 GHz channels have a resolution of ~5km, while the 36.5 GHz channels are at ~12km). However, one obtains better SIC accuracy by using low-frequency channels as these are less susceptible to atmospheric effects. Thus, remote sensing of sea-ice concentration from microwave radiometry is always a trade-off between accuracy and spatial resolution (Comiso et al., 1997). The PMR satellite can produce daily SIC products (sub-daily over polar regions), thanks to the large swath. For all existing passive microwave sensors, the characteristics of the orbit, and the width of the swath leave a small unobserved region around the poles (polar observation hole). Many sea-ice concentration algorithms have been developed in the past decades. A recent inventory was compiled in the context of the ESA Climate Change Initiative (CCI) Sea Ice projects (Ivanova et al., 2015). It is also recognized that the algorithms that combine brightness temperatures into SIC estimates are not the only elements making a good SIC product. Atmospheric correction (requiring Radiative Transfer Models), Weather Filtering, correction for land spill-over effects, dynamic tuning of the algorithm tie-points are all elements of a modern SIC processing chain. An assessment of SIC retrievals from L-band radiometry has also been done (Gabarro et al., 2017)

SIC maps can be obtained from SAR imaging missions (e.g Sentinel-1, RADARSAT-2,...), independently of the polar night, and mainly independent from the weather. Weather effects

Co-funded by the Horizon 2020 programme of the European Union

such as wind and precipitation over the ocean yield ambiguities in the single, co-polarization channel of older SAR sensors. The SAR-based products have substantially higher resolution than those from microwave radiometry. A limitation is that the spatial coverage is limited to relatively narrow (4-500 km) SAR scenes, and pan-Arctic maps require several days of aggregation, or more satellites[1], while some regions (e.g. the region around Svalbard and the Barents Sea) are mostly covered daily using the two Sentinel-1 satellites. Discrimination of water from sea ice is better when using the cross-polarization channel of multi-polarization SAR systems (e.g. the dual-polarization of RADARSAT-2 or Sentinel-1).

Optical spectrometry (e.g. Sentinel-3 OLCI, Sentinel-2, MODIS, VIIRS,...) is another tool for monitoring sea-ice concentration, but here the main limitation is cloud cover and the need for sunlight. In the light season, and cloud-free conditions, high-resolution images can be classified in ocean/ice pixels and aggregated to the desired spatial resolution. Thin, high-altitude clouds can sometimes prevent automatic algorithms to work on such images, although they can still be useful for visual/manual interpretation. Interestingly, this type of imagery is the only technology allowing mapping of melt ponds on sea ice in the Arctic summer (e.g. Rösel et al., 2012, Istomina et al., 2015a,b) as it can discriminate the lighter blue of the pond water from the darker blue of the ocean water in leads and cracks. Thermal infrared imagery that can be recorded also during the Polar night is also used for ice monitoring during the Winter period where the surface temperature of ice is significantly lower than that of water.

Interestingly, several investigators have recently adopted multi-sensor approaches to combine the strong points of the individual techniques and reduce ambiguities. For example, sea-ice concentration products based on a merging of passive microwave and SAR are (independently) studied at the Finnish, Danish, and Norwegian meteorological institutes (e.g. Karvonen, 2014). Also, Ludwig et al. (2019) attempted to merge passive microwave with MODIS cloud-free imagery. In all these cases, the rationale for adopting a multi-sensor approach is to build upon the nearly daily complete coverage of the passive microwave products and improve the spatial resolution where SAR or visible imagery is available. These multi-sensor techniques should receive more attention.

1 Even using two Sentinel-1. The situation is expected to improve when S1C is operational, and when/if the Radarsat Constellation Mission (RCM) is seamlessly available to Copernicus users.

Co-funded by the Horizon 2020 programme of the European Union

SAR images are the main input for National Ice Services to produce their ice charts, which are targeted at end-users for navigation. The process is at present mostly manual, with trained ice analysts drawing and labelling polygons. These polygons encompass classes of similar sea-ice conditions, and the labels assign several characteristics to the polygon following nomenclatures standardized by WMO [WMO No. 259]. The principal characteristics attached to the polygons are the total sea-ice concentration, reported in tens (e.g. 3/10s, 8/10s,...), and sea ice type based on the observed stage of development.

Sea ice can be detected with a variety of other satellite techniques, including altimetry, scatterometry, and even GNSS signals. But none of these techniques allow the mapping and quantification of sea-ice concentration.

1.2. Characteristics of the parameter

	Spatial resolution	**Frequency**	**Latency**
Based on Passive Microwave	5-25 km (highly depends on sensor and frequency channels used)	Sub-daily in both polar regions from a single mission (polar observation hole)	Often collected as daily maps, but latency can be less than 3h after sensing for swath data. Target <1h achievable.
SAR	80-100m (sometimes aggregated to <1km)	Varies regionally. No full Arctic coverage from single missions.	At present no automatic SIC products based on SAR only.
Optical imagery	10s meter to 1km	Varies regionally and with the season. The main limitations are solar light and cloud cover.	Can be less than 3h after sensing for swath data.

1.3 Validation

Co-funded by the Horizon 2020 programme of the European Union

The validation of sea-ice concentration is far from a simple task, as no *In situ* observation technique exists that is autonomous and covers scales that are directly comparable to those of the satellite products. An additional difficulty is that sea ice is always on the move, so that accurate space/time collocation between the ground estimate and the satellite product is difficult.

One can split the validation of sea-ice concentration in three broad aspects: validation at very high (100% SIC) and very low (0% SIC) conditions, validation at intermediate conditions (typically in the Marginal Ice Zone), and validation in specific conditions (thin sea ice, melt ponds,...).

Validation at the 0% SIC range is possibly one of the most straightforward aspects. Indeed, it is not difficult to detect large areas of open-ocean conditions in navigational ice charts, and assess the accuracy of the other satellite products there. It is a more useful exercise if the open-ocean conditions are sampled not too far from the actual sea ice, in order to be representative of the conditions (ocean temperature, wind waves, atmospheric conditions) prevailing at the ice edge. However, it is noteworthy that many products use techniques to actually report 0% SIC in open-ocean conditions. These techniques range from Weather Filters, to climatology masks, to using SST products for masking warm waters. As a result, validating over open ocean targets does not always result in useful information for improving the products or assigning accuracy numbers.

Validation at 100% SIC has long been a difficult task, as it is *apriori* challenging to detect where and when large extents of sea ice are fully closed. Andersen et al. (2007) used visual inspection of SAR images to detect the location and time of 100% SIC conditions in the high-Arctic and used these conditions to intercompare SIC algorithms. Kwok (2002) used a related but different method by selecting convergence/divergence zones as observed by a SAR-based sea-ice motion product (in that case the Radarsat Geophysical Processor System). This approach was adopted and expanded upon during the ESA CCI project (Ivanova et al. 2015; Pedersen et al. 2019) using motion vectors derived from the CMEMS/DTU-Space product based on Sentinel-1 data. Areas identified as converging over at least two days, and -in addition- in winter freezing conditions are considered as 100% SIC, and used to validate SIC products from microwave radiometry in Lavergne et al. 2019 and Kern et al., 2019. Limitations to this validation method are the coverage of the underlying SAR ice motion product, and the applicability to the winter season only (local convergence while surface melting does not

Co-funded by the Horizon 2020 programme of the European Union

guarantee 100% SIC). It is noteworthy that the validation statistics close to 100% SIC are largely influenced by the cut-off applied to most SIC products to the =< 100% SIC range. Indeed, geophysical retrieval noise (e.g. of algorithms using microwave radiometry) results in values being both lower and above 100% SIC. This symmetric noise distribution is very seldom made available to the users, and thus validation teams, because SIC products are thresholded to the physical range [0%;100%]. Recently, Kern et al. (2019) investigated how the non-thresholded, symmetric distribution of noise can be inferred from thresholded products.

There is a general lack of accurate validation data for the intermediate range of SIC. Very often (higher resolution) satellite products are used as validation sources for (coarser resolution) satellite products, e.g. SIC derived from Landsat or MODIS is used as validation data for passive microwave estimates. This is however problematic as all satellite products have their challenges and short-comings that should first be characterized via validation. Also, relying for example only on visible imagery to validate microwave products might induce a bias towards spring/summer (sunlight) or cloud-free condition.

Some ship-based manual visual observations exist, and are collected from the bridge of ice-going vessels. Two protocols exist, one for the Antarctic (ASPeCt) and one for the Arctic (Ice Watch - Arctic Shipborne Sea Ice Standardization Tool (ASSIST)). The ASSIST protocol builds upon that of ASPeCt and adds focus on observing and reporting melt ponds. Observers are tasked to survey the sea-ice conditions around the ship at regular intervals (typically hourly). The line of sight and the motion of the ship along its track typically result in an elongated field of view. Depending on the protocol, and the level of training of the observer, both the total sea ice concentration, the concentration of ice types, the fraction of melt ponds, the sea-ice thickness, etc… are estimated and reported. The interested reader is directed to a newly compiled dataset of both ASPeCt and Ice Watch ASSIST reports in Kern et al. (2019) and references cited there. Using such ship-based observation to validate (especially coarser resolution) satellite products is challenging both due to the accuracy of the observation, preferential sampling, and the mismatch of scales between the observation and satellite product. Alternative sampling methods could include drone-based camera systems that would survey a larger area around the ship (because flying higher) and whose imagery would be processed automatically.

Co-funded by the Horizon 2020 programme of the European Union

Despite its key importance to both climate and near-real-time applications in the polar regions, the validation of satellite-based sea-ice products is a very challenging task that should receive more attention.

1.4 Error sources/Accuracy/uncertainty

The error sources and accuracy of sea-ice concentration retrievals vary widely with the methodology used. In the following, we review these characteristics for the main techniques outlined at the beginning of this section.

Using microwave radiometry, the standard deviation of the error against ground truth is typically between 1% to 7% for the most widely used algorithms (Ivanova et al. 2016). These values are valid for winter freezing conditions, and the accuracy is often slightly better in the Southern Hemisphere because of the relative preponderance of first-year ice. Lavergne et al. (2019) report uncertainties below 2% over open ocean for their EUMETSAT OSI SAF - ESA CCI Climate Data Records (thanks to an explicit correction of the brightness temperatures with radiative transfer models). At 100% SIC conditions, the same CDRs show uncertainty of ~2% when using C-band frequency channels (6.9 GHz) and ~3.5% when using the "classic" Ku and Ka bands (18.7 GHz and 36.5 GHz). More recently Kern et al. (2019) validated and intercompared 10 SIC products derived from passive microwave radiometer data (including those from OSI SAF - CCI). They found uncertainty values ranging from 4% to 7% at 100% SIC conditions. Algorithms using higher frequency channels (e.g. ASI using near 89 GHz channels) exhibit the largest uncertainties. Interestingly, Kern et al. (2019) also reveal that some products are biased high by a few percents. Such a high-bias (after truncation to the =< 100% SIC range) results in removing and hiding a larger uncertainty in some products. Despite these seemingly small uncertainty values, there still exist large differences between products on a daily basis (e.g. Comiso et al., 2017). These differences result from the algorithms themselves, and the way they combine frequency channels, that result in different sensitivity to error sources such as sea-ice type, the effective temperature at the emission layer, the snow-depth on sea-ice, the thickness and brine content of sea ice (for thin ice), the atmospheric wetness, etc… Differences in daily SIC products translate into differences in monthly trends of sea-ice extent and area (Comiso et al., 2017; Kern et al., 2019). Part of these differences in integrated quantities arise from differences in grid spacing, projection, land mask, etc. and others from the SIC algorithms. Part of these discrepancies are attributed to the Weather Filters used by

Co-funded by the Horizon 2020 programme of the European Union

all products, but that has so far not received as much attention as the SIC algorithms themselves (Ivanova et al., 2016).

Due to the lack of ground truth data, it is very difficult to provide accuracy measures for automatic SAR-based SIC products or those derived from optical imagery. Most of the time, the validation of such products is based on evaluating how the algorithm performs on reference scenes/images that were for example classified by visual inspection.

The accuracy associated with manually drawn ice charts is an area of open research. The lack of validation data led to relying more on comparing ice charts (the polygons themselves and/or the SIC value assigned to polygons) from different analysts (e.g. Karvonen et al., 2015; Cheng et al., 2019). Given the importance of sea-ice charts, more efforts should be put into validating them and provide uncertainty estimates.

1.5 Known limitations and gaps

The retrieval of SIC can be achieved using several satellite technologies (microwave radiometry, radars, visible imagery, etc.). However, with the current observing systems, none of these techniques fully answer the user requirements (both for navigation and ingestion in forecasting models).

The applicability of microwave radiometry to generate global daily-covering products is limited by the rather coarse resolution achieved by these products. At the time of writing, the best resolution that can be achieved (just below 5km) is only available from one satellite mission (JAXA's AMSR2), and by relying on imaging channels with high microwave frequencies, which result in rather large uncertainties. This trade-off between spatial resolution and accuracy will be partly solved with the Copernicus Imaging Microwave Radiometer (CIMR) mission.

At the other end of the resolution spectrum, Synthetic Aperture Radar missions continue to improve, both in coverage (better power allowing longer duty cycle) and technology (dual-frequency imagery). Nevertheless, at the time of writing, there are no fully automated algorithms that solely rely on SAR images and return SIC maps and that are not limited by ambiguities. Automatic classification of SAR images is even more difficult because of persistent artifacts in the imagery itself (thermal noise, Park et al. 2018), a problem that

Co-funded by the Horizon 2020 programme of the European Union

central processing facilities have not solved despite the missions being in the in orbit for several years.

Although several teams are actively researching efficient algorithms to provide multi-sensor SIC products (e.g. that merge microwave radiometry and SAR), we are at the infancy of such approaches for global or regional mapping of SIC, and more efforts are needed generally to make better use of multi-sensor capabilities to automatically map SIC on an operational basis.

As the case for many (if not all) sea ice variables, the existing capabilities work best in freezing conditions. When temperatures rise near the melting point and further when surface snow starts melting and melt ponds form at the top of sea ice, the accuracy of most algorithms is greatly reduced. Not only the accuracy is reduced, but there is doubt about what SIC products actually measure -the total sea-ice concentration, or the ice surface fraction? Simply put, are melt ponds on top of sea ice accounted as water or sea ice). Answering these questions and reducing our uncertainties in summer SIC (and Sea Ice Area) is required to address key questions of the future of sea-ice in a changing climate, such as when the Arctic Ocean would be ice-free during the summer (Niederdrenk and Notz, 2018).

1.2.2. Sea ice thickness

Sea ice thickness is a physical parameter that indicates the distance from the bottom of the ice pack, which is in contact with the seawater, and the sea ice upper surface. Sea ice thickness is becoming an increasingly important parameter for climate change monitoring due to the thinning of the sea ice and the increase of the thin sea ice extent (i.e. less than one meter). This is due to the fact that thin sea ice dominates the ocean-atmosphere heat exchange in polar regions. Sea ice thickness is also very important for operational ice monitoring (Ice charting) although today no large scale higher resolution observational capability exists. Ice chart estimates of ice thickness is therefore mostly based on indirect information from ice type observations and meteorological data (freezing degree days).

2.1. Technologies used and retrieval methods

a) Altimetry (Cryosat)

Co-funded by the Horizon 2020 programme of the European Union

The altimeters measure the ice freeboard, and then the hydrostatic equilibrium equation is used to derive the ice thickness as a function of the ice freeboard. Freeboard is obtained as the difference between the local sea surface and the ice pack surface height.
The discrimination of the echo is based on the surface reflectivity variation. This variation depends on whether the echo is dominated by specular or diffuse reflections (leads or ice floes). Two main parameters are used to characterise the surface, the "pulse peakiness" and the "stack standard deviation" based on the multilplemodes the sensor collects the data in (Laxon et al., 2013). The freeboard measurements are averaged in order to reduce the speckle size.

A major technological change from the "conventional" low-resolution measurement (LRM) sensors was the introduction of instruments with a delay-Doppler or SAR Measurement (SARM) processing capability. This latter mode of operation enables a finer along-track resolution and lower noise levels due to the accumulation of looks (multi-looking) from multiple viewing geometries. The resultant radar echoes ("waveforms") have a narrower shape. This technology was first demonstrated by CryoSat-2 and has become more operational with Sentinel-3A and the recently-launched Sentinel-3B (Quartly et al., 2019).

b) Lidar Altimetry (ICESat2)

Sea ice thickness is derived using freeboard measurements. Freeboard is obtained as the difference between the local sea surface and the ice pack surface height. This is a relative measurement and it is not affected by the error sources that affect absolute height measurements, such as geoid error, long-wavelength laser pointing error, tidal error and dynamic ocean topography (Zwally et al., 2008).

A first calculation of the relative height is calculated using a 20 km running mean which is considered the reference level. The reference sea level is afterward estimated from this relative altimetry profile using leads. The reference sea level is calculated from the average of the lowest 2% of the relative heights in a 50 km section profile. Freeboard height is calculated as the difference between the relative height and the reference sea level. Finally, sea ice thickness is obtained by converting the freeboard values to ice thickness by making some assumptions on ice and snow densities and snow depth through the hydrostatic equilibrium equation (Zwally et al., 2008).

Co-funded by the Horizon 2020 programme of the European Union

However, at the moment of writing this document, no operational data is available (no real-time data is processed), since this is a research mission, so data might not be useful for the final user.

c) L-band radiometry (SMOS, SMAP)

L-band radiometry can retrieve sea ice thickness from brightness temperatures (Kaleschke et al., 2012). This methodology relies on the fact that the brightness temperature of sea ice is related to ice thickness. The retrieval of ice thickness using this method is limited to the thickness of less than ~0.5-0.8 meters (Kaleschke et al., 2012; Huntemann et al., 2014). The spatial resolution is also limited to ~35 km. Temporal resolution is daily for the sea ice thickness product in the Arctic region, however the sensor leaves a gap at the north pole (~83ºN).

There are two types of retrieval methods. The theoretical retrieval, developed by Kaleschke et al. (2012), Tian-Kunze et al. (2014) and the empirical retrieval implemented by Huntemann et al. (2014) and Gupta et al. (2019). The theoretical retrieval algorithm begins with an initial guess from the algorithm developed by Kaleschke et al. (2012). This initial guess is used in conjunction with a parameterization of the ice temperature and salinity to estimate a modelled temperature brightness (TB). The difference between the observed TB and the modelled one is used to produce a new estimation of the ice thickness until convergence is reached (Tian-Kunze et al., 2014). The empirical retrieval is trained with *In situ* measurements and data from models to obtain daily sea ice thickness estimates. Huntemann et al. (2014) calibrated the empirical retrieval with model-based sources such as: HIRLAM, the Cumulative Freezing Degree Days (CFDD) algorithm, NCEP and TOPAZ.

d) Optical sensors (MODIS)

This type of retrieval is based on the use of thermal imagery. Moderate Resolution Imaging Spectroradiometer (MODIS) is used for retrieving thin sea ice thickness (Mäkynen et al., 2013). The ice surface temperature is acquired under cloud-free night-time conditions. MODIS RGB images are generated from bands 20 (red), 31 (green) and 32 (blue). The band differences 32-31, 31-22 and 31 are used in the manual cloud-masking procedure. Further cloud masking of MODIS night-time data is essential in order to obtain reliable sea ice thickness. The thickness of ice is estimated from the observed ice temperature by using a model that relates both quantities and other physical parameters (mainly radiative fluxes and latent heat fluxes) estimated from the HIRLAM model (Mäkynen et al., 2013). The estimated thickness is adjusted for the presence of snow over the ice.This type of retrieval is heavily affected by the presence of clouds on the scenes. Therefore, a continuous track of the ice over a location is difficult. Also, a snapshot of a large geographical region is most of the time

Co-funded by the Horizon 2020 programme of the European Union

impossible and weekly products are provided as a replacement for a result with a geographical continuous coverage. The maximum retrievable ice thickness is 35-59 cm considering typical weather conditions (Mäkynen et al., 2013).

e) SAR

Single attempts have been made to use SAR data for the retrieval of the thickness of thinner ice on local and regional scales. Correlations between the ice thickness and radar intensities at different polarizations or the co-polarization ratio HH/VV were noticed by Wakabayashi et al. (2004) and Nakamura et al. (2009). The sensitivities to ice thickness are similar at C- and L-band. L-band radar signatures are less affected by the small-scale roughness of the ice surface and are more strongly influenced by deeper portions of the ice. The difference between the radar intensities at VV- and HH-polarization is affected by the dielectric constant of the near-surface ice layer, which changes depending on the near-surface ice salinity. In one study from the Antarctic, even ice thicknesses up to about 1.2 m could be retrieved with a sufficient accuracy based on the co-polarization ratio at C-band (Nakamura et al., 2009). As a special case the thickness of pancake ice covers can under certain conditions be retrieved from wave dispersion retrieved from SAR images (e.g. Wadhams et al. 2018).

2.2. Characteristics of the parameter

Some products provide the sea ice thickness data onto a user-friendly 5 km square Polar Stereographic grid by averaging all thickness measurements within a 25 km radius of the centre of each grid cell, with all points receiving equal weighting.

	Temporal resolution	**Spatial Resolution**	**Accuracy and precision**	**Latency of the geophysical parameter**
Radar Altimeter CCI sea ice thickness products	Monthly EASE2 (Hendricks 2018)	25 Km (Hendricks 2018)	STD: 0.624m At 0.4º(lon) *4º(lat) (Laxon et al., 2013)	15 days
Laser Altimeter Not operational	Sea ice freeboard NSICD: 90 days (Kwok et al., 2019)	variable	0.02+/-0.72m (Kern and Spreen, 2015)	15 days

Co-funded by the Horizon 2020 programme of the European Union

Passive Microwave	Daily up to 85º latitude (Kerr et al., 2010) 25km	35km at nadir and 50km at 60º incidence angle	Retrieval uncertainty varies with thickness (Tian-Kunze et al., 2014). Best retrieval in the 10-30 cm range (Kaleschke et al., 2016)	12 h
Optical Sensor	Bad coverage during freeze-up periods. Weekly (Mäkynen et al., 2013)	1km at nadir. At a scan angle of 40º: ~2 km (Mäkynen et al., 2013)	Accuracy is best for the 15-30 cm thickness range: ~38% (Mäkynen et al., 2013)	12h

2.3 Validation procedure

There are several methods to evaluate the satellite-derived sea-ice freeboard and thickness. Satellite altimetry, *In situ* observations, airborne campaigns, submarines, and drifting and moored buoys have all been used through the years. However, such observations are still sparsely distributed in space and time (Quartly et al., 2019).

There are two reasonably extensive datasets for a direct satellite sea-ice freeboard evaluation. One is from NASA's Operation IceBridge (OIB), with the sea-ice freeboard given by the total freeboard (snow + sea ice) measured by a laser altimeter minus the snow depth measured by the snow radar. The other is from the airborne campaigns carried out as part of ESA's CryoSat Validation Experiment (CryoVEx), where an airborne version of the CryoSat-2 SIRAL altimeter provides coincident Ku-band radar freeboard data.

Other observations commonly used to evaluate satellite-derived SIT are from upward-looking sonars (ULS) either from submarine cruises or moored buoys (for example, during the Beaufort Gyre Experiment -BGEP). The Ice Mass Balance (IMB) buoys have also been used for validation (Laxon et al., 2013, Quartly et al., 2019). Nonetheless, this data needs to be resampled (temporally and spatially) in order to be comparable with the sea ice thickness analysed. Given the scarcity of the reference data for validation some studies use the gaussian error propagation for estimating the uncertainty in sea-ice thickness (Kern and Spreen, 2015).

Co-funded by the Horizon 2020 programme of the European Union

The correlation between OIB and CryoSat-2 SIT estimates is often found to be lower than with submarine, moored buoys and AEM observations. The cause of this is still unclear and subject to further investigation (Quartly et al., 2019).

SMOS derived sea-ice thickness presents its peculiarities (i.e. retrieval of thin ice) which prevents the usage of most of the validation data available. Electromagnetic induction systems (EM) on a helicopter have been used to validate the SMOS data, but those measurements are usually acquired during the end of March and April, when the ice is mostly thick. ULS has also been used for the validation of L-band estimates of sea ice thickness. An extensive field ESA campaign took place in the Barents Sea during March 2014 with the RV Lance ship for L-ban radiometry validation. Moreover, sea ice thickness was measured using an EM system from the bow of the boat and another EM-system towed below the helicopter (Kaleschke et al., 2016).

The lack of reference validation data is reported in many studies (Huntemann et al., 2014). A similar issue is found when validating MODIS derived ice thickness, compounded by the presence of clouds difficulting a timely acquisition of ground truth (Mäkynen et al., 2013).

2.4 Error sources/Accuracy/uncertainty

The document 'User Requirements for a Copernicus Polar Mission Phase 2 Report - High-level mission requirements' set the accuracy requirement (goal) of the sea-ice thickness (thin and thick) as following: for thickness larger than 0.5 m: 0.5m while for thin ice (thickness < 0.5 m) the accuracy goal is 0.1.

Despite these challenges and the many assumptions in the processing chain, recent studies find relatively good correlations (0.5–0.9) with mean differences − 0.21 to 0.12 m between the CryoSat-2-derived SIT products and the evaluation data in the central Arctic winter (October–March) (Tilling et al., 2018).

Individual freeboard measurements have a standard deviation averaging 9 cm Arctic-wide and can be calculated through the propagation of errors as the root-sum-square combination of the two sources of error. The standard deviation arises through (a) uncertainties in the floe height measurement due to speckle in the radar echoes, and (b) uncertainties in sea surface height. When gridding monthly data (typically 4 or more passes) results in a 2 cm freeboard

Co-funded by the Horizon 2020 programme of the European Union

uncertainty. This scales to 20 cm thickness, or 11% of a typical growth season thickness of 1.8 m for gridded monthly thicknesses (Tilling et al., 2018).

The monthly CryoSat-2 data have been compared to EM bird data, both data sets were gridded onto the **same 0.4º latitude by 4º latitude grid.** The root-mean-square difference includes both the errors in CS-2 ice thickness and the EM data and differences due to the temporal and spatial sampling of the two data sets. The mean difference between *In situ* and CS-2 data is 0.066m and the STD 0.624 m (Laxon et al. 2013, Graham et al., 2019).

ICESat2 sea ice thickness estimates within 25-km segments have an uncertainty of ~0.7 m and this figure is dependent on the relative thickness of the total freeboard and snow depth (Kern and Spreen, 2015). The mentioned uncertainty is higher over thicker multi-year ice. The main contributors to thickness uncertainty are freeboard and snow depth (accounting for more than 80% in all cases).

For the L-band radiometers, the retrieval uncertainty varies with the thickness (Tian-Kunze et al., 2014). But, the best retrieval varies in the range of 10-30 cm (Kaleschke et al., 2016).

The optical sensors can measure sea ice thickness with enough accuracy for the thickness range of 15-30 cm and the accuracy is ~38% (Mäkynen et al., 2013)

2.5 Known limitations and gaps

a) Radar altimetry: Operational applications today require high-resolution products over the Arctic with a minimal time delay, which is not achieved nowadays.

One important limitation of altimeter measurements is the lack of precise snow depth measurements, which are fundamental to derive the ice thickness from freeboard measurements. However, this parameter (snow depth) has a large uncertainty.

The operational Sentinel-3 mission (2 satellites) covers areas up to about 81 degrees of latitude which leaves a significant pole hole in the Arctic which the CRISTAL HPCM mission aims at filling in.

b) Laser altimeters: A clear limitation of Laser altimeters is that no operational mission exists and none is planned, so data is for science purpose only.

Co-funded by the Horizon 2020 programme of the European Union

c) L-band radiometers: permit estimating sea ice thickness with high temporal resolution (daily product), but the spatial resolution if poor (25 Km) and can only estimate thin ice thickness below half a metre. Also, for L-band radiometry of thin ice thickness there are currently only science missions but the CIMR HPCM could take over.

e) SAR: In the retrieval of ice thickness with SAR instruments, "disturbing" factors such as frost flowers or rafting processes that influence the radar signature have to be taken into account and may overlay the effect of ice growth. The methods tested for the retrieval of ice thickness from SAR image analysis are in a very preliminary stage of development and not suited for operational applications.

Therefore, a sea ice thickness product with high temporal resolution covering the whole ice thickness range is missing. A higher resolution sea ice thickness product (100s of meters to a few kilometer resolution) is also missing.

1.2.3. Sea ice drift and deformation

3.1 Technologies used and retrieval methods:

(a) Measurements of position changes of buoys deployed on sea ice ("Lagrange approach": continuous tracking of a single object), are described, e.g., in Itkin et al. (2017).

(b) The use of satellite image pairs for drift retrieval has been investigated in several studies (Lavergne et al., 2010; Hollands et al., 2011; Girard-Ardhuin et al., 2012; Karvonen, 2012; Berg et al., 2014; Muckenhuber et al., 2016; Korosov et al., 2017; Demchev et al., 2017). Two approaches are popular: correlation techniques and tracking of distinct features. In the former approach, small windows are distributed as regular grids in the master image. For each window its shift of position in the second image is systematically determined by applying spatial correlation ("pattern matching"). The search can be organized in resolution pyramids and cascades. Feature tracking works by identifying distinct ice cover structures such as ridges, leads, cracks in the master image and trying to find them in the slave image. Image data originating from optical, SAR, scatterometer or passive microwave sensors are used. Drift vectors obtained from pattern matching are mostly shown on the vertices of a fixed eulerian approach. If single distinct features are tracked, the grid resulting from connecting single adjacent drift vectors is irregular. Pattern matching and feature tracking can be combined. The rotational motion requires additional retrieval procedures. The advantage of using satellite images is the high spatial density of drift vectors, which, however, depends on the spatial resolution of the image. The Radarsat Geophysical Processor System (RGPS) employs a temporal sequence of satellite images covering the same region to follow ice structures identified in the first image over a longer period (at maximum as long as those structures can

Co-funded by the Horizon 2020 programme of the European Union

be identified in the successive images). This approach creates an irregular grid composed of single cells with their vertices on the tracked features. In particular, when using passive microwave radiometers and scatterometers, a Laplacian filter is applied on daily images for enhancing the structures in the ice that are to be tracked. Ice displacements are calculated based on the Continuous Maximum Cross Correlation (CMCC) method (Lavergne et al., 2010). The CMCC relies on a continuous step for optimizing the components of the motion vector, located at the maximum of the cross-correlation function between a reference and a candidate block. In practice, virtual image pixels are interpolated from neighboring pixels in each candidate block. The main effect of using the CMCC is the removal of the quantization noise.

(c) When sea-ice drift estimates are available from different sensors, they can be merged for generating a multi-sensor drift product. The multi-sensor product aims at gaining confidence in the retrieved ice motion by a synergetic use of several instruments and reducing the number of missing data. The merging methodology is based on two steps. First, all grid locations where at least one single-sensor product has a valid motion vector are assigned a merged motion vector, as a weighted average of the available estimates. Weights are related to the standard deviations of single-sensor datasets. The second merging step consists of a spatial interpolation of missing vectors from the motion vectors in the closest vicinity. Current merging methodologies are rather crude and limited in scope (see known limitations and gaps below).

(d) While methods of the category (b) need pairs of satellite images as input and output the two-dimensional displacement field, the instantaneous (sub-second) sea ice motion along the line-of-sight (LoS) between the radar and a surface element can be retrieved from the Doppler frequency derived from SLC (single-look complex) data based on a single SAR scene (Kræmer et al., 2015, Kræmer et al., 2018)

(e) Instantaneous LoS components of drifting ice can also be derived from along-track interferometry, but in this case, again two images are required from a satellite tandem (two identical SAR instruments) for which the along-track (temporal) baseline is on the order of milliseconds and the across-track baseline is short enough to minimize the influence of ice topography on the interferometric phase (Dammann et al. 2019). The spatial resolution is higher than for the Doppler approach (c). From methods (c), (d), single sub-second LoS velocity component fields are obtained, which are usually separated by hours to days. In which way they are representative for an assessment of the actual two-dimensional ice velocity field and its changes on temporal scales of hours is still unclear. Whether split-beam InSAR processing (to obtain the azimuthal component of velocity, see Bechor et al. (2006)) can be applied for sea ice has to be checked.

Co-funded by the Horizon 2020 programme of the European Union

3.2. Parameter Characteristics

➔ Ocean and Sea Ice Satellite Application Facility OSISAF (EUMETSAT)
http://osisaf.met.no/p/ice/#lrdrift
The sea ice drift product in the OSISAF product's portfolio is based on low resolution (10-15 km) passive and active microwave instruments such as SSMIS, AMSR-E, and ASCAT. The spatial resolution of the drift field is 62.5 km, projected on a Polar Stereographic Grid similar to the one used for the other OSISAF sea ice products. It is a 2 days (48 hours) ice drift dataset processed daily.

➔ EU Copernicus Marine Service / Technical University of Denmark
http://resources.marine.copernicus.eu/documents/PUM/CMEMS-OSI-PUM-011-006.pdf
Drift data are provided near-real-time on a 10 km grid (originally from Envisat ASAR, then Radarsat-2, now Sentinel-1 at 300 m spatial resolution), based on the application of the maximum cross-correlation method on single geographically overlapping image pairs from consecutive dates. Also available is a 24-hour mean-value composite.

➔ Centre ERS d'Archivage et de Traitement (CERSAT) at IFREMER
http://cersat.ifremer.fr/data/products/catalogue
CERSAT makes available a continuous winter time (beginning of September to end of May) series of drift vectors over the Arctic, provided on a polar stereographic grid every 62.5 km, over 3-days or 6-days overlapping periods. A monthly drift is also available. The drift field is inferred from the combination of the respective sea-ice drift vectors retrieved separately using respectively QuikSCAT (from winter 1999-2000)/ASCAT (available from 2007-2008) and SSM/I (in horizontal and vertical polarization, from winter 1991-92) observations. The estimation of sea-ice drift for each one relies on a correlation technique applied to the field of the second spatial derivative of 12.5km resolution composite maps separated by a few days (backscatter maps for QuikSCAT/ASCAT and brightness temperature for SSM/I. This time series is ongoing. Archived Arctic drift fields from AMSR-E (Oct 2002 – April 2011) are also available.

➔ Research-based on SAR imagery
The spatial resolution of the drift field varies between 300 m and 10 km, dependent on the SAR image mode and the size of grid cells. The temporal resolution depends on the time interval between revisits of a single satellite or different satellites over a given area (note that also SAR images acquired at different frequencies can be combined for drift analysis). The time between revisits decreases with increasing latitude. For the Sentinel-1a and 1b constellation, e.g., this is less than a day in the Arctic.

Co-funded by the Horizon 2020 programme of the European Union

ICE DRIFT				
Resolution	OSISAF-EUMETSAT	Copernicus-DTU	CERSAT	SAR
Temporal	daily	daily		
Spatial	62.5 km	10 km	62.5 km	300 m - 10 km
Accuracy and Precision	2-5km/2days	300 m/day		
Latency	48h	NRT	1.5-3 day	< 1 day

- Latency: time from observation (satellite pass) to product readiness. If a product is generated every 3 days (average of measurements from day D0, D0-1, D0-2), then on average latency is 1.5 days.

3.3 Validation procedure

(a) Displacements derived from the tracking of sea ice buoys, beacons or drifters are used as a reference for judging results of retrievals from satellite data. This, of course, requires to consider the uncertainties in buoy positions. In the framework of the International Arctic Buoy Programme (http://iabp.apl.washington.edu/), e.g., positions of about 200 buoys drifting in the Arctic and of 120 buoys in operation in Antarctic waters can be obtained (status end April 2019). The areal density of buoys, however, is in general not sufficient for rigorous validation of satellite drift products. This type of validation procedure was applied, e.g., in studies by Korosov et al. (2017), Lindsay et al., (2003), Muckenhuber et al. (2017).

(b) The error of ice displacements automatically retrieved from a pair of two satellite images can be achieved by manually determining displacement vectors using the same image pair. Since this requires the existence of clearly identifiable structures that show up in both images, this method corresponds to the automated feature tracking but can also be used in comparisons to results from pattern matching. This approach was employed, e.g., in Hollands et al. (2011).

(c) Lindsay and Stern, 2003, estimated the tracking error (which is caused by imprecisions in pattern matching or feature tracking applied on pairs of satellite images) by combining two efforts of automated retrieval of displacements applied on the same satellite image. They

Co-funded by the Horizon 2020 programme of the European Union

compared results from two RGPS-processors, implemented at different places, with different initializations (i.e. identifications of trackable features in the first image).

3.4 Error sources/Accuracy/uncertainty

(a) Buoys: Error sources are spatial and temporal uncertainties of position readings. The accuracy of the absolute buoy position includes both a possible bias and a random component and may be larger for drifting than for stationary buoys. Magnitudes are given, e.g., as 25 m for stationary buoys (Itkin et al 2017), but these numbers vary depending on buoy type. E.g. uncertainties of buoy locations from the International Arctic Buoy Program (IABP) "C" data set are 0.5 km (https://nsidc.org/data/eg/nsidc0116-icemotion-buoy), uncertainties of Argos buoys (Argo 2000) are between 350 m and 150 m, and of buoys with GPS receivers below 50 m (http://imkbemu.physik.uni-karlsruhe.de/~eisatlas/ HTML/ eisatlas_buoydoc.html). In arrays of buoys (spatial extension of a few kilometers), position uncertainties relative to one another are on the order of 1-2 m (J. Hutchings, pers. com. 2019). The accuracy of the GPS time is better than a millisecond. Hence, the temporal error can be ignored.

(b) Satellite images: Displacements retrieved from a pair of satellite images are prone to geo-location errors of the two images, and to the tracking error (Lindsay and Stern, 2003). (Note that the tracking error is zero for buoys). Already for Envisat ASAR, e.g., the position (geolocation) error was better than 0.04 times the pixel size of the corresponding image product, and for the modern satellite missions it has even further improved (Small et al., 2005, Schubert et al., 2008, Schubert et al., 2017). Position errors can hence be neglected for satellite images. In comparison to manually derived displacements, Hollands and Dierking (Holland et al., 2011) found uncertainties (standard deviations) of displacements retrieved from Envisat wide-swath images pairs acquired under winter conditions between 0.8 and 1.6 times the size of an image pixel (here 150 m). These numbers were given for time intervals of 2 to 6 days between the acquisitions of the two images used for drift retrieval and represent the tracking error. When applying Envisat Image mode (pixel size 25 m), the corresponding numbers are between 0.9 to 1.2 for winter image pairs (time intervals 2 to 6 days), and 1.5 for one summer pair (1.2 days). However, in single cases tracking errors were up to 4.8 pixels for winter and even 11.6 pixels for the summer pair (both: Image mode). Lindsay and Stern, (Lindsay et al., 2003) reported a tracking error of 100 m for Radarsat ScanSAR images (pixel size 100 m) for a time interval of 3 days (based on results from two different RGPS processors). In comparison with buoys, they found differences in displacements of 320 m (median). These differences include the geolocation error of the buoys and the satellite images (in which the latter may be negligible) and the tracking error. Muckenhuber and Sandven (2017) did their retrievals based on Sentinel-1 Extra Wideswath (EWS) image pairs (40 m pixel size) and in comparison to buoys found displacement differences of 540 m (HH-polarized images) and 350

Co-funded by the Horizon 2020 programme of the European Union

m (HV-polarization) (median). Korosov and Rampal (2017), also used Sentinel-1 EWS image pairs and found uncertainties between 1.2 and 1.4 km for the x- and y- components of displacements relative to ice drifters. Kraemer et al. (2018) compared Doppler line-of-sight sea ice drift velocities derived from Sentinel-1A EWS data with GPS tracks from a drifting ice station as well as with vector fields obtained using a conventional cross-correlation approach. They found that in EW mode it is not possible to obtain Doppler estimates with the required precision for typical Arctic ice drift speeds, which vary mainly between 0.03-0.2 m/s.

(c) Validation of OSISAF low-resolution sea ice drift dataset was conducted in the Arctic against *In situ* drifters. Trajectories were made available as hourly (and sub-hourly) GPS records for an optimum temporal collocation. The validation exercise extended over 3 Arctic winters starting October 2006 and ending April 2009. Statistical results and graphs document an excellent agreement between the OSISAF low-resolution sea ice drift datasets and the reference data.

Provision of uncertainty information

Usually, magnitudes of errors derived empirically in single studies are taken as information on the error to be expected in general. However, since the retrieval of displacement vectors from satellite images depends on the temporal stability of visible features or patterns in the ice that can be traced over image sequences, it can be expected that the tracking error varies spatially and temporally. In the case of radar intensity images and images of brightness temperatures (passive microwave sensors), the contrast between features/patterns may considerably change during the transition phase between freezing and melting conditions. To be able to automatically provide a preliminary judgment of the retrieval quality that only depends on the characteristics of the image pair/sequence, Hollands et al. (2015) used a "confidence factor" (CFA) that combines thresholds for the cross-correlation coefficient and selected image texture parameters. The magnitude of the CFA (quantifying how often thresholds are exceeded) is used to identify regions of less reliable displacement information, in which pattern matching is difficult due to the lack of distinct ice structures or due to very low-intensity contrasts. A second possibility for judging the reliability is back-matching, i.e. the displacement field is calculated twice. In the first calculation image 1 is employed as a reference, in the second image 2. Drift vectors are regarded as less reliable if results obtained from image constellations 1-2 and 2-1 reveal larger differences. For this approach it is necessary to carry out calculations for pair 1-2 on a grid different from pair 2-1, otherwise the difference is always zero. It must be noted that the reliability metrics introduced by Hollands et al. (2015) is not directly correlated with the uncertainty. There is at present no accepted algorithm for uncertainty propagation adapted for sea-ice drift products.

- **Retrieval of deformation**

Co-funded by the Horizon 2020 programme of the European Union

The calculation of deformation parameters (divergence/convergence, vorticity, shear, total deformation) is carried out based on the retrieval of displacements, e.g. (Weiss et al., 2013). Such data can be obtained from arrays of buoys (Itkin et al 2017) or pairs of satellite images (Lindsay and Stern, 2003), with the restrictions regarding spatial density or temporal resolution as discussed above. Hence, uncertainties in the displacement vectors affect the estimates of deformation parameters. The latter is calculated from line integrals that are calculated on the boundary of grid cells (in the case of satellite images) or of buoy arrays. In addition, one has to consider the so-called boundary-definition error when the grid cell boundaries and deformation zones are unfavourable oriented to each other. Solutions to reduce this effect are proposed in (the latter showing up as discontinuities in the displacement field) .

3.5 Known limitations and gaps

(a) It is necessary to agree on standard procedures so that products showing drift or displacement fields are comparable. It has to be stated which type of uncertainty is shown: only the tracking error, or a combination of tracking and geolocation errors. In the latter case, the geolocation errors can be provided for the satellite images and buoys/beacons/drifters. The tracking error depends on the intensity contrast of the satellite images, e.g. on the visibility of structures on/in the ice that can serve as objects for feature tracking and pattern matching. Hence, a set of image parameters is needed that quantifies the expected uncertainty of the displacement field.

(b) For satellite images, the temporal resolution is often not sufficient to reflect hourly and sub-hourly changes of the magnitude of drift velocity and the direction of the drift vector.

(c) While the advantage of buoys is a high temporal resolution of the drift pattern, the disadvantage is that the spatial coverage is sparse. Another drawback is that buoys are usually deployed on thicker, more stable ice.

(d) The strategy of merging drift vectors from different satellite sensors includes the loss of a certain level of dynamic and aliasing during the merging process. As a consequence, rapidly changing drift patterns, such as when a low-pressure system travels over sea ice, might be better described by single-sensor datasets than in the multi-sensor product. It should however be recognized that only limited effort was put so far in designing advanced merging algorithms for sea-ice drift estimates. There is for example to date no operational product that merges radiometry-based with SAR-based sea-ice drift products, which would however

Co-funded by the Horizon 2020 programme of the European Union

fill a key gap (complete daily coverage, with higher resolution and accuracy where SAR is available).

1.2.4. Ice type and ice edge

4.1. Technologies used and retrieval methods

Ice chart production in operational services is mostly carried out using SAR images at wide-swath modes. With scatterometer and passive microwave radiometer, which offer a much wider coverage at the cost of lower spatial resolution, the entire Arctic and Antarctic can be covered within a short time and long-term temporal variations of regional ice type distributions can be monitored. While most pixels in SAR images cover only one ice type, the much larger pixels in scatterometer images may often contain mixtures of different types. However, as stand-alone these coarse-resolution instruments are not well suited for operational ice mapping. Even today ice charts are still generated based on manual interpretation of experienced ice analysts. Nevertheless, there is an interest in applying automated procedures as is demonstrated in several published studies. The separability of ice types in SAR images and scatterometer data depends on radar frequency, polarization, incidence angle, and the spatial resolution. The interpretation and analysis of the images rely on the intensity and textural variations which are caused by differences in surface roughness, volume inhomogeneities (both on length scales of the radar wavelength), and macro-scale ice structures (e.g. ice ridges, leads, floe margins), all of which can vary considerably with the time of year and prevailing environmental conditions.

Methods that can potentially be used for automated ice classification are, e.g., knowledge-based thresholds, Bayesian classifiers, decision trees, Neural Networks, Support Vector Machine (SVM), and the Random Forest Classifier. These methods require training data (supervised classification schemes). Clustering techniques such as k-Means and Isodata identify pixels with similar statistical properties and do not depend on training data.

Two advanced automated processing schemes for the production of ice charts from SAR images are ARKTOS (Advanced Reasoning using Knowledge for Typing of Sea ice), and MAGIC (Map-Guided Ice Classification). ARKTOS mimics the decision strategies of ice analysts when they categorize ice conditions (Soh et al., 2004). Besides SAR, ARKTOS uses sea ice concentration from passive microwave radiometers and ice climatology data. Different ice regions are first separated through the application of a watershed algorithm. For each region, a set of parameters is then calculated based on image intensity, texture, and geometric properties. Those parameters are based on the criteria used in the visual ice classification and are applied for the final ice type labelling. MAGIC makes use of the polygons manually drawn

Co-funded by the Horizon 2020 programme of the European Union

by the ice analysts (Ochilov and Clausi, 2012). For each polygon, an unsupervised pixel-wise classification is performed. Whereas a manually drawn ice chart only provides information on average ice conditions for each polygon, a pixel-level characterization can be achieved when using MAGIC. Details of the processing chain, including the iterative region growing with semantics (IRGS) and automatic labelling can be found in different publications, e.g. Yu and Clausi, (2007), Maillard et al. (2005), and Ochilov and Clausi (2012). Neither approach has performed to a sufficiently satisfactory level to be used in an operational context (see 4.4).

If quad-polarization SAR images are available, various polarimetric parameters can be used for separating ice types. The major shortcoming for operational ice charting is the small swath typical for the fully polarimetric imaging mode. This problem does not occur for the compact-polarimetric data acquisitions (but the information content is less). The practical gain of quad-pol measurements is the availability of two additional parameters besides the like- and cross-polarization intensities, namely correlation and phase difference between VV- and HH-polarization. From the basic polarimetric data, different polarimetric parameters can be calculated that are valuable for enhancing the visual interpretation and the automated ice classification. Examples are given in, e.g., Scheuchl et al. (2004), Moen et al. (2013) Geldsetzer et al. (2015). Investigations on the optimal combination of polarimetric features in terms of ice separability, computational effort, and robustness are still ongoing. Algorithms developed for single intensity data can also be applied to individual polarimetric parameters. More efficient is the use of feature vectors as input, i.e. combination of intensities and/or polarimetric parameters that differ between ice types (e.g. Moen et al., 2013).

The combination of different frequencies is another issue, which has been investigated using airborne SAR imagery and to a lesser extent satellite data (see section 3.2.4.2). Combinations of radar bands L+C or L+X are most useful. The same algorithms can be used for polarimetric data.

The spatial arrangement of grey tones (texture) in a satellite image can be quantified by, e.g. elements from the grey-level co-occurrence matrix (GLCM), Gabor filters and Markov Random Fields. Clausi (2001) found that the GLCM achieved the highest accuracy in classifying sea ice types in SAR images compared to the two other methods. From the GLCM, many different texture parameters can be calculated for either separating several ice types (Maillard et al., 2005; Zakhvatkina et al., 2017) or for distinguishing ice and water for the determination of ice concentration (Leigh et al., 2014). In contrast to intensity and many polarimetric parameters are texture parameters usually only weakly sensitive to the incidence angle. However, windows are required for their calculation, which blurs sharp boundaries between ice types. The systematic comparisons of texture features and their relative importance for ice type separation, however, are rare.

Co-funded by the Horizon 2020 programme of the European Union

On a global scale, several techniques for separating ice types exist using scatterometer or passive microwave radiometers, or a combination of both. As for sea ice concentration, multi-frequency passive microwave radiometers have been common to use in the classification of sea ice, among others the NASA Team algorithm and the Bootstrap algorithm, see e.g. Cavalieri et al. (1984), Comiso (1990, 2012) and references therein.

In Belmonte Rivas et al. (2018), ice and water are distinguished in scatterometer data by applying an ocean-wind and a sea ice geophysical model function (GMF). The sea ice GMF is empirically derived from stable wintertime intensity levels because backscattering intensities of single ice types change during the melting season. Parameters that can be derived from scatterometer data are radar intensity, its azimuthal anisotropy and incidence angle gradient, and polarization difference or ratio (e.g. for QuikSCAT).

Remund et al. (2000) propose a method that combines brightness temperatures measured at different frequencies and polarizations with the radar intensity at a fixed incidence angle and the gradient of the intensity with respect to the incidence angle. If parameters are measured in very different units, data fusion techniques can be used to give equal weighting to all of the data. The number of parameters available for classification may be reduced by employing a principal component analysis. The final ice separation is achieved by using, e.g., a Bayesian classifier or by applying one of the other methods mentioned above.

The EUMETSAT OSI SAF sea ice edge and type are both multi-sensor products which have been available operationally since 2005 (Aaboe et al. 2016). For their retrieval is used a Bayesian approach to combine active backscattering and spectral gradient ratio of brightness temperature at the vertically polarized 19 GHz and 37 GHz channels, plus the polarisation ratio at both low and high frequency to detect the ice edge. A similar approach is used in Lindell and Long (2016). The operational OSI SAF algorithm is trained by a dynamical set of training data updated on a daily basis in order to take into account temporal variabilities of the surface signatures and to be more flexible when adding or replacing sensors. The Copernicus Climate Change Service (C3S) has modified the operational classification algorithm from OSI SAF in order to receive long climate consistent data records based on passive microwave radiometers back to 1979 and up to the present time, with daily updates (Aaboe et al. 2018).

4.2 Parameter Characteristics

The table below shows spatial and temporal resolution requirements for monitoring of different ice parameters that are considered in ice charting based on SAR images. The table is based on Flett et al. 2004 and Scheuchl et al. 2004. It is distinguished between strategic and tactical information. The former refers to the regional survey as provided in the daily ice charts (useful for ship route planning), the latter refers to the judgement of the ice conditions

Co-funded by the Horizon 2020 programme of the European Union

in the vicinity of a vessel to support immediate operations. Ice concentration can be regarded as a special case of ice classification, i.e. separation of ice and water areas. The latency for the availability of satellite data is between less than one hour and two hours in Canada (D. Flett, CIS, personal communication, 2018). However, this is not the case for European ice charts where latency can often be up to 6h (Charts are issued at 15 UTC based on satellite acquisitions in the early morning (6-8 UTC).

	strategic		tactical	
Parameter	**spatial resol.**	**temp. resol.**	**spatial resol.**	**temp. resol.**
Ice edge location	5 km	daily	< 1 km	6 hours
ice concentration	< 100 m (±10% accuracy)	daily	< 25m (±5% accuracy)	6 hours
ice types	50 – 100 m	daily	< 20 m	6 hours
leads/polynyas	50 – 100 m	daily	< 20 m	6 hours
ridges	< 50 m	daily	< 10 m	6 hours
ice decay stage	20 km	weekly	5 km	daily
iceberg location	< 50 m	daily	< 5 m	hourly

(Polynyas are openings in the ice with sizes between 10 and >10000 km2 that occur if strong katabatic winds from land push the ice away from the coast or if a spot of warm surface water hampers ice growth.)

Co-funded by the Horizon 2020 programme of the European Union

4.3 Validation

Automatically generated ice classification maps are mostly validated by comparing them with manually generated ice charts. The latter are in general based on SAR images but consider visual observations from ships and airplanes. At the Canadian Ice Service (CIS), e.g., the production of ice charts which is mainly based on RADARSAT-2 dual-pol ScanSAR Wide imagery is supplemented by Sentinel-1 IW and EW images, data from AMSR-2 (Advanced Microwave Scanning Radiometer 2), VIIRS (Visible Infrared Imaging Radiometer Suite), MODIS (Moderate Resolution Imaging Spectroradiometer), and GOES (Geostationary Operational Environmental Satellite). Also considered are meteorological conditions. The most recent ice charts are cross-checked with the results of preceding analyses. Optical images are also a useful complementary source but only for snow- (and cloud-) free ice areas. If the occasion arises, satellite images are compared with *In situ* observations of ice conditions and/or with observations from airplanes and helicopters. Such comparisons are very much limited in time and space. Results from scatterometer and passive microwave radiometers are usually validated in comparison to classification results obtained from high-resolution data such as SAR images. However, passive microwave ice concentrations are typically more accurate than these validation data, so this validation method is unsatisfactory.

4.4 Error sources/Accuracy/uncertainty

The process of ice classification is complicated by the fact that the discernibility of ice types and structures in SAR images depends on the relative influence of cm-scale ice properties such as small surface undulations or air bubbles in the ice on the backscattered radar signal. These properties do not differ consistently between different ice types and may cause false interpretations.

With respect to the accuracy of classification results of automated procedures, studies carried out in close collaboration with the ice centers can be regarded as the most reliable. For MAGIC, classification accuracies between 71% and 89% (assessed by the ice analyst) were reported in Maillard et al. (2005) for conditions with three to six different ice classes. For the automatic separation of ice and water, Leigh et al. (2014) found an average accuracy of 96% when using MAGIC, and Ochilov et al. (2012) reported pixel-level accuracies between 78% and 100% and region accuracies between 81% and 100%. With ARKTOS, Soh et al. obtained

Co-funded by the Horizon 2020 programme of the European Union

mean absolute differences between 4.3% and 23.5% for ice type separation and 8.4% for the determination of ice concentration. Nevertheless, automated procedures are yet not fully implemented in the production of ice charts.

Another issue arises with regard to the number of different characteristics that have to be taken into account to describe ice conditions. Moen et al. (2013) describe the results of manual analyses of a satellite SAR image (acquired in polarimetric mode) carried out by two ice analysts. The SAR image was complemented by additional information from a field campaign. The two independently generated ice charts revealed considerable differences which were attributed to the fact that the selected classification scheme was too detailed.

4.5 Known limitations and gaps

During the summer season, ice mapping based solely on C-band SAR is extremely challenging both for manual ice chart interpretation and automated methods, since the separability of ice types decreases under melting conditions. Signature contrasts between FY and MY ice are larger at L-band during the beginning and end of the melting season but can be very low at both C- and L-band when melting is strong (Casey et al., 2016). Classification in temporal sequences of SAR images is particularly difficult when meteorological conditions alternate between melting and freezing within short time intervals. Algorithms specifically designed and optimized for ice type separation under melting conditions have yet not been published.

The characterization of an ice “type” or “class” (whereby “class” can be viewed as a collection of “types”) requires the knowledge of different ice characteristics. Different ice parameters that are regarded as essential or useful for a most detailed mapping of ice types – but are not available on a basis suitable for operational monitoring - are thickness (see above), the degree of deformation (e.g. expressed as a percentage of ridged ice), and stage of melting.

1.2.5. Snow on sea ice

Snow (depth) on sea-ice is at present the “holy grail” of sea-ice remote sensing. It is an especially important parameter, both for the retrieval of sea-ice thickness from (radar) altimetry and for ingestion in forecast models (due to the insulation effect of snow). Snow-depth on sea ice also has a key role in navigation, as it slows down ice breaking.

5.1. Technologies used and retrieval methods

Several techniques are being investigated for the retrieval of snow-depth on sea ice. Three classes of methods are: (a) from microwave radiometry (especially using low-frequency

Co-funded by the Horizon 2020 programme of the European Union

channels such as those of SMOS, AMSRs, and CIMR), (b) from dual-frequency altimetry (e.g. Ka/Ku altimetry combining AltiKa and CryoSAT2, or CRISTAL), and (c) from modelling approaches (snow precipitation from atmospheric reanalysis are advected and accumulated using ice drift information). At this stage, none of these techniques outperforms the others, and all show rather limited accuracy wrt validation data.

5.2 Characteristics of the parameter

To our knowledge, there are no operational snow-depth on sea ice products. What can be said at present is that the variable is snow-depth (measured in meters) although as for land surfaces, this depth can be associated with different snow densities (also a rather unknown parameter) to yield snow water equivalent.

5.3 Validation

The validation data available for sea-ice thickness (see section 2 Sea ice) often contain valuable information on snow-depth. These include Ice Mass Balance buoys (IMBs) with transistor chains, snow-depth buoys with sonic ranging sensors, helicopter- and sled-borne ElectroMagnetic (EM devices), airborne radars (Operation Ice Bridge -OIB- and CryoVex), and snow-pit manual observations. Also, snow-depth can be reported as part of the ASPeCt and ASSIS/IceWatch ship-based protocols.

Collecting, processing, and quality control of these validation data is time consuming and is currently mostly limited to research efforts (maybe to the exception of OIB, but here again, several versions exist). Validation of snow-depth can be very time-dependent because of wind-driven snow redistribution processes (snow is easily advected by winds).

5.4 Error sources/Accuracy/uncertainty

There are many caveats for the retrieval of snow-depth on sea ice from satellite data, one of which is the lack of dedicated satellite missions (CRISTAL could be one in the future) and the relative lack of validation data.
Snow processes (depth, insulation, layering, grain size, etc.) have often been considered as error sources in the retrieval of other variables such as sea-ice concentration and sea-ice type, and it is only rather recently that the community have focused on measuring it from space.

Co-funded by the Horizon 2020 programme of the European Union

5.5 Known limitations and gaps

Being an area of active research, with prototype algorithms and products only, the whole "snow-depth on sea ice" variable is a gap, that will hopefully be bridged as more teams investigate its retrieval, and new validation campaigns are carried upon. In that respect, the integrated on-ice laboratory deployed with MOSAiC will hopefully bring the community forward. At present, the first gap is the lack of an international, community-driven, intercomparison exercise, that would help to take the pulse of the snow-depth on sea ice EO community, and get a status of what the current state-of-the-art is with each technique.

1.2.6. Albedo

The sea ice Albedo is mainly measured with the same technologies and similar retrievals than snow albedo. Therefore, we encourage the reader to read albedo on land chapter 5 from land parameters.

6.1. Technologies used and retrieval methods

Sea ice albedo can be computed with the optical AVHRR sensor. Albedo is also computed with MERIS data, onboard EnviSAT. The broadband sea ice albedo is calculated as an average of the six spectral albedo values at 400–900 nm in steps of 100 nm.

6.2 Characteristics of the parameter

Specific available products of sea ice albedo have the following characteristics:
University of Bremen - MERIS:

- Temporal resolution: daily average sea ice albedo products
- Spatial resolution: gridded on a 12.5 km polar stereographic grid, for May-September 2002-2011
- https://seaice.uni-bremen.de/melt-ponds/.

6.3 Validation

See validation of albedo on land section 7 and Melt Pond validation Section 7.

6.4 Error sources/Accuracy/uncertainty

The Error of specific products of sea ice albedo is:

- uncertainty from AVHRR: 0.028

Co-funded by the Horizon 2020 programme of the European Union

- uncertainty from MERIS product: 0.068-0.089 (Istomia et al., 2015)

6.5 Known limitations and gaps

An important limitation of the sea ice albedo products is that the optical sensors measurements are limited when solar light is illuminating the target (so from March to September in the Arctic circle) and when not dense clouds are present on the sky, which is not very frequent in the Arctic Ocean summer period. More limitations can be found in albedo on snow, chapter 5 from land parameters.

1.2.7. Melt ponds

The presence of melt ponds on the Arctic sea ice strongly affects the energy balance of the Arctic Ocean in summer. It affects albedo as well as transmittance through the sea ice, which has consequences for the heat balance and mass balance of sea ice. In the context of changing Arctic climate, knowledge of melt pond fraction, its spatial distribution and the length of the melt season are required to reflect and predict the role of the sea ice cover in the radiative balance of the region (Istomina et al., 2015).

The temporal dynamics of the melt can be subdivided into four stages (Eicken et al., 2002):

1. Melt onset: widespread ponding and lateral meltwater flow.
2. Drainage: both the surface albedo and melt pond fraction decrease due to the removal of snow cover and due to pond drainage.
3. Melt evolution: the meltwater penetrates deeper into the ice, the pond coverage continues to evolve and melt pond fraction to grow.
4. Freeze-up: surface albedo is still affected by the now over-frozen ponds.

The melt pond fraction during each of these stages, their duration and the date of their onset/end are specific to sea ice type and can provide a lot of information on the state of the sea ice and its change.

Satellite retrieval of the melt pond fraction and albedo allows to observe the melt evolution and how it is reflected in the surface optical properties throughout the whole Arctic summer.

Melt pond fraction information is also required to validate and improve as much as can be done summertime sea-ice concentration products based on passive microwave data (see the section above). Due to the penetration depth of microwave radiation in water, passive

Co-funded by the Horizon 2020 programme of the European Union

microwave sensors cannot distinguish between the ocean and meltwater. At the same time, the microwave emissivity of bare, melting sea-ice in between ponds is largely unknown. These two factors strongly limit our capacity to improve estimates of summer sea-ice concentration from passive microwave radiometry. There is an urgent need for more, longer, and better melt-pond fraction information products to improve other satellite products (e.g. summer sea-ice concentration) and to develop and tune parameterization in forecast models (e.g. Kern et al. 2016, Kern et al. 2020).

7.1. Technologies used and retrieval methods

a) Optical sensors

Different algorithms are used to derive melt pond fraction products from optical frequency sensors.

a1) ESA-MERIS: Zege et al. 2015 describes an algorithm to derive the melt pond fraction from ESA - MERIS (MEdium Resolution Imaging Spectrometer) sensor data onboard EnviSat. This is based on an analytical solution for the reflection from the sea ice surface, called Melt Pond Detector (MPD). This algorithm produces maps of the melt ponds area fraction and the spectral albedo of sea-ice, from the MERIS Level 1B data, including the radiance coefficients at ten wavelengths and the solar and observation angles (zenith and azimuth). This algorithm, in contrast to other algorithms, does not use a priori values of the spectral albedo of the sea-ice constituents. The algorithm includes the correction of the sought-for ice and ponds characteristics with the iterative procedure based on the Newton–Raphson method. Also, it accounts for the bi-directional reflection from the ice/snow surface, which is particularly important for Arctic regions where the sun is low. The algorithm includes an original procedure for the atmospheric correction, as well. The numerical verification shows that the MPD algorithm provides more accurate results for the light ponds than for the dark ones. The spectral albedo is retrieved with high accuracy for any type of ice and ponds. Istomina et al., 2015a presents the validation against *In situ* data, aerial and ship observations. University of Bremen offers daily average melt pond fraction products, gridded on a 12.5 km polar stereographic grid, for May-September 2002-2011 retrieved from MERIS based on the MPD algorithm, in https://seaice.uni-bremen.de/melt-ponds/. Validation, case studies and weekly trends are presented by Istomina et al. (2015 a,b).

Co-funded by the Horizon 2020 programme of the European Union

a2) NASA - MODIS:

MODIS surface reflectances are used to retrieve three surface fractions: open water, snow and ice, and melt ponds. *In situ* spectral measurements of spectral albedo and Bidirectional Reflectance Distribution Function (BRDF) were performed by Tschudi et al. (2008) on the sea ice with significant ponding in order to characterize the surface reflectances of each ice and water surfaces types. Once the spectral reflectances were defined, a set of linear equations are used to characterize the contribution of each surface component to the total spectral reflectance from the MODIS sensor. However, the surface reflectances are described by linear equations that are not well-conditioned.

To constrain the interval of the solution between zero and one, a cost function is introduced. by Rösel et al., 2012 and use an artificial neural network to accelerate the processing. This algorithm uses a level 3 MODIS surface reflectance product. The root-mean-square errors range from 3.8 % - 11.4 % depending on the dataset. University of Hamburg offers an 8-day composite product at a 12.5 Km grid point based on MODIS for the period 2000-2011. This product is available at https://icdc.cen.uni-hamburg.de/1/daten/cryosphere/ arctic-meltponds.html

University of Bremen is working on running an algorithm to derive the melt pond fraction from OLCI on Sentinel-3 (personnel communication from Gunnar Spreen).

b) SAR

Multiscale feature extraction algorithms can be used for automatically extracting melt ponds and derived statistics. A comparison of high-resolution spaceborne SAR systems (e.g. TerraSAR-X) against airborne SARs has shown that the former is unable to resolve small melt ponds and, when detected, the estimated area is smaller than the actual one. Furthermore, the estimated melt pond fraction from spaceborne systems is significantly smaller.

More recently, machine learning processes have been used to classify high-resolution SAR dual-polarization imagery (e.g. TerraSAR-X). The two algorithms used in the classification were the decision tree and the Random Forest (RF) (Han et al., 2016). RF showed its superior performance when used with the HH backscatter coefficient as the most contributing variable to the RF model. Other contributing variables to the RF model are the co-polarization phase

Co-funded by the Horizon 2020 programme of the European Union

differences and the alpha angles (Han et al., 2016). The melt pond fraction estimated in such a way has an RMSD of 4.9%.

Sentinel-1 40 meters resolution SAR images were used for estimating the melt pond fraction in the Canadian Arctic region (Scharien et al., 2017). The analysis demonstrated that melt pond fraction using backscatter from HH polarization can be characterized with a RMSE of 0.09. This value is close to the error bounds of estimations using optical and radar data (Rösel et al., 2012; Istomina et al., 2015).

7.2 Characteristics of the parameter

Melt pond products consist of providing the % of the pixel which is covered by melt pond. Due to cloud cover, current datasets often consist of daily or 8-day composites of the melt pond fraction and broadband albedo for May-September.

The mean melt pond fraction per grid cell for the entire Arctic Ocean derived from MODIS satellite data of the last 12 years shows a strong increase in June. By the end of June the maximum with a mean melt pond fraction above 15 % is reached, followed by a second maximum at the end of July.

	Temporal resolution	Spatial Resolution	Latency	Error
Optical Sensor MERIS	daily	12.5 Km		6.5 - 22 %
Optical Sensor MODIS	8-day	12.5 Km		3.8-11%
SAR	-	40m		4.9%-9%

7.3 Validation

The melt fraction products are usually validated against *In situ* field campaign sites spread over the entire Arctic, airborne measurements and ship cruise, hourly bridge observations and visual estimation (Istomina et al., 2015a, b).

Co-funded by the Horizon 2020 programme of the European Union

In general, the airborne measurements are performed with high-resolution digital imagery acquired by Aerosonde unmanned aerial vehicle (UAV) flights within the area of interest.

Some of the specific campaigns to validate melt pond products are: C-ICE 2002 (Yackel (2005)), HOTRAX 2005 Ship cruise (Perovich et al. (2009)), POL-ICE 2006, MELTEX 2008 (Birnbaum et al. (2009)), Barrow 2009 (Polashenski 2011), NOGRAM-2 2011 (Lehmann (2012)), TransArc 2011 (Nicolaus et al. (2012)), among others. Recently, Buckley et al. (2020) extracted melt-pond coverage and indication of depth (colour) in High Resolution Operation Ice Bridge Imagery.

These validation data sets contain a wide range of pond fractions and were obtained over landfast ice, FYI and MYI of various ice concentrations. Therefore, the performance of the satellite retrieval can be thoroughly tested for a variety of conditions and conclusions on the more or less suitable conditions for the application of the MPD retrieval can be drawn.

7.4 Error sources/Accuracy/uncertainty

The uncertainty of the different products are the following which depends on the time and region:

- Optical Sensor- Meris RMS: between 0.065 and 0.22 depending on the validation campaign
- Optical Sensor MODIS RMS: between 0.038 and 0.11, depending on the validation campaign
- SAR: between 4.9% and 9%

It is important to remember that this parameter can not be measured with optical sensors during night periods and if clouds are present.

7.5 Known limitations and gaps

An important limitation of the melt pond products, as well as the albedo one is optical sensors measurements are limited when solar light is illuminating the target (so from March to September in the Arctic circle). Moreover, a clear sky is required to observe the ice, so not dense clouds in the sky, and this is not very frequent in the Arctic Ocean summer period.

Co-funded by the Horizon 2020 programme of the European Union

To discriminate between open water in leads and meltwater in ponds requires enough imagery channels in the blue/green region of the spectrum. In the past, these types of channels have not been selected onboard heritage missions such as AVHRR, and this limits our ability to process a long time series of melt-pond fractions.

Several prototypes, research-based melt-pond fraction products exist (see some example above). There is a lack of concerted initiative to improve the maturity of these algorithms and products, and to prepare the needed long-term and error characterized data records that are required to improve other EO products (e.g. sea-ice concentration) or tune parameterizations in forecast models. By the same token, there are no operational, near-real-time satellite-based products of the melt-pond fraction.

1.2.8. Ocean and Ice Surface Temperature

The Ice Surface Temperature (IST) is one of the most important components in the Arctic surface-atmosphere energy balance. The surface temperature strongly affects the atmospheric boundary layer structure, the turbulent heat exchange, and sea ice temperature controls sea ice melting and growth rates. Advanced thermodynamic sea ice models treat the temperature of the snow and ice surfaces as vital parameters for freezing and melting of sea ice.

8. 1. Technologies used and retrieval methods

a) Thermal infrared sea surface and ice surface temperature

Measurements of the Sea Surface Temperature (SST) and Ice Surface Temperature (IST) using satellite infrared radiometry is a challenge because of difficulties in distinguishing clouds from snow-covered surfaces, as both appear white in the visible and cold at thermal infrared wavelengths. However, recent initiatives show that the IST at L2 is retrievable within a standard deviation of 3.0ºC compared to drifting buoys, and 1.5ºC compared with radiometers, using state of the art multispectral cloud masking (Eastwood et al., 2018). This accuracy is sufficient for using this data in model assimilation and validation schemes, if there is a quantitative description of the uncertainty provided.

Co-funded by the Horizon 2020 programme of the European Union

OSISAF is serving the product OSI-203a/b L3 SST/IST which is a 12 hourly product based on L2 Metop-B AVHRR and NPP VIIRS SST/IST, with a resolution of 5 km polar stereographic grid. The input to compute the SST/IST is thermal infrared data from the Advanced Very High Resolution Radiometer (AVHRR) on-board the EUMETSAT Metop satellites and the Visible Infrared Imaging Radiometer Suite (VIIRS) on the Joint Polar Satellite System (JPSS) National Polar-orbiting Partnership (NPP) satellite.

The input data used to compute the surface temperature and cloud probability algorithms are: Tb and reflectances, sun/satellite/earth geometrical information and the cloud mask data. Daily SST climatologies from the OSTIA system (Donlon, 2012) provided by the UK MetOffice are also used by the daytime SST algorithm as a first SST guess. All other data are ancillary fields of information that can be used as filters (Eastwood et al. 2017).

SLSTR (Sea and Land Surface Temperature Radiometer) instrument onboard Sentinel-3, also, provides sea, ice and land surface temperatures. The accuracy of the global sea-surface temperature maps is better than 0.3 ºC, with a spatial resolution of 0.5 Km^2.

NOAA JPSS Visible Infrared Imaging Radiometer Suite (VIIRS) also serves Ice Surface Temperature products at the ice surface including snow and meltwater on the ice. The VIIRS IST provides surface temperatures retrieved at 750-meter spatial resolution for snow/ice-covered oceans for both day and night. The IST algorithm uses two VIIRS Infrared bands, and is based on the Advanced Very High Resolution Radiometer (AVHRR) legacy IST algorithm.

b) Multi-spectral microwave radiometry

Deriving the temperature profile through the snow and ice layers, from the surface down to 0.5 m into the ice, is feasible from a combination of the available satellite data. The satellite data used here are thermal infrared (TIR) and microwave radiation data at different wavelengths and polarizations from 1.4GHz (SMOS and SMAP) to 89GHz (AMSR). The satellite data are compared with coincident data from Ice Mass-balance Buoys and numerical weather prediction data. This combined dataset is analyzed for empirical relationships between the satellite measurements and different snow conditions, and ice parameters are derived using linear regression, for particular the snow and ice temperature profile.

Co-funded by the Horizon 2020 programme of the European Union

The satellite channels of lower frequencies can retrieve temperatures from deeper levels in the snow and ice (ICE-ARC H2020 report). The comparisons between measured and simulated temperatures derived with the empirical models show a high correlation with R^2-values ranging from 0.43 to 0.90. The differences in correlation between the IMB buoys indicate a spatial dependency, as well as strong dependency on differences in snow and ice thickness. The models derived in this study are based on conditions with intermediate snow and ice thickness.

However, this is a science product and is not served in a continuous mode, so this is not an operation product at the moment.

8.2 Characteristics of the parameter

Monthly accuracy requirements (Target precision) for SST and IST for OSI-205-a/b. IST requirements split between validation against radiometers and buoys.

The target precision of the sea surface and sea ice surface temperature data are 1.0 K and 4.0 K, respectively, expressed as the standard deviation of the difference with traditional buoy measurements (extracted from ATBD for OSISAF SST and IST L2 OSI-205-a/b processing chain SAF/OSI/CDOP2/DMI/SCI/MA/223, EUMETSAT)

Parameter	Target accuracy Std Dev. / Bias	Temporal Resolution	Spatial Resolution	Latency
SST OSISAF 203-a/b	Day: 1-2ºC / 0.8ºC Night: 0.5 C/0.8ºC (Eastwood et al. 2011)	12 h	5 km	6h
IST OSISAF 203-a/b against Buoys	Day: 3ºC / 3.5ºC Night: 4.0ºC / 4.5 ºC	12 h	5 km	6h

Co-funded by the Horizon 2020 programme of the European Union

IST OSISAF 203-a/b against radiometer		12 h	5 km	6h
OSISAF 205-a/b against Buoys	Monthly accuracy 3ºC / 3.5ºC (Dybkjær et al., 2018)	12h	0.75/1km	6h
OSISAF 205-a/b against radiometer	Monthly accuracy 2ºC / 1.5ºC (Dybkjær, et al., 2018)	12 h	0.75/1km	6h

8.3 Validation

In situ observations of ice surface temperatures in Arctic regions are typically measured by buoys on the sea ice. Such measurements are often dubious because the instrument can be buried under snow or sticking up in the air and thus measuring either internal snowpack temperatures or air temperatures. Snow, snow skin and air temperatures can in fact be several degrees apart and validation of the skin temperatures measured from a satellite is therefore complicated. For this reason, the validation requirements products have been split in two, one set of requirements for validation based on *In situ* IR radiometers and one set for validation based on *In situ* temperature buoys. The requirements for IST radiometer validation are more precise and accurate than those for buoy validation, since radiometers provide a more representative observation of the temperature that the IST product delivers. The IST requirements are partly based on Stammer et al. (2007).

8.4 Error sources/Accuracy/uncertainty

The uncertainty on the satellite SST and IST retrievals have been divided into three components: a random uncertainty, a locally systematic uncertainty and a large-scale systematic uncertainty. These uncertainty components represent errors that have distinct correlation properties and have been modelled (see (Steiner et al. 2018) for additional details).

Co-funded by the Horizon 2020 programme of the European Union

The target (expected) accuracy, named std and bias values are 1.0 and 0.7 for SST and 3.0 and 3.5 for IST, as specified by scientists. The OSI-203-a accuracy of the SST is within target accuracy (1.0 of std and 0.7 of bias), while the IST during day time is within the target (3.0 of std and 3.5 of bias). At night time the OSI203a is not within the target requirement, but within the threshold requirement of 4.0 K standard deviation for SST and within or close to the threshold requirement of 4.5 K bias for IST.

8.5 Known limitations and gaps

Satellite infrared radiometry has difficulties in distinguishing clouds from snow-covered surfaces.

The satellite sensors are sensitive to changes in snow emissivity, associated primarily with snow precipitation and snow cover metamorphosis processes and with melting processes initiated by surface air temperatures around the freezing point of water. This is primarily affecting the simulated temperature estimates in the snowpack.

Co-funded by the Horizon 2020 programme of the European Union

1.3 Ocean Parameters:

1.3.1. Surface ocean biogeochemical compounds and light

Ocean colour is the change in the colour of the ocean, and other water bodies such as seas and lakes, due to the substances dissolved and particles suspended within the water. Ocean colour remote sensing primarily aims to derive the spectrum of marine or other surface water reflectance (also defined as remote sensing reflectance, RRS) from satellite observations. In turn, RRS can be used to determine inherent optical properties (absorption and back-scattering coefficients, marine fluorescence) and concentrations of optically significant constituents present in the upper layer of the ocean.

Among these is the concentration of chlorophyll-a (Chl), a photosynthetic pigment found in phytoplankton cells. Ocean colour remote sensing is thus the only satellite remote sensing technique that opens a window onto ocean biology. Also suspended sediments and coloured dissolved organic matter (CDOM) can be derived from RRS. Chl is present in all phytoplankton and a good indicator of phytoplankton biomass, which represents about 1-2 % of the global plant's biomass. However, phytoplankton contributes to about 50% of the World's primary production, Chl, but also other ocean colour products related to other particles, decaying organisms, underwater light are used parameters for assessing, developing, and assimilated in local, regional and global biogeochemical and ecosystem models (which can be coupled to ocean or Earth System model) with a wide range of applications in climate and biodiversity research and water quality, fisheries, coastal management.

Considering the various products that can be derived from marine reflectance data as well as the role of marine phytoplankton in the carbon cycle (responsible for approximately half of the Earth's total carbon fixation), the Global Climate Observation System lists both the spectrum of marine reflectance and the chlorophyll-a concentration as Essential Climate Variables (ECV).

1.1. Technologies used and retrieval methods

The so-called "ocean colour" products are derived from optical sensors with between five to ten spectral bands between 400 to 700 nm at least 20 nm band resolution and an SNR above 400. Algorithms and products described for standard products require atmospherically corrected top of atmosphere data (L_{TOA}; provided as L1 products) to derive the water-leaving

Co-funded by the Horizon 2020 programme of the European Union

radiance and by accounting for the incoming radiance the RRS (sr^-1, Level-2 products) at each waveband is derived. Only about 10% of the radiance measured by a satellite instrument in visible blue and green wavelengths originates from the water surface and significantly less in the red. The sensors thus require very low radiometric and spectral uncertainties and a high signal to noise ratio (SNR), particularly for the 'blue' bands (~400-450 nm). Ocean colour instrument design must therefore incorporate extremely sensitive and stable radiometry, dedicated on board calibration and spectral channels located at wavelengths of specific interest

RRS are derived from multispectral sensors with several, e.g. nine for MODIS sensors on Aqua and Terra satellite (since 2002 and 1999, respectively) and 21 for OLCI on Sentinel-3 (since 2016 and 2018 on S-3A and S3B, respectively) wavebands from 400 to 1080 nm suitable for ocean colour exploitation and its atmospheric correction. The later can be very challenging, especially in the polar oceans where the observations are generally taken under high zenith angles (therefore the light is not penetrating much into the ocean the RRS signal is low) and the adjacent effect of sea ice and higher possibility of cloud cover introduce more uncertainty. Most ocean color sensors, such as SeaWiFS, MODIS, MERIS and OLCI are low earth polar-orbiting satellites flying in a sun-synchronous orbit, therefore acquiring also polar observations and if sunlight, sea ice and weather conditions allow, several orbits per day can be achieved, Only one ocean colour sensor in the past measured the entire spectrum in the visible (128 bands with 5.7 nm bandwidth between 380 to 1080 nm). However, since the HICO sensor was operated from the ISS, it was not providing any polar observations. In addition to the RRS products at each waveband, also the daily average photosynthetically available radiation (PAR) at the ocean surface (in Einstein m^{-2} d^{-1}) is available which is similarly retrieved from the L_{TOA} data but further using plane-parallel radiative transfer modelling to assess the whole PAR spectrum (e.g. Frouin et al., 2002; Aiken and Morre, 1997). PAR is defined as the quantum energy flux from the Sun in the 400-700nm range. For ocean color applications, PAR is a common input used in modeling marine primary productivity. Implementation of this algorithm is contingent on the availability of observed L_{TOA} in the visible spectral regime that does not saturate over clouds.

The RRS product is an ECV. It is useful to assess the radiation budget in the ocean and serves as input data for retrieving surface ocean biogeochemical compounds and information on the underwater light environment (all Level-2 products). In the following we list available products from OLCI, MODIS and merged (currently from SeaWiFS, MODIS and MERIS) OC-CCI.

Co-funded by the Horizon 2020 programme of the European Union

(Products only available from OC-CCI are indicated with * and only from OLCI with **). Chl (in mg/m^3), the diffuse downwelling irradiance attenuation (KD in m^{-1}) at 490 nm (KD490), the total absorption (at*, in m^{-1}), the absorption of CDOM and non-algal particles (adg, in m^{-1}; for OLCI only available as case-2 water product at 443 nm) and particle back-scattering (bbp, in m^{-1}) coefficients at the RRS wavebands. The KD490 products are often used as an indicator for turbidity.

Chl, KD490, particulate inorganic carbon (PIC) and particulate organic carbon (POC) -the latter two are only available from MODIS- can be retrieved with simple band ratio algorithms (still used for all operational case-1 products) using the blue and green bands with coefficient derived from fitting a large set of *In situ* data (e.g., O'Reilly et al., 1998; Morel et al., 2007; Balch et al., 2005; Stramski et al., 2008) or via semi-analytical algorithms e.g. the quasi analytical algorithm by Lee et al. (2002) which is used for MODIS and OC-CCI products and first retrieves the IOPs (at, adg, bbp and phytoplankton absorption aph, the later is only available from MODIS) and from that retrieves KD490 (OC-CCI product only), and Chl (often directly derived from aph443 by an empirical factor derived from a large *In situ* database). The merged GlobColour ocean colour Chl products are available from band-ratio (Chl_avg) and semi-analytical (Garver-Siegel-Maritorena 2002; Chl-GSM) algorithms.

Standard products are typically developed for open ocean waters where phytoplankton also determines the abundance of other optical constituents such as coloured dissolved organic matter (CDOM) and non-algal particles. However, band-ratio algorithms which mostly show the best global performance when compared to *In situ*, often fail in coastal and inland waters (so-called case-2 waters), where the abundance of these constituents is not correlated. On the other hand semi-analytical algorithms often succeed there since they allow the determination of these compounds independent from Chl. For MERIS and OLCI also case-2 water products for Chl (Chl_nn) are available together with adg443 and TSM. These are derived following Doerffer and Schiller (2007) from neural nets trained with case-2 water collocated *In situ* data on apparent (RRS) and inherent (at, bbp, adg, aph) optical properties (AOP and IOP, respectively) and geophysical quantities (Chl, TSM) which are further amplified via bio-optical modelling to allow optimal training of the net to obtain reliable values for Chl_nn, adg443_nn and TSM.

1.2 Characteristics of the parameter

Co-funded by the Horizon 2020 programme of the European Union

- Temporal Resolution The operational data are acquired close to daily at the equator for each MODIS sensor and the two S3 OLCI sensors together, while several orbits per day across the polar regions are likely. The non-operational but high spatially resolved ocean colour data from Sentinel-2 (with two instruments in orbit) and Landsat-8 are much less well temporally resolved with about five to 10 days between overpasses at the equator at the same spot.

- Spatial Resolution: The spatial resolution currently ranges from 300m (OLCI on Sentinel-3) to 1 km (MODIS) for globally acquiring ocean colour sensors. The merged SeaWiFS-MODIS-MERIS-VIIRS data sets provide 4 km resolution globally, but are available at 1 km scale for the Arctic and European region. Non-operational products for turbidity and even Chl are available from Landsat-8 and MSI/Sentinel-2 at 100 and 10 m scale.

- Latency: However, ocean colour is limited to the light lit time of the year, so at SZA below 60° no ocean colour data can be acquired in addition to that cloud-and high glint-free conditions are required. In the polar oceans this leads rather to a weekly than daily resolution of the ocean colour data during the sun-lit time of the year which is mainly limited to April to September for the Arctic and October to March for the Antarctic Ocean.

1.3 Validation

To infer in-water properties such as chl-a from satellite observations of ocean colour requires retrieval of the RRS that, as noted above, may be less than 10% of the top of atmosphere detected signal and, hence, requires high precision in the satellite sensor calibration (Groom et al. 2019). To achieve the required ocean colour product uncertainties, in addition to instrument pre-launch and onboard calibrations, a System Vicarious Calibration (SVC) must be applied (see e.g., Sentinel-3 Mission Requirements Traceability Document; IOCCG Report 13; Zibordi et al., 2012). SVC uses highly accurate *In situ* measurements of water-leaving radiances, which are the best quality radiometric Fiducial Reference Measurements (FRMs) for ocean colour. SVC employs these FRMs to reduce residual biases in Level-2 products.

Validation is focused on independently assessing the accuracy and stability of the satellite products. For ocean colour this involves inter-comparisons with high-quality ground-truth *In situ* measurements (FRMs) of both the radiometry and bio-optical parameters and inter-

Co-funded by the Horizon 2020 programme of the European Union

comparisons with corresponding products from other stable missions and climatologies. In ocean colour, *In situ* FRMs provide critical knowledge of the ground truth but are sparse due to the complexity of radiometric and bio-optical measurements from ships and instrumented platforms. Mission inter-comparisons allow for large-scale global time-series evaluations. Since most measurements have to be obtained from ships, the ground-truth data coverage is low and biased to certain regions. Especially the polar oceans are sparsely sampled due to the difficult access of these remote areas and harsh environmental conditions.

Lately, validation data sets are complemented by inline measurements of continuously operated optical sensors either operated on ships (e.g., Brewin et al., 2016; Liu et al., 2018) or even on autonomous platforms such as bioARGO floats (Organelli et al., 2017; Wojtasiewicz et al., 2018). These enable better to characterize the spatial and temporal variability of satellite products, such as Chl, RRS, KD490, bbp, adg and even enable real-time validation. However, the require thorough validation with FRMs themselves.

In addition also cross-comparisons among satellite sensors are necessary to assess the long-term stability of sensors on a global scale.

1.4 Error sources/Accuracy/uncertainty

Since Chl and RRS (or normalized water-leaving radiance) are ECVs, for climate purposes, the Global Climate Observing System (GCOS) specifies the uncertainty requirements with 30% and 5% at blue and green wavelengths, and a stability per decade of 3% and 0.5%, respectively (https://www.ncdc.noaa.gov/gosic/gcos-essential-climate-variable-ecv-dataaccess-matrix/gcos-ocean-biogeochemistry-ecv-ocean-color).

In compliance to the above also the other ocean colour products would require similar uncertainties. Based on user consultation results, the uncertainty information delivered together with the parameter-related product in the OC-CCI products (except for the bbp product were no uncertainties could be provided due to the sparse *In situ* data set) contains the root mean square difference (RMSD) and bias, computed based on comparison to match-up *In situ* data divided up into their membership to a specific optical water class based on their spectrum from the OC-CCI RRS data (Jackson et al. 2019). Uncertainty information provided with each product is critical for the design and set up of assimilation systems and for prediction quality assessment to users.

Co-funded by the Horizon 2020 programme of the European Union

1.5 Known limitations and gaps

The gap on spatial resolution: OLCI provides full ocean colour capability to 300 m but higher resolution (of order 10–100 m) to detect in bays or estuaries at the polar coasts. In addition, the observation of colour in inland waters are not adequately supported, since missions providing such data are focused on land applications (e.g., Sentinel 2 or Landsat 8). Such missions have limited capabilities for retrieval of SPM concentrations, and in some cases of Chl-a concentrations. Mission requirements to meet these needs were presented in International Ocean Colour Coordinating Group [IOCCG] (2018). Improvements to the capability of Sentinel 2 or Landsat 8 sensors could partly meet these requirements, along with HAP or nanosatellites, assuming that issues of calibration are addressed.

Gap temporal resolution: Often the temporal resolution is too low, especially in the polar regions were often even during sun-light conditions weather conditions are not favorable (waves to high, too many clouds) and sea ice adjacency effects deteriorate retrievals. Merging of OC products from different sensors will improve the coverage. However, when there is very low or no sunlight, coupled bgc-ocean models well-calibrated with remote sensing products and FRMs must fill the gap.

No products on phytoplankton functional types are available which would help to a) improve predictions for water quality, HABs, fishery, coastal management by themselves but also indirectly by improving the quality of Chl products, since they are biased towards 1) a global mean of phytoplankton absorption which is quite different in the polar oceans (in polar oceans they are much more adapted to low light conditions), and 2) a constant relationship to absorption by detrital and CDOM. While CDOM is particularly low in the Antarctic Ocean it is rather very high in the Arctic Ocean with very high Arctic riverine inputs.

Information on chlorophyll fluorescence is only available as a product from MODIS with FLH; still, the product is difficult to use for interpretation further phytoplankton health and other physiological features (iron limitation, etc.). In general the retrievals are questionable for the polar oceans since in the spectral range they are retrieved RRS data are at the noise level due to the low sun in this region.

Although *In situ* validation and other forms to ensure the assessment of OC product stability is mostly well-coordinated, it needs to continue and be sustained, because FRM protocols and round-robins to assess the FRMs uncertainty and to train researchers to obtain FRMs are still

Co-funded by the Horizon 2020 programme of the European Union

sparse and need to be enlarged. Especially in the polar oceans sampling due to difficult access of the region is sparse and the exploitation of using autonomous platforms' optical data needs to be further developed and harmonized, as it is well on the way for the bioARGO floats.

Especially the SVC platforms need to be sustained, last year (2018) MOBY was not able to take measurements for most of the year and also Boussole was on and off, so only the coastal FRMs from AERONET-OC could provide SVC. This limited especially the ability to characterise S3B OLCI OC products and therefore its L2 products are still not operational. Therefore SVC needs to be sustained and enlarged by at least two more platforms to secure VC of sensors.

1.3.2. Sea Surface Temperature

Sea surface temperature (SST) is a key indicator of the Arctic changes and the role of the ice-albedo feedback mechanism in any given summer melt season. As the area of sea-ice cover decreases, more incoming solar radiation is absorbed by the ocean and, in turn, the warmer ocean melts more sea ice. Summer SST in the Arctic Ocean is driven mainly by the amount of incoming solar radiation absorbed by the sea surface. Solar warming of the Arctic surface ocean is influenced by the distribution of sea ice (with greater warming occurring in ice-free regions), cloud cover, ocean optical properties, and upper-ocean stratification. In the Barents and Chukchi Seas, there is an additional source of ocean heat contributed by the advection of warm water from the North Atlantic and North Pacific Oceans, respectively.

IMPORTANT NOTE: Since the instruments that measures SST is the same as the ones that measures Ice Surface Temperature (IST), the description of the instrument technology, parameter characteristics, validation and error sources of SST is with the description of IST in section 8: Ocean and Ice Surface Temperature, from the section SEA ICE PARAMETERS.

1.3.3. Sea Surface Salinity

Sea Surface Salinity (SSS) is a key indicator of the freshwater fluxes and an important variable to understand the changes the Arctic is facing. Since *In situ* salinity measurements are very sparse in this region, remote sensing salinity measurements are of special relevance. SSS has been observed from satellite since 2009 when the ESA SMOS (Soil Moisture and Ocean Salinity) mission was launched. This was the first satellite to measure this important oceanographic parameter.

Co-funded by the Horizon 2020 programme of the European Union

3.1. Technologies used and retrieval methods

The salinity of the ocean can be measured only by using L-band passive microwave radiometers. The three L-band missions—the SMOS mission; the NASA Aquarius mission; and the NASA SMAP (Soil Moisture Active Passive) observatory provide an unprecedented source of salinity information over the Arctic Ocean, which can be assimilated in the models and help to improve them.

The retrieval of sea surface salinity in cold oceans is a challenge, since the sensitivity of the brightness temperatures to sea surface salinity get considerably reduced when the sea surface temperature is below 10ºC. Moreover, some undesired effects are present in the brightness temperatures acquired by the radiometers, such as the land-sea and ice–sea contaminations, which affect the quality of the salinity retrieval close to coasts and ice edges.

The Barcelona Expert Center (BEC) is serving a dedicated product for the Arctic Ocean (freely available at: http://bec.icm.csic.es/ocean-arctic-sss/) (Olmedo et al., 2018). It has been derived by applying the debiased non-Bayesian salinity retrieval, a methodology focused on mitigating the systematic salinity biases (Olmedo et al., 2017). The on-going ESA Arctic+ Salinity project (Dec 2018 – June 2020) will contribute to reducing the knowledge gap in the characterization of the freshwater flux changes in the Arctic region by developing a better quality SMOS SSS product in the Arctic region (https://arcticsalinity.argans.co.uk/). The impact of assimilating the new SSS products in the TOPAZ system will be assessed. If an improvement is demonstrated, the assimilation of SMOS SSS products in TOPAZ will be part of the new Arctic reanalysis and forecast products on the CMEMS portal.

The Laboratoire d'Océanographie et du Climat, Expérimentations et Approches Numériques (LOCEAN) has recently developed another SMOS SSS product in the Arctic Ocean. Very recently, they have shown that this data, first compared to ARKTIKA-2018 campaign, can be used for studying the variability of surface water masses of the Laptev and the East-Siberian seas (summer 2018) (Tarasenko et al., 2019, Supply et al., submitted).

SMAP SSS data reveal a much stronger interannual variation of SSS than HYCOM. Given HYCOM's relaxation of SSS to seasonal climatology and the use of seasonal climatology of river discharges, SMAP SSS may provide a more reliable dataset to study interannual

Co-funded by the Horizon 2020 programme of the European Union

freshwater changes of the Arctic Ocean in regions where no or few *In situ* data are available to constrain HYCOM.

SMAP SSS global products are served by two teams: NASA-JPL and REMSS which use different algorithms. Both are served at PODAAC data server (https://podaac.jpl.nasa.gov/dataaccess).

3.2. Characteristics of the parameter

Product	Spatial resolution	Temporal resolution	STD error (from Fournier et al., 2019
SMOS BEC ARCTIC SSS product	25 Km	served daily - 9 days average	1.07
SMOS CATDS Arctic SSS product	25 Km	9 days	1.12
SMAP L3 JPL global SSS product	0.25º	8 days	2.38
SMAP L3 REMSS global SSS product	0.25º	8 days	0.84

Latency is not important in this variable since it is not required for near-real-time.

3.3 Validation procedure

The quality assessment of the product is done by comparing it with *In situ* measurements. Much less Argo buoys are deployed in the Arctic Ocean than in the rest of the ocean. The *In situ* measurements used are:

Co-funded by the Horizon 2020 programme of the European Union

Argo floats: Most of the Argo buoys are located between 60ºN and 70ºN, and few of them are inside the Arctic Ocean. The uppermost salinity measurements (not deeper than 10 meters) are considered and no measurements shallower than 0.5 m are used due to the formation of bubbles and foam.

Tara Polar Circle Expedition dataset: This campaign took place in the Arctic Ocean from June to October 2013 (Reverdin et al., 2014), and a thermosalinograph (TSG) Seabird SB45 and a temperature sensor (SBE38) recorded sea surface temperature and salinity at 3 m depth during the whole cruise. Since TARA salinity data presents a large range of spatial variability in the Arctic Ocean (≈ 26 to 35), it becomes a very valuable source for assessing the annual SSS reference salinity field used for the generation of the SMOS SSS product.

Transects of TSG: This salinity data source is provided by Copernicus (available on http://marine.copernicus.eu/services-portfolio/access-to-products/).

3.4 Error sources/Accuracy/uncertainty

The accuracy of the salinity reduces in cold oceans, since the sensibility to salinity gets considerably reduced when the temperature of the ocean is below 10ºC. The accuracy of the BEC SSS dedicated product for high latitudes (more than 50ºN,) varies between 0.4 and 0.8 psu, depending on the region (Olmedo et al 2018), when compared with TARA *In situ* data. When comparing the BEC SMOS SSS product with Argo floats data the standard deviation ranges is between 0.2 psu and 0.35 psu, but take into account that Argo floats are located between 50ºN and 70ºN, and none are located inside the Arctic Ocean.

The accuracy with SMAP data depends on the product developed as well as the averaged days. The accuracy varies between 0.84 to 2.38 as std deviation in the Arctic.

3.5 Known limitations and gaps

A known limitation is that measurements near the coast (less than 50 km) will suffer from land-sea contamination errors, and also on sea-ice contamination.

The product could be improved if the combination of different sensors (ie. SMOS and SMAP) is assessed.

Co-funded by the Horizon 2020 programme of the European Union

There is an urgent need for *In situ* measurements of salinity in the polar regions. Currently, there are very few *In situ* salinity data available in the areas North of the Arctic Circle. A sufficient *In situ* database would not only provide a robust assessment of satellite SSS uncertainties in the Arctic Ocean, but also support the retrieval algorithm refinement, leading to enhanced satellite salinity products.

The precision degrades in cold water as the sensitivity of L-band radiometer signal to SSS decreases when SST decreases, even though this effect on temporally averaged maps is partly compensated by the increased number of satellite measurements at high latitudes.

Co-funded by the Horizon 2020 programme
of the European Union

1.3.4. Sea Surface Height

4.1. Technologies used and retrieval methods

Satellite measurements of Sea Surface Height are based on the data provided by Radar altimeters. Such instruments measure the range between sea surface and instrument antenna. Then, Sea Surface Height can be estimated, if satellite height is known. The resulting measurements, once corrected from atmospheric contributions, contain two main contributions: the oceanographic signal due to currents, tides, heat content and atmospheric load; and the undulations of the geoid. The oceanographic signal, away from the strongest currents, is of the order of 20 cm and variably in time. The undulation of the geoid, on the contrary, is much bigger and constant at typical oceanic scales. If the geoid is not sufficiently well known, which has been the case for most of the time, temporal anomalies have to be computed (Sea Level Anomalies) and the mean sea level due to ocean currents (Mean Dynamic Topography) has to be independently estimated and added (Robinson 2004).

From a technological point of view, Radar Altimeters can measure Sea Surface Height at their nadir with a footprint of the order of 7 km (Robinson 2004). During the last years a new generation of radars that use the Synthetic Aperture approach have been developed (e.g. Sentinel-3constellation; e.g. Ray et al. 2015). In spite of the improvements in the instrument, all current altimetric measurements are flawed by the same problem: the sampling limitations due to their swath. To solve this limitation a new mission concept, the SWOT mission, has been proposed and is expected to be able to provide high resolution maps of sea level in the years to come.

4.2. Characteristics of the parameter

These are the characteristics of some of the most popular altimetric products. There are additional products devoted to the long-term evolution of sea level or to assimilate into ocean models.

Product	Spatial resolution	Temporal resolution	Latency
CMEMS Global along-track L3 SSH NRT	14 km	instantaneous	< 3 h

Co-funded by the Horizon 2020 programme of the European Union

CMEMS Global gridded L4 SSH NRT	¼ º	irregular	1 day
CMEMS Global gridded L4 SSH reprocessed	¼ º	irregular	irregular

4.3. Validation

There are multiple strategies to validate measurements such as the comparison with GPS buoys and tide gauges.

4.4. Error sources/Accuracy/uncertainty

Radar altimeter data is noisy not only due to instrumental noise and errors in the atmospheric correction, but also due to the sea state. This has a major implication: when analysis along-track data the effective spatial resolution of observations will change. Along-track products from Jason-2, for example, have an error range between 1.5 and 3.5 cm rms at 1Hz (Dufau et al. 2016). Obviously, at higher frequencies (20Hz) they are bigger. Another source of error is the errors due to the sampling, which can be theoretically derived when performing the optimal interpolation to generate two-dimensional maps. These errors are usually included in L3 and L4 altimetric products.

4.5. known limitations and gaps

Since current altimeters are only able to measure sea level in its nadir, measurements are composed of lines, which brings the need to perform spatio-temporal interpolations to retrieve two-dimensional fields. These maps have a limited resolution of about 100 km and a temporal frequency of the order of 10 days in spite of their higher nominal resolution and frequency. This is a major limitation since the Rossby radius of deformation is smaller and decreases with latitude. This is the so-called altimetric gap. Notice, however, that in the arctic area satellite tracks are closer. Finally, it's worth mentioning, however, that this is not the only limitation. Smaller scales have smaller sea level amplitudes, which requires to reduce the noise level, and other dynamical processes such as internal waves, start to contribute to the signal.

Co-funded by the Horizon 2020 programme of the European Union

1.3.5. Sea Surface Currents

5.1. Technologies used and retrieval methods

Measuring ocean currents from satellites is a key challenge of satellite oceanography. Although significant advances have been done in the recent years and new concepts have been proposed, current operational measurements mainly rely on indirect approaches and are constrained to surface currents.

The basic principle of the direct measurement of velocities relies on the Doppler effect, i.e. on the change of frequency of the returned signal. Such measurements are currently done by Synthetic Aperture Radars (SAR), allowing for the retrieval of surface velocities (see Ardhuin et al. 2019 for a short review). Currently there are two approaches: use two interferometric SAR or the single centroid from the same instrument. While both approaches provide equivalent information, they have different resolutions and revisit capabilities (Romeiser et al. 2014). Present day, the European Space Agency provides Level-2 products with radial velocities, i.e. ocean surface velocities in the direction of the line connecting the sensor and the measured point. These products can be found for Envisat, Sentinel-1a and Sentinel-1b but their application for monitoring ocean currents is rather limited due to the difficulties to extract the geophysical signal from other contributions and, then, to separate the contribution of surface currents from the contribution of waves (Rodríguez et al. 2018). It worth mentioning that, during the recent years, different mission concepts, such as SEASTAR (Gommenginger et al. 2018); SKIM (Ardhuin et al. 2018); and WaCM (Chelton et al. 2019), have been proposed to measure ocean currents although two of them have been already discarded (SEASTAR and SKIM).

The major consequence of the difficulties to retrieve ocean velocities from direct measurements is the need to estimate them from indirect approaches. At present, velocities can be estimated from Sea Surface Height, Sea Surface Temperature, Sea Surface Salinity, a sequence of tracer images or Surface Winds (see Isern-Fontanet et al 2017 for a review on this subject). However, the only truly operational approach to the retrieval of ocean velocities is based on applying the geostrophic approximation to Sea Surface Heights (SSH) measurements provided by altimeters and, eventually, complement these measurements with the wind-driven component derived from wind measurements. Within this framework, the link between velocities and SSH is direct where is sea surface topography (see the section on Sea Surface Heights), the vertical normal vector, is gravity and is the Coriolis parameter. Wind induced velocities, usually known as Ekman velocities, can be added to these geostrophic velocities to improve the estimation of currents. The approach followed consists of fitting an empirical model to the velocities derived from surface drifters, which is then used to estimate the Ekman component from Surface Winds (Isern-Fontanet et al. 2017).

Co-funded by the Horizon 2020 programme of the European Union

5. 2. Characteristics of the parameter

Here, we report the characteristics of the L4 global velocity fields provided by Copernicus Marine Service These total velocity fields are obtained by combining CMEMS NRT satellite Geostrophic Surface Currents and modelled Ekman current at the surface and 15m depth (using ECMWF NRT wind). This product has been initiated in the frame of CNES/CLS projects. Then it has been consolidated during the Globcurrent project (funded by the ESA User Element Program).

Product	Spatial resolution	Temporal resolution	Latency
NRT CMEMS Global Total Surface Current (Geostrophic + Ekman) at 0m and 15m.	1/4º	6h	1 day
Reprocessed CMEMS Global Total Surface Current (Geostrophic + Ekman) at 0m and 15m.	1/4º	3h	1 year

It's worth mentioning that geostrophic velocities are easily derived from altimetric measurements and Ekman velocities can be estimated from surface wind data. Consequently, we refer the reader to the characteristics of these variables for further information about spatial and temporal resolution, as well as data latency.

5.3. Validation

The validation of surface products is based on the direct comparison with *In situ* measurements, which mainly consist of surface drifters (e.g. Rio et al. 2003).

5.4. Error sources/Accuracy/uncertainty

The standard approach for the estimation of ocean currents is based on the combination of geostrophic velocities derived from altimetric measurements with Ekman velocities derived from atmospheric models. This implies that there are three sources of errors: instrumental

Co-funded by the Horizon 2020 programme of the European Union

noise, sampling limitations and theoretical limitations. Instrumental noise can be assessed and sampling errors can be theoretically derived. The validity of the theoretical approach used, e.g. the geostrophic approximation or the Ekman model use, is more difficult to assess. As a consequence measurement errors have to be determined empirically. Based on the GlobCurrent outcome, 15 cm/s can be considered as a global value for the product accuracy.

5.5. known limitations and gaps

The limitation of geostrophic velocities derived from altimetric measurements are well characterized and understood. On one side, there are the limitations due to the combination of noise level and sampling characteristics of the current constellation of altimeters (see the section on Sea Surface Heights). On the other side, the limitations due to the geostrophic approximation.

1.3.6. Sea Surface Stress (wind)

Ocean surface wind and wind stress observations are essential and relevant for a wide range of applications, e.g., coastal protection, ship routing, off-shore wind energy, climate-scale circulation, water cycle and ocean forcing. As meteorological analyses more and more focus on mesoscale processes, wind measurements are needed globally. Mid and high latitude, high wind events (cold air outbreaks) lasting several days can lead to the formation of deep water that helps drive global ocean circulation patterns. High winds also help exchange disproportionately large amounts of carbon dioxide. Moreover, high-latitude surface winds play an important role in the generation of polar lows. In addition, although satellite-derived surface winds can only be retrieved over ice-free ocean areas, such observations in combination with sea ice derived information helps in the understanding of ocean-ice interactions as wind-generated waves propagate into the sea ice covered regions.

6.1. Technologies used and retrieval methods

Space-borne microwave passive and active sensors are used to derive sea surface wind observations globally at various spatial and temporal resolutions.

Passive microwave sensors or radiometers (e.g., SSM/I, TMI, GMI) measure the wind speed over the ocean. The retrieval is based on a physical radiative transfer model that calculates the microwave emission from flat and rough ocean surfaces and the absorption and emission by the Earth's atmosphere (Meissner and Wentz 2012). Radiometers are usually equipped with multiple receiving channels (typically between 6 GHz and 37 GHz) to derive wavelength-dependent emission characteristics of the atmosphere and Earth's surface from the measured brightness temperatures (Ulaby and Long, 2014). However, the presence of rain is known to

Co-funded by the Horizon 2020 programme of the European Union

degrade the quality of the retrieved wind speeds. Polarimetric radiometers (e.g., Windsat) provide complementary information on the wind direction relative to look direction (Yueh et al. 1999). This allows the determination of the ocean vector winds, i.e., both scalar wind speed and wind direction, although the latter is of poor quality below 8 m/s (Ricciardulli et al. 2012). L-band (1–2 GHz) radiometers (e.g., SMOS, Aquarius, SMAP) are minimally affected by rain or frozen precipitation and are sensitive to high and extreme winds (Reul et al. 2012; Meissner et al. 2017). However, due to their relatively low spatial resolution (around 50 km) they cannot well resolve high-gradient regions, such as the eye and eyewall of hurricanes. Moreover, the L-band signal is little sensitive to low and moderate winds.

The altimeter measurements of the power and shape of the radar echo are not only used to determine significant wave height (SWH) and mean square slope (mss) of the ocean surface, but also near-surface wind speeds. Global Navigation Satellite System Reflectometry (GNSS-R) techniques (i.e., bistatic radar configuration) have shown their capability to observe sea surface wind speed (Zavorotny and Voronovich, 2000). The GNSS-R wind inversion relies on a geophysical model function (GMF) which relates the measured Delay-Doppler Map (DDM) to the sea surface wind speed for a certain observing geometry. The wind speed sensitivity though sharply decreases for winds above 6-7 m/s and in turn the derived wind quality (Lin et al., 2019). Both altimeters (e.g., Saral Altika, Jason-2) and GNSS-R (TDS-1) winds have relatively limited coverage.

At incidence angles above 20° (and especially above 30°), the radar backscatter over the ocean results from scattering off wind-generated capillary-gravity waves, which are generated by, and generally in equilibrium with, the near-surface wind vector over the ocean. Synthetic aperture Radars (SARs) can provide very high resolution information about the sea surface roughness and are particularly relevant in coastal areas and marginal ice zones. However, since SARs provide a single azimuth view, one cannot infer whether backscatter variations are due to wind speed or wind direction variation (Portabella et al. 2002). Several retrieval methodologies have been proposed to attempt overcoming such problem, by adding to the radar backscatter measurements either SAR imaging capabilities to detect wind streaks (Horstmann et al., 2002) or Doppler measurements of radial wind speed (Mouche et al., 2012). In general, SAR lacks absolute calibration, temporal sampling, and complete information for wind vector retrieval (Gade and Stoffelen, 2019).

Unlike SAR, the space-borne radar scatterometer samples the sea surface at different azimuth views, thus enabling sea-surface wind vector inversion from the backscatter measurements (Stoffelen, 1998). It is therefore a unique system in terms of its all-weather, global sea-surface wind (stress) vector capabilities. In fact, high quality, high resolution (20 km) scatterometer-derived global sea-surface wind vectors are routine and successfully used in a wide variety of oceanographic, atmospheric, and climate applications, e.g., NWP data assimilation,

Co-funded by the Horizon 2020 programme of the European Union

nowcasting, ocean forcing, wind energy, analyses of mesoscale processes such as moist convection and turbulence, etc.

6.2. Characteristics of the parameter

The table below summarizes the sea surface wind characteristics of the most widely used sensors (for wind applications) described above.

Characteristics of widely used global ocean satellite wind measurement systems (Gade and Stoffelen, 2019)

Parameter	**Sea surface wind vector**	**Spatial Resolution**	**Temporal Resolution**	**Latency**
Radiometer	Only speed [a]	50 km	12 h	3 h
SAR	Partial information[b]	1 km	Infrequent	3 h
Scatterometer	Yes	20 km	12 h	0.5-3 h

[a] WindSat provides credible wind direction for speeds above 8 m/s

[b] Only one component is measured, with similar sensitivity to both speed and direction

The temporal resolution refers to a single satellite/sensor. However, there is typically a constellation of such sensors (which varies with time), leading to improved temporal sampling. In particular, there are currently six scatterometers in different sun-synchronous orbits: the Advanced Scatterometer (ASCAT) on METOP-A, -B and -C, OSCAT on ScatSat-1, CFOSAT and HY-2B. The sea surface wind products from the first four are served in near real time (NRT), while the last two (CFOSAT and HY-2B) are expected to become available in NRT soon.

6.3. Validation

Co-funded by the Horizon 2020 programme of the European Union

The validation of satellite-derived sea surface wind products is generally carried out with the following auxiliary reference datasets:

NWP model output: Global NWP model output, e.g., the ECMWF sea-surface wind output, is spatially and temporally interpolated to the satellite acquisitions. Global NWP winds well resolve the large scale wind although they largely miss small scale processes, such as moist convection.

Moored buoy winds: The moored-buoy anemometer winds are widely used to calibrate and validate satellite sea surface winds. Several moored buoy arrays are used as reference. However, most of the buoys are either tropical (e.g., TAO, TRITOAN, PIRATA, RAMA) or coastal (e.g., NDBC, ODAS). Very few moored buoys are available at high latitudes, i.e., beyond 55°N or 55°S.

Precipitation data: To analyse precipitation effects on the satellite wind retrieval quality, collocations with passive microwave systems are performed. Polar sun-synchronous systems like the SSM/I provide rain data at all latitudes. Other satellite rain products from more inclined (e.g., TMI or GMI) or geostationary (MSG) orbits are often use, but do not provide (reliable) precipitation information beyond 65°N or 65°S.

Other validation sources: Inter-comparison between different satellite-derived wind products is also often used for validation purposes. For example, the C-band ASCAT is often used to analyse rain contamination effects on Ku-band scatterometer (Lin and Portabella, 2017) or radiometer winds. Also, at high latitudes, cloud imagery is used to verify how well satellite-derived winds resolve polar lows (Furevik et al., 2015).

6.4. Error sources/Accuracy/uncertainty

The accuracy of the radiometer-retrieved wind speeds has been assessed through comparisons with NWP and buoys. While in rain-free scenes, the accuracy matches that of a scatterometer (Wentz et al. 2017), in precipitating scenes, significant errors start to appear in light rain (surface rain rates > 1 mm/h, Meissner and Wentz 2009).

The SAR-derived wind quality is very much situation or image dependent. Because of its very high resolution, several non-wind-related atmospheric (e.g., gravity waves, rain cells) and oceanic (e.g., waves, tides, shallow-water bathymetry) processes can be seen in a SAR image, further negatively impacting the wind retrieval process. The SAR wind accuracy is reported to be around 2 m/s in favorable conditions.

Scatterometer wind vector errors estimated through triple collocation analysis (Stoffelen, 1998) are typically between 1 m/s (C-band systems) and 1.6 m/s (Ku-band systems, more

Co-funded by the Horizon 2020 programme of the European Union

affected by rain and viewing geometry issues) (Vogelzang et al., 2011). At high latitudes, the scatterometer wind quality is not degraded (Furevik et al., 2015).

6.5. Known limitations and gaps

There are two main areas of ongoing concern for satellite-derived wind quality. The first is degradation of the retrievals in rain and the other is retrievals at high wind speeds, which in tropical and sub-tropical latitudes often occur with rain.

Consecutive sun-synchronous orbits have gaps between them and thus only cover portions of the globe in one day. Multiple scatterometers greatly improve the temporal sampling (Stoffelen et al. 2019; Trindade et al. 2020), notably at high latitudes.

One goal of the remote sensing community is to add Doppler capability to future scatterometers in a manner that allows for simultaneous measurements of surface winds and currents and improve directional accuracy (Rodriguez et al. 2018). Very few observations are made in the upper few meters where there is great deal of variation related to winds and waves. These variations impact the calibration of winds and stress and applications that depend on stress retrievals.

Mesoscale air-sea interaction requires much finer scale observations, with grid spacing of roughly 5 km or finer. Observations on these scales, with sufficient averaging in space and time, would allow investigation of most mesoscale features.

Co-funded by the Horizon 2020 programme of the European Union

Section 2: Current and in-development satellite products

This section provides a link to the work done in work package 2 on the provision of Copernicus services for polar regions. WP2 provides an inventory of the products currently available in the two most relevant services for polar regions: CLMS and CMEMS. In addition, WP2 also highlights relevant products either provided by C3S or ESA related projects (ESA-CCI and ESA Data User Element, DUE). Here, we only provide a summary of the inventories from WP2 and refer to the deliverable reports D2.1 'Final report on ways to improve the description of the changing Polar Regions in the Copernicus Land Monitoring Service (CLMS)' and D2.2 'Final report on ways to improve the description of the changing Polar Regions in the Copernicus Marine Environment Monitoring Service (CMEMS)' for more details.

Table 2. 1 details those variables presently served in Copernicus Marine Environment Monitoring Service and whether or not they can be derived from satellite measurements. Orange boxes emphasize that a RS product can be derived with sufficient quality, but is not today offered by Copernicus. Therefore, we recommend Copernicus to provide these RS products in the future. This shall involve R&D activities to maturate the prototype products before they can be served in CMEMS.

Table 2. 2 collects variables served in Copernicus Land Monitoring Service and whether or not they can be derived from satellite measurements.

Table 2. 1: Cross-reference between sea parameters provided by CMEMS, both models and observations and which ones are/can be measured by remote sensing techniques, either in real-time or delayed mode. Note that In situ measurements are not considered here Orange boxes *emphasize that a RS product can be derived with sufficient quality, but is not today offered by Copernicus.*

Theme	Variable	WP2.2 CMEMS	CMEMS product from models/RS[1]	WP3.1/3.3 Remote Sensing
Sea Ice	SIC	Yes	both	Yes
	SIT	Yes	both	Yes
	SIDrift	Yes	both	Yes
	IS Temperature	Yes	RS	Yes
	SIType	Yes	both	Yes
	SIAge	Yes	model	Yes
	Melt ponds	No	-	Yes

Co-funded by the Horizon 2020 programme of the European Union

	Sea ice Albedo	Yes	model	Yes
	Ice salinity	No	-	Not possible
	Leads detection	No	-	Yes
	Pressure ridge size and distribution	No	-	Possible
	Snow depths	Yes	model	Possible
Cross-disciplinary	Iceberg Density	Yes	RS	Yes
Physical Ocean	SST (EOV)	Yes	both	Yes
	SSS (EOV)	Yes	both	Yes
	SSH (EOV)	Yes	both	Yes
	Surface geostrophic currents (EOV)	Yes	RS	Yes
	Surface currents (EOV)	Yes	model	possible
	Subsurface Temperature (EOV)	Yes	model	Not possible
	Subsurface salinity (EOV)	Yes	model	Not possible
	Subsurface Currents (EOV)	Yes	model	Not possible
Sea state	Sig. wave heights	Yes	both	Yes
	Surf. Stress (Wind)	No	-	Yes
	Spectra	No	model	Possible (SWIM on CFOSAT)
	Peak Period	Yes	model	Yes (from spectra)
	Ocean Albedo	No	-	Yes
Biogeochemical Ocean	Oxygen (EOV)	Yes	model	Not possible
	Ocean Colour (EOV)	Yes	RS	Yes

Co-funded by the Horizon 2020 programme of the European Union

	Chl profiles (EOV)	Yes	model/RS(surface)	Yes (surface)
	Nutrients (NO2, NO3, NH4, PO4, Si, Fe) (EOVs)	Yes	model	Not possible
	Zooplankton (EOV)	Yes	model	Not possible
	Phytoplankton Group Chl (EOV)	Yes	RS	Yes (surface)
	Phytoplankton (PHYC+PP) (EOVs)	Yes	model	Not possible
	Light Attenuation (KD)	Yes	both	Yes

[1]: See Deliverable WP2.2, Annexe 1, 2 and 3 to have more information on the type of model that produces each parameter.

Table 2. 2: Cross-reference between land parameters provided by CLMS and which ones are/can be measured by remote sensing techniques.

Theme	Parameter	WP2.1 CLMS	CLMS product from MODEL/RS	WP3.1/3.3 Remote Sensing
Cryosphere	Snow cover extent	Yes	RS	Yes
	Snow water equivalent	Yes	RS	Yes
	Lake Ice Extent	Yes (Baltic region[1])	RS	Yes
	Lake Ice duration	No[2]	-	Yes
	Lake Ice Thickness	No	-	Yes[3]
	Snow melt	No	-	Yes
	Snow depth	No	-	Yes[4]
	Snow avalanche	No	-	Yes
	Permafrost	No	-	No[5]
Energy	Surface albedo	Yes	RS	Yes

Co-funded by the Horizon 2020 programme of the European Union

	Land Surface Temperature	Yes	RS	Yes
	Top Of Canopy Reflectance	Yes	RS	Yes (Not considered in this document)

[1]: Baltic region defined as upper left corner: 5ºE, 71ºN to lower right corner: 45ºE, 45ºN

[2]: Can in principle be derived from the daily Lake Ice Extent product, but regionally limited to the Baltic Sea region. Polar night is also an issue in the north as the lake ice extent product is based on MODIS. The product needs to be complemented with SAR-observations to capture the ice formation period.

[3]: Only for large lakes using PMR instruments.

[4]: Depending on the validation of the method suggested by Lievens et al. (2019). Low-resolution products could be derived from SWE (based on PMR measurements) via models for density.

[5]: Permafrost variables are not directly available via RS, but can be estimated in some cases by using certain parameters as proxies (ground deformation, land cover, water storage, lake extent), or by a combination of modelling and satellite data products of ground temperature, soil moisture, vegetation cover, and snow cover (see part 1 of this report).

Co-funded by the Horizon 2020 programme of the European Union

Section 3: Parameters from future missions

In this section, we discuss which impact the various upcoming satellite missions can have on the agreed list of land and sea parameters that Kepler wants to address. For each parameter/satellite combination where we see a synergy, we comment briefly on the impact the sensor could have on the retrieval of the parameter. In some cases, a new sensor could revolutionize the parameter retrieval, whereas for other parameters, information from the new sensor could advance knowledge, bridge gaps or by other means contribute to improvements in the product retrieval methods.

Table 3. 1 reports the parameters observable mainly with the future ESA HPCMs missions, since of course we cannot assess all planned missions from all countries. We have also presented a few other satellites we think could have a large impact. Below, the parameter quality and the advantages with respect to the current missions are discussed per parameters and following the numbers used in Table 3.

Table 3. 1: Cross-reference between land/sea parameters of relevance to Kepler/Polar regions and future satellite missions. Numbers refer to comments in the sections following the table.

Parameter	**HPCM Satellites**							
Land	**CHIME**	**CIMR**	**CO2M**	**CRISTAL**	**LSTM**	**ROSE-L**	**FORUM**	**Others**
Snow extent		1				2	3	
Snow wetness					1	2		
SWE	1	2		3		4		5,6
Snow depth		1				2		
Snow albedo	1							
Avalanche						1		
Lake ice extent					1	2		
Lake ice thickness	1			3		2		
Permafrost		1		2	3	4		

Co-funded by the Horizon 2020 programme of the European Union

Soil moisture		1				2		
Soil organic carbon content (SOC)	1[1]							
Biophysical vegetation parameters (e.g. LAI, FAPAR)	1[1]							
Inland water biogeochemical parameters (PFT, Chl, etc.)	1							2
Sea ice / Ocean	**CHIME**	**CIMR**	**CO2M**	**CRISTAL**	**LSTM**	**ROSE-L**	**FORUM**	**Others**
SI Concentration		1				2		
SI Thickness (>1m)				1				
Thin SI Thickness (<0.5m)		1				2		3, 4
SI Drift		1				2		
SI Type		1		2		3		
Snow-depth on SI		1		2		3		
Melt ponds								1
Icebergs				1		2		
SI Surface Temperature		1						
Sea Surface Temperature		1						
Sea Surface Salinity		1						2

Co-funded by the Horizon 2020 programme of the European Union

Ocean Winds		1				2		3
Ocean Colour	1							
Atmosphere	**CHIME**	**CIMR**	**CO2M**	**CRISTAL**	**LSTM**	**ROSE-L**	**FORUM**	**Others**
CO_2 & CH_4 concentration			1[1]					

[1]: These parameters are included here for completeness but are not discussed in Section 1 because the focus of this report is on cryosphere-relevant parameters. For more details on these parameters see Deliverable WP2.1 which reports on the parameters served in the Copernicus Land Monitoring Service.

3.1 Land surfaces

Snow extent/area

1: <CIMR> shall generate L2 products of terrestrial total snow area with a standard total uncertainty of ≤ 10 % at a spatial resolution of ≤15 km with daily coverage of the Polar Regions. [MRD-950 in CIMR MRD v3]

2: <ROSE-L> contribution with wet snow detection in multi-sensor approaches for snow cover fraction estimation (see also Snow wetness-ROSE-L).

3: <FORUM> information from the far-infrared spectrum could be used for separating snow/bare ground during night time (polar darkness) when normal sensors have little sensitivity. The coarse-scale is, however, a challenge in matching products.

Snow wetness

1: <LSTM> Surface snow metamorphism can be studied.

2: <ROSE-L> more penetration, potentially more sensitive to degrees of wetness.

Snow Water Equivalent (SWE)

1: <CHIME> can potentially be used to quantify surface snow grain size distribution (SSG). Snow grain size has an impact on radar backscatter on high frequencies (>8 GHz), and is important for several SAR retrieval algorithms for SWE (synergy with SWE5) [(CHIME MRD, section 3.2.3.2 Hydrology/ Cryosphere)].

2: <CIMR> shall generate L2 products of terrestrial snow water equivalent (SWE) with a standard total uncertainty of < 40 mm at a spatial resolution of ≤15 km with daily coverage of the Polar Regions. [MRD-960 in CIMR MRD v3].

3: <CRISTAL> (CRISTAL MRD).

Co-funded by the Horizon 2020 programme of the European Union

4: <ROSE-L> SWE can be retrieved by repeat pass interferometric techniques. At L.band, the decorrelation is less critical (see below: snow depth). For incidence angles < 40 degrees, the relationship between phase delay and SWE is almost independent of snow density. Theory shows that an L-band (35 deg incidence angle) 130 mm water equivalent causes a phase shift of 2pi, which corresponds to about 0.5 m snow depth, whereas one fringe at C-band is equivalent to 11 cm snow depth. (ROSE-L MRD)
5: X-band sensors such as Iceeye, in tandem with C-band or higher frequencies (Ku/Ka) can potentially be used in backscatter based retrieval algorithms to resolve ambiguities.
6: NISAR and other 3rd party L-band SAR missions (see also SWE-ROSE-L) could improve SWE retrieval via interferometry.

Snow depth
1: <CIMR> snow depth information can be derived from CIMR SWE-product (see SWE2) when density can be retrieved or assumed by other means.

2 <ROSE-L> From theory it is concluded that snow depths up to 0.5 m can be retrieved without ambiguities of the interferometric phase at higher incidence angles (> 30 deg). At C-band, the 2π phase ambiguities are already reached about 0.1 m snow depth. The use of L-band data is also beneficial because of the lower temporal coherence decay compared to C-band. Furthermore, the application of L-band has advantages in slightly vegetated areas because of the larger penetration depth compared to C- and X-band. In densely vegetated areas, snow depth retrieval also does not work at L-band (ROSE-L MRD).

Snow albedo
1: <CHIME> Hyperspectral information allows to derive knowledge of physical snow properties such as albedo.

Avalanche
1: <ROSE-L> Possible sensitivity to other types of avalanches.

Lake ice extent
1: <LSTM> Differentiate between various ice stages (snow-covered ice, bare ice, melting ice and partial ice) [LSTM MRD].
2: <ROSE-L> The combination of C- and L-bands improves the capability to distinguish ice and water and hence to determine lake ice extent.

Lake ice thickness

Co-funded by the Horizon 2020 programme of the European Union

1: <CIMR> L-band has the potential for measuring ice thickness (Tikhonov et al., 2018).
2: <ROSE-L> SAR images acquired at X-, C-, and L-band have been used to distinguish between the floating ice and bedfast ice regime. Comparisons with field measurements revealed achievable accuracies of 93% using C-band imagery (Engram et al., 2018). L-band reveals less sensitivity since it is affected by the presence of large ebullition bubbles trapped under or in lake ice which may complement information related to studies of methane flux (Engram et al., 2013). X-band intensities were used in conjunction with an ice growth model to determine lake ice thickness and showed a good agreement (Antonova et al., 2016). Since the penetration depth is larger at L-band, ROSE-L data may also be useful for ice thickness retrieval.
3: <CRISTAL> Snow depth (on sea ice and glaciers) is one of the objectives of CRISTAL (see MRD). Lake ice thickness and snow depth on lake ice can potentially also be measured on large and medium-sized lakes according to Beckers et al., 2017.

Permafrost
Permafrost variables are not directly observable from space, but can often be estimated from one or several proxies (ground deformation, land cover, water storage, lake extent) or a combination of modelling and satellite data products of ground temperature, soil moisture, vegetation cover, and snow cover. Thus, permafrost can particularly profit from synergistic use of several instruments.
1: <CIMR> can generate products of snow cover and depth.
2: <CRISTAL> Land elevation change, and the snow and surface state are some of CRISTAL's mission priorities (see MRD).
3: <LSTM> Its main objective is the retrieval of land surface temperature with a spatial resolution target of 50 m. The thermal infrared sensor will enable day and night time measurements, and is designed to cover the full temperature range required for permafrost applications.
4: <ROSE-L> interferometry can quantify land surface movements due to freeze/thawing of the active layer. The retrieval of ground movement and deformation in vegetated areas is hardly possible with C- and X-band systems. An L-band SAR penetrates further through the vegetation canopy and provides stable long-term coherent information on the surface movement. ROSE-L backscatter information can be used to quantify freezing/thawing of the active layer (similar to S1, but L-band penetrates deeper, and can thus provide complementary information). Also, the L-Band SAR mission will provide the ability to monitor soil moisture conditions below the vegetation canopy over most vegetated land cover types throughout the growing season, with a spatial resolution of 1 km for L2 products.

Soil moisture
1: <CIMR> can similarly to SMOS (L-Band) and AMSR2 (C-band) PMR generate soil moisture or drought indices, but only when the soil is not frozen and at a rather coarse resolution. This

Co-funded by the Horizon 2020 programme of the European Union

can be useful as a precursor indication of forest fires. Since CIMR combines L- and C-band there is a potential for improved accuracy and resolution wrt SMOS and AMSR2.
2:<ROSE-L> The L-Band SAR mission will provide the ability to monitor soil moisture conditions below the vegetation canopy over most vegetated land cover types throughout the growing season, with a spatial resolution of 1 km for L2 products.

Soil organic carbon
1: <CHIME> Topsoil organic carbon content can be derived from hyperspectral imagery, potentially relevant for the carbon stored in Arctic peatlands and permafrost regions.

Biophysical vegetation parameter
1: <CHIME> Remotely sensed hyperspectral data together with radiative transfer modelling has the potential to provide high accuracy complex biophysical parameters such as e.g. LAI or FAPAR.
2: <ROSE-L> L-band enhances information and classification accuracy of land cover and land cover changes, in particular when combined with other Copernicus missions. L-band SAR generally provides clear distinction between vegetated and non-vegetated areas. It is hence useful for mapping forest/non-forest areas as well as the location and extent of broad forest types.

Inland water biogeochemistry
1: <CHIME> and 2: <NASA-PACE>: Hyperspectral imagery is expected to provide information on phytoplankton abundance, coloured dissolved organic matter and total suspended matter as can be derived from multispectral sensors such as OLCI. In addition, these hyperspectral satellite data sets are expected to reliably retrieve the abundance of phytoplankton types. For CHIME due to the sensor swath probably no open ocean region can be covered, however inland and coastal waters will be covered with a spatial resolution fine enough to resolve horizontal patterns in these waters. However, revisit time will be probably only every couple of days which probably only allows snapshots of these waters. However, NASA is planning to launch around 2023 the PACE hyperspectral ocean colour sensor which will allow for global ocean colour detection on a 1km scale within 1-2 days. It will especially deliver for the open ocean the possibility to retrieve phytoplankton types. The atmospheric satellite sensor SCIAMACHY (on Envisat) has been used to derive globally quantitative retrievals of major phytoplankton groups (see Bracher et al. 2009, Sadeghi et al. 2012). However, retrievals were limited by very large pixel size and low temporal resolution. Hyperspectral remote sensing reflectance data measured in water or above water (from stations or airplanes) have also been explored to enable the retrieval of phytoplankton groups at coastal or inland waters and develop further algorithms for future hyperspectral satellites like PACE and CHIME. National hyperspectral sensors have launched in the past (HICO, CHRIS-PROBA) so far have not delivered data sets on phytoplankton types, however the recently launched terrestrial

Co-funded by the Horizon 2020 programme of the European Union

sensors DESIS and PRISMA are currently explored to show if even sensors with a rather low signal to noise ratio in the blue and green band can also be used for phytoplankton retrievals over water. All these efforts are important to have algorithms ready when suited sensors like PACE and hopefully also CHIME will provide on an operational scale well-calibrated hyperspectral data sets.

3.2 Sea ice

Sea Ice Concentration

1: <CIMR> shall generate L2 sea ice concentration (SIC) and Sea Ice Extent (SIE) products at a spatial resolution of ≤5 km and a standard total uncertainty of ≤5% with sub-daily coverage of the Polar Regions and daily coverage of Adjacent Seas. [MRD-890 in CIMR MRD v3]. SIC is one of the two primary objectives of the CIMR mission.

2: <ROSE-L> The separation of open water and sea ice is a special case of ice type classification with only two classes. Since C- and L-bands reveal different sensitivities to the influence of wind on scattering from the open ocean, they complement one another and may improve the ice-water separation (further investigations required).

Sea Ice Thickness (>1m)

1: <CRISTAL> The system shall be capable of delivering sea ice thickness measurements with a vertical uncertainty of less than 0.1 m. The horizontal resolution of sea ice thickness measurements shall be 80 m. The system shall be capable of delivering sea ice thickness at a grid-scale resolution of at least 3 km. It shall be capable of delivering sea-ice thickness measurements within 24 hours of acquisition. [Several requirements under section 4.2.1 Sea Ice thickness in CRISTAL MRD v2].

Thin SI Thickness (<0.5m)

1: <CIMR> shall generate thin (≤0.5 m) sea ice thickness L2 data products in freezing conditions at a spatial resolution of <60 km, with a thickness standard total uncertainty goal of 10% and daily coverage of the Marginal Ice Zone in the Polar Regions and Adjacent Seas. [MRD-910 in CIMR MRD v3].

2: <ROSE-L> Correlations between ice thickness (up to 1.2 m) and the co-polarization ratio were reported at C-band. In another study, L-band was found to be less sensitive to the thickness of thin ice which may be due to a lower SNR. L-band offers the advantage of larger penetration depth and a lower sensitivity to frost flowers on thin lead ice. (Dierking et al., 2013).

3: <FSSCAT> They carry a dual microwave payload (a GNSS-Reflectometer and an L-band radiometer with interference detection/mitigation), and a multi-spectral optical payload to measure soil moisture, ice extent, and ice thickness, and to detect melting ponds over ice (Alonso-Arroyo et al., 2017).

4: <COSSM> The Chinese Ocean Salinity Satellite Mission will be launched in 2020 and will

Co-funded by the Horizon 2020 programme of the European Union

carry different sensors. Two interferometric L-band radiometers: one in Y shape form (similar to SMOS), and the other with 1D array as well as an active L-band. Moreover, the satellite will also carry on C and K-band microwave radiometers.

Sea Ice Drift

1: <CIMR> shall generate daily sea ice drift L2 products with a standard total uncertainty of ≤3 cm/s at a spatial resolution of ≤25 km with daily coverage of the Polar Regions and Adjacent Seas. [MRD-920 in CIMR MRD v3].

2: <ROSE-L> In general C- and L-band SAR images complement each other since single ice floes of different ages can be easier identified in C-band images, whereas structures such as ridges and cracks stand out more clearly at L-band. Both characteristics are useful for ice drift retrieval, the relative contribution of each frequency depends on the ice conditions. L-band SAR images provide more contrast during the melt and freeze-up periods and are hence preferable compared to C-band during the initial and final phase of the melting season (ROSE-L MRD).

Sea Ice Type / Stage of Development

1: <CIMR> shall generate the L2 Ice stage of development/Ice type products at a spatial resolution of <15 km with daily coverage of the Polar Regions and Adjacent Seas [MRD-930 in CIMR MRD v3].

2: <ROSE-L> For ice charting, L-band delivers information that is complementary to C-band. L-band is much better suited for the detection and characterization of ice deformation such as ridges, rubble fields and fractures, for delineation of ice floes, and for separating rough and smooth ice surfaces. This is necessary for operational ice services. Dependent on environmental conditions and ice cover characteristics, areas of thin ice may be easier to identify. L-band provides sufficient radar intensity contrast between first-year and multi-year ice during early melt onset and during the drainage phase of advanced melt. (ROSE-L MRD)

3: <FSSCAT> (GNSS-R + L-band radiometer): Sea ice edge, to be launched not before mid-2020 (Alonso-Arroyo et al., 2017).

Snow-depth on Sea Ice

1: <CIMR> shall generate snow depth on sea ice L2 products in freezing conditions with a standard total uncertainty of ≤10 cm at a spatial resolution of ≤15 km with daily coverage of the Polar Regions and Adjacent Seas. [MRD-940 in CIMR MRD v3].

2: <CRISTAL> The mission shall be capable of retrieving the depth of dry snow on sea ice. Derived from co-temporal observations at Ku- and Ka-band. The uncertainty of snow depth measurements over sea ice shall be less than 0.05 m. The horizontal resolution of snow depth retrievals over sea ice shall be identical to sea ice thickness. [Several requirements under section 4.2.3 Snow depth on sea ice in CRISTAL MRD v2].

Co-funded by the Horizon 2020 programme of the European Union

Icebergs

1:<CRISTAL> Altimeters can measure the height of relatively tall and flat icebergs (more common in the Southern Ocean, Tournadre, et al. 2008). This is limited by the along-track visibility of the altimeter instrument. Knowing the height of an iceberg can improve the accuracy of forecasting its path.

2:<ROSE-L> First investigations carried out by different operational ice centers and the International Ice Patrol IIP indicate that L-band may be more suitable to detect icebergs than C-band (report in preparation). More investigations are required, but in combination with Sentinel-1 C-band imagery, an L-band mission at least enhances iceberg detection. One reason is that L-band reveals a lower sensitivity to wind-effects on the ocean surface than C-band (ROSE-L MRD).

Sea Ice Surface Temperature

1: <CIMR> shall generate L2 products of Ice Surface Temperature (IST) in freezing conditions with a standard total uncertainty of ≤1.0 K at an effective spatial resolution of ≤15 km with daily coverage of the Polar Regions and Adjacent Seas [MRD-970 in CIMR MRD v3].

3.2 ocean

Sea Surface Temperature

1: <CIMR> shall generate L2 Sea Surface Temperature (SST) products at a resolution of 15 km in the open ocean, with a standard total uncertainty of 0.2 K for 95% global coverage and sub-daily coverage in the Polar Regions and Adjacent Seas [MRD-900 in CIMR MRD v3]. SST is one of the two primary objectives of the CIMR mission.

Sea Surface Salinity

1: <CIMR> shall generate daily L2 products of sea surface salinity (SSS) over the 95% global ocean from at a resolution of <60 km and a standard total uncertainty of ≤0.3 pss over monthly timescales [MRD-980 in CIMR MRD v3].

2: <COSSM> The Chinese Ocean Salinity Satellite Mission will be launched in 2020 and will carry different sensors. Two interferometric L-band radiometers: one in Y shape form (similar to SMOS), and the other with array form (one dimension) as well as an active L-band. Moreover, the satellite will also carry C and K-band microwave radiometers.

Ocean Winds

1: <CIMR> shall generate daily L2 products of wind speed and direction over 95% global ocean at a resolution of <40 km (TBC) and a standard total uncertainty of ≤2 ms -1 [MRD-990 in CIMR MRD v3].

2: <ROSE-L> Enhancements to existing information obtained at C-band are expected since L-

Co-funded by the Horizon 2020 programme of the European Union

band may likely reveal a higher sensitivity to high wind speeds due to lack of saturation in the signal. This promises better measurements needed for, e.g., better predictions of the fate of hurricanes (ROSE-L MRD).
3: <COSSM> The Chinese Ocean Salinity Satellite Mission will be launched in 2020 and will carry different sensors. Two interferometric L-band radiometers: one in Y shape form (similar to SMOS), and the other with a 1D array as well as an active L-band. Moreover, the satellite will also carry C and K-band microwave radiometers. L-band radiometer can detect very high winds (Reul et al., 2016).

Ocean Colour
1: <CHIME> For coastal waters, see text under Inland Water Biogeochemistry

Melt Ponds
1: <FSSCAT> This mission will carry a dual microwave payload (a GNSS-Reflectometer and an L-band radiometer with interference detection/mitigation), and a multi-spectral optical payload that could be used for the detection of melting ponds over ice (Alonso-Arroyo et al., 2017).

3.4 Atmosphere

CO_2 & CH_4
1: <CO2M> provides total column concentrations of CO_2 and CH_4 in the atmosphere, which is an integrated signal of air-sea and air-land exchange fluxes of these greenhouse gases [CO2M MRD].

Co-funded by the Horizon 2020 programme of the European Union

Section 4: Feasibility of synergies

For the HPCM missions, synergies between the Radar Observing System for Europe at L-band (ROSE-L), the Copernicus Imaging Microwave Radiometer (CIMR), and the Copernicus polar Ice and Snow Topography ALtimeter (CRISTAL) are recently under discussion. The findings reported below are derived from former radar, passive radiometer, and radar altimeter missions and are hence of a broader validity. Synthetic Aperture Radar (SAR), scatterometers, passive microwave radiometers (PMR) and radar altimeter (RA) missions differ considerably in their technical design and major monitoring tasks, as defined in other sections of this report.

The tables below review the potential synergies that have been identified, organized by land, sea-ice and ocean targets. The proposed synergies are supported by published papers that emphasize the feasibility of those new products. Moreover, the HPCM missions which could also provide new products are also specified. Users of these new products are identified following the WP1 definition (intermediate users, land end-users and ocean end users). Finally, the type of societal impact is assessed in three categories: high, middle and low impact.

4.1 Synergies for land applications

A wide range of synergies can be envisaged for the land parameters we consider (snow cover fraction, snow water equivalent, snow depth, snow wetness, avalanche and lake extent/thickness, soil moisture). By using SAR together with optical sensors several studies have shown that retrieval of snow cover fraction can be improved during periods of cloud cover. Similarly, snow water equivalent products may be improved at the edge of the snow cover or for low values of SWE (limited sensitivity) by combining SWE estimates (at low spatial resolution) with snow cover fraction (at higher spatial resolution) see e.g. Muñoz et al. (2013). Also in the case of SWE retrieval using ROSE-L, optical or even C-band SAR snow products may play a synergistic role in masking out false SWE retrievals during no-snow conditions, or low estimates of SWE during wet snow conditions. Snow wetness (using C-band SAR) can also be improved by taking into account optical snow cover data to allow separation between dry snow and bare soil, which C-band SAR data usually are insensitive towards. Within snow avalanche monitoring there is a potential to combine SAR detection of avalanches with optical detections. In a study at Greenland (Aberman et al., 2019) showed that some avalanches were only observable by optical sensors (S2), whereas many others were only seen by SAR (S1). Combining the observations would obviously result in better mapping.

Current Lake ice extent products based on medium resolution optical sensors (MODIS/S3) can be improved significantly in Arctic regions by combining them with SAR derived ice cover, in particular during the polar night period when ice formation occurs, but also allowing more precise mapping of the ice break up period when the timing is crucial and optical observations often suffer due to cloudiness. Lake ice thickness estimates can potentially be improved by combining radar altimeter

Co-funded by the Horizon 2020 programme of the European Union

measurements with other sensors like Lidar (ICESat-2) even other sensors (SAR, optical or even passive microwave sensors for the largest lakes).

Permafrost variables are not directly observable from space, but can often be estimated from one or several proxies (ground deformation, land cover, water storage, lake extent) or from a combination of modelling and satellite data products of ground temperature, soil moisture, vegetation cover, and snow cover. Thus, permafrost can particularly profit from synergistic use of several instruments, specifically CIMR (snow cover & depth, soil moisture), CRISTAL (snow & surface state, land surface movements), LSTM (land surface temperature), and ROSE-L (land surface movements, freeze/thawing data, soil moisture).

Soil moisture products are based on L-, C-, X and K-band radiometers or SARs. In general, soil moisture estimated from radiometry is more accurate than that from SAR, but radiometers have a coarse spatial resolution. In the last decade, several polynomial or physical-based methods have addressed the soil moisture disaggregation (with a resulting resolution of 100 m-10 km). Two different strategies were used: i) synergy of passive microwave + optical and thermal infrared (TIR) data and ii) synergy of passive + active microwave data. For instance, SMOS was combined with optical and TIR data from MODIS in a soil evaporative efficiency model (Merlin et al., 2008) and in a linear model (Piles et al., 2011; 2014; Portal et al., 2018). SMAP was also combined with ASTER and Landsat-7 data (Merlin et al., 2013) and SEVIRI data (Piles et al., 2016). In SMAP, active and passive L-band data were combined (Das et al., 2014) and also passive L-band with C-band SAR data from Sentinel 1 (Das et al, 2019).

The above synergies are resumed in Table 4. 1.

Table 4. 1: Synergies for land applications, specifying the HPCM sensor who could provide the synergy and references.

Parameter	Sensor combinations	Synergy aspect	HPCM provide the synergy	Current synergy & Reference
Snow extent	SAR + optical + PMR	Optically based Snow extent products can be improved during polar nights and cloudy conditions by taking SAR (wet snow) and PMR (dry snow/presence of snow). In complex terrain where PMR fails, ROSE-L SWE retrievals may play a role. **Beneficiary**: Intermediate Users	ROSE-L, CIMR, CHIME	S1/S2/S3 AMSR-2

Co-funded by the Horizon 2020 programme of the European Union

		Impact: high impact		
Snow water equivalent/ Snow depth	PMR + SAR + optical	SWE estimates from PMR can be improved taking into account higher resolution products. **Beneficiary**: Intermediate Users and land end users **Impact:** high impact	CIMR, ROSE-L CHIME	S1, S3, AMSR-2Muñoz et al. (2013)
Snow wetness / LWC (Liquid water cont.)	SAR, Optical	Optical snow extent products can be used to differentiate between dry snow/bare soil in wet snow detections from SAR. LWC retrieval should be considered. Assimilation with hydrological models is needed to quantify LWC. **Beneficiary**: Intermediate Users **Impact:** middle impact	ROSE-L, CHIME	S1, S2 , S3
Snow Avalanche monitoring	SAR, Optical	Optical sensors can contribute to improving SAR detections of avalanches under unfavourable conditions (masked terrain/small avalanches). **Beneficiary**: Land end users **Impact:** high impact	ROSE-L, CHIME	S1, S2 Aberman et al., 2019
Lake ice extent	Optical, SAR	SAR can improve optically based lake ice extent products during polar night/cloudy conditions **Beneficiary**: Intermediate and land end users **Impact:** middle impact	ROSE-L, CHIME	S2/S3 + S1

Co-funded by the Horizon 2020 programme of the European Union

Lake ice thickness	RA, LIDAR, PMR, SAR, Optical	Several sensor combinations could be used to quantify errors in thickness estimates from RA and generalize the estimates outside the RA-footprints on the lakes (similarities of ice types). **Beneficiary**: Intermediate and land end users **Impact:** middle impact	CIMR, CRISTAL, CHIME	RA (CryoSat)+ S1/S2/S3
Permafrost	PMR, RA, Thermal, SAR	Permafrost estimation by combining several RS proxies and/or RS data and model runs. **Beneficiary**: Intermediate and land end users **Impact:** high impact	CIMR, CRISTAL, LSTM, ROSE-L	RA (CryoSat), S1 Landsat, TerraSAR-X, MODIS, GRACE Trofaier et al., 2017
Soil Moisture	PMR, Optical, SAR	Improved spatial resolution **Beneficiary**: Intermediate and land end users **Impact:** middle to high impact	CIMR, CHIME, ROSE-L	SMOS, SMAP, MODIS, SEVIRI, ASTER, Landsat7, S1. Piles et al, 2016; Portal et al., 2018; Merlin, et al., 2013; Das et al., 2019.

Co-funded by the Horizon 2020 programme of the European Union

The practical implementation of the respective data fusions, however, depends on the designs of the different missions regarding orbit constellations and acquisition times relative to each other.

4.2 Synergies for ocean and ice applications

Over the oceans, SAR systems are used, e.g., for wind speed and wave spectrum retrieval, oil spill monitoring, ship and iceberg detection, and sea ice classification, and drift retrieval. Data from scatterometers are beneficial for their synoptic coverage, e.g., for wind speed and direction retrieval over the ocean, for monitoring of snow cover and sea ice extent, sea ice classification, retrieval of sea ice drift, and start and end of the melting season over sea ice and the ice sheets. Passive microwave imagers can be employed to determine, e.g. surface temperature, wind speed and direction, sea surface salinity, ice concentration, ice extent, thin sea-ice thickness, ice drift and timing and duration of the ice melting season over the ocean, or timing and extent of melting of the Greenland and Antarctic ice sheets. The primary objectives of radar altimeters are to measure and monitor the variability of Arctic and Southern Ocean sea-ice thickness, as well as the surface elevation and changes of glaciers, ice caps and the Antarctic and Greenland ice sheets. This list demonstrates that synergies are possible by combining instruments with different spatial resolutions and spatial coverage, different penetration depths into the ground, and different sensitivities to single geophysical parameters. A caveat to this is that all microwave sensors have limitations as to their utility over ice and snow surface during melting conditions. As this is the period of most activity in the polar regions, additional synergies with cloud-free optical data, and other sources of data including *In situ* and forecast models are necessary.

The feasible synergies on sea ice and ocean applications are resumed in Table 4. 2. It also contains information on the User (intermediate or end-user) and the impact of the synergy.

Table 4. 2: Possible synergies for sea ice and ocean applications with the list of the possible HPCM providing them and references.

Parameters/Task	Sensor combinations	Synergy aspect	HPCM provide the synergy	Current synergy & reference

Co-funded by the Horizon 2020 programme of the European Union

Global sea-ice concentration and sea ice type separation.	SAR and PMR	With their hemispherical view, PMR data define the boundary conditions for regional maps of SAR concentration/type mapping. SAR images are used to "sharpen" the PMR data, reduce ambiguities, and potentially provide coverage of sea ice concentrations below the level of PMR detectability. **Beneficiary**: Intermediate users **Impact:** middle to high impact	CIMR & ROSE-L	AMSR-2, S1 For SIC: Karvonen, 2014. Wang et al. (2016)
Global sea ice drift mapping	SAR and PMR (potential VIS/IR as well)	With their hemispherical view, PMR data define the boundary conditions for regional maps of ice drift. Within SAR coverage, PMR adds more frequent revisits. VIS/IR can complement at intermediate resolution (cloud permitting). **Beneficiary:** intermediate users **Impact:** middle impact	CIMR & ROSE-L	AMSR2 and S1 (not realized today).
Calibration and validation of PMR data products	SAR, PMR and optical/thermal radiometers	The high spatial resolution of SAR and optical/thermal radiometers permits the calibration and validation of data obtained from PMR. A key element is the summer season where sea ice concentration, type, and melt-pond fractions are available from SAR or optical/thermal radiometers but are an ambiguity for PMR. **Beneficiary**: Intermediate users **Impact:** middle to high impact	CIMR, ROSE-L & CHIME	AMSR-2, S1, S3 For melt-ponds: Kern et al. 2020.

Co-funded by the Horizon 2020 programme of the European Union

High-resolution sea ice mapping concentration and type mapping to support maritime end users.	SAR and optical/thermal radiometers	Improved automatic classification of sea ice concentration and type through a combination of multi-polarimetric SAR at different frequencies. Low frequency (L-band) SAR provides greater penetration into the ice and higher contrast for deformation features. High spatial resolution of SAR and optical/thermal radiometers are complementary in providing information on sea ice rheology. **Beneficiary**: Intermediate users & Marine end users **Impact:** high impact	S1 & ROSE-L, S2, S3 CHIME	S1, S2 and S3 For SAR frequencies: Singha et al, 2018.
Thickness retrieval for thin ice classes	SAR, PMR, and thermal radiometers	The thickness of thin ice can be retrieved from PMR (L-band), thermal radiometers, and from L-band SAR data. Scales are different: with PMR one obtains the average thickness over areas > 50 km in extension, whereas SAR and thermal radiometers are optimally suited for retrieving changes of thin ice thickness on scales of 10s of meters. Mutual comparisons of the thickness retrievals are helpful in judging the reliability and robustness of the individual results. **Beneficiary**: Intermediate users & Marine end users **Impact:** high impact	CIMR, ROSE-L & CHIME	SMOS, S1, S3 Kaleschke et al. 2012; Dierking, 2013

Co-funded by the Horizon 2020 programme of the European Union

Ice type separation Ice age	SAR, RA, and PMR. (specifically S1, ROSE-L, and CIMR), and optical/thermal radiometers	CRISTAL is planned as a dual-frequency altimeter system operating at Ku and Ka-band, which provides data along with profiles from which the thickness of sea ice and potentially of the snow layer on the ice can be retrieved with a horizontal resolution of 80m. Ice thickness profiles and indications of the presence of snow on the ice may be used to complement the ice classification based on SAR imagery. Sea ice type information can also be retrieved from PMR by exploiting the difference in emissivity of the different ice types. Sea ice age can be computed with ice drift from PMR, supplemented with *In situ* (buoys) or other satellite sensors including SAR or optical during the melt season, and used as an input to freeboard-to-thickness conversion, and to tune and quality control PMR-based sea-ice type information. Sea ice type classification from microwave sensor synergies will work outside of the melt season, but will be reliant on synergy with *In situ* data and optical sensors during the melt season. **Beneficiary**: Intermediate users **Impact:** middle impact	CRISTAL, ROSE-L & CIMR	AMSR-2, CryoSat, S1, S3

Co-funded by the Horizon 2020 programme of the European Union

Tracking of sea ice thickness and deformation evolution	RA and SAR	Sea ice deformation data can be retrieved with lower frequency (L-band) SAR, providing improved deformation mapping capability, RA data deliver ice thickness profiles. **Beneficiary**: Intermediate users **Impact:** middle impact	CRISTAL, ROSE-L	CryoSat, S1 Hendricks et al., 2011
Retrieval of iceberg properties	RA and SAR	For icebergs that are equal or larger than the altimeter footprint, RA may deliver iceberg height and SAR areal extension (i.e.horizontal cross-section). Low frequency (L-band) SAR provides better detection of icebergs within sea ice. **Beneficiary**: Intermediate users & Marine end users **Impact:** middle impact	CRISTAL, ROSE-L	Tournadre et al., 2008
Global Sea-ice thickness maps **(already operational in CMEMS)**	RA and PMR	Outside of the melt season; 1) Sea-ice thickness maps for all range of thickness can be obtained by merging RA thick sea- ice thickness and L-band PMR thin sea-ice thickness, and 2) PMR provides ice age which can either be input to ice thickness calculations or directly approximate ice thickness. **Beneficiary**: Intermediate users **Impact:** high impact	CIMR & CRISTAL	CryoSat, SMOS Ricker et al., 2017 Guerreiro et al. 2017, Liu et al. 2020
Sea and Ice Surface Temperature	PMR and IR imagery	PMR (with C-band microwave frequency) can measure cold polar SST, IST through clouds. IR radiometers can measure it more accurately, but not through clouds.	CIMR and Sentinel-3 (SLSTR)	S3, ASMR-2 Dybkjær et al., 2018

Co-funded by the Horizon 2020 programme of the European Union

(already operational in CMEMS)		PMR and IR imagery can be combined to achieve improved SST and IST products, particularly for the coastal zone. **Beneficiary**: Intermediate users **Impact:** high impact		

4.3 Synergies for ocean biogeochemistry applications

Synergies between different sensors retrieving information on surface biogeochemistry products in ocean, coastal and inland waters have been scarce. Two example studies by Losa et al. (2017) and Vanhellemont et al. (2014) have shown that the combination of different sensor types can improve especially the products temporal and spatial resolution and coverage (see Table below).

By combining via optimal interpolation the hyperspectral SCIAMACHY with the multispectral OC-CCI PFT-CHL products the synergistic SynSenPFT algorithm has been developed (Losa et al. (2017)). This led to daily and 4 km by 4 km resolved PFT-CHL data set from 2002 to 2012 globally which enabled to overcome the limitations of the two input algorithms: SCIAMACHY PFT products which are based on analytical inversions are limited by the coarse spatial and temporal coverage of the atmospheric sensor SCIAMACHY. Multispectral ocean color PFT-CHL products are based on purely empirical derived functions for each PFT which have a good spatial and temporal coverage. Recently SynSenPFT products were used for evaluating the successful OC-CCI CHL data assimilation into a global coupled ocean biogeochemical global model predicting PFTs (Pradham et al. 2019) which would not have been possible for the low coverage SCIAMACHY products themselves. Applying analytical methods to retrieve PFTs from the current atmospheric sensor on S5P in synergy with the even higher spatially (300 m) resolved and slightly higher temporal (~1 day) resolution data of S3 ocean color sensor OLCI will prolongate the previous global PFT-CHL data set supplying better resolution needed in more dynamical systems such as the coastal ocean. Combining coastal or inland water retrievals from high spatial but low temporal resolved hyperspectral data from national sensors (DESIS, PRISMA, EnMAP) and HPC-CHIME, with S3 OLCI data, will enable high spatial and temporal resolved PFT-CHL data in these waters which are urgently needed in these hotspots for human activities (recreation, pollution, fisheries,...). Similarly to PFT-CHL products also phytoplankton fluorescence products can benefit from combining hyperspectral land or atmospheric sensors with ocean color sensors.

The geostationary meteorological sensor SEVIRI with a single visible band has demonstrated capability to observe suspended particulate matter (SPM) and turbidity dynamics, however, with high uncertainty (e.g., Kwiatkowska et al., 2016). SEVIRI turbidity and SPM products have been used in synergy with the same, but high quality and high spatially resolved, products of polar-orbiting ocean colour sensor MODIS-A (Vanhellemont et al., 2014). The resulting product is an improvement over both data sources especially in the highly dynamic coastal waters. A geostationary ocean colour sensor

Co-funded by the Horizon 2020 programme of the European Union

over Europe would provide invaluable data concerning our marine environment. The cost of increasing the spatial resolution of a geostationary sensor is very high, so combining a lower spatial resolution geostationary ocean colour sensor with a high resolution polar orbiting sensor, can provide a high frequency synergetic product with high spatial resolution. Likewise, the forthcoming Meteosat Third Generation meteorological-focused Flexible Combined Imager has three visible bands and simulations have shown CHL retrieval capability if data are averaged in space and time (Lavigne and Ruddick,2018). In addition, combining geostationary hyperspectral Sentinel-4 UVN PFT-CHL retrievals with S3 could enable even much higher coverage of PFT-CHL products over the entire Atlantic and European Waters.

Table 4. 3 : Synergies for ocean biogeochemistry applications, specifying the HPCM sensor who could provide the synergy and references

Parameter	Sensor combinations	Synergy aspect	HPCM provide the synergy	Current synergy & reference
Global Ocean PFT CHL	High spectral atmospheric (SCIAMACHY) and multispectral ocean color sensor	Phytoplankton group biomass (PFT CHL) at high temporal (daily) and spatial (4 kmx4 km) resolution in the global open ocean, in future also for coastal and inland applications and also for marine CHL-fluorescence; currently S3/S-5P synergy developed. **Beneficiary**: Intermediate users **Impact:** high impact	HCPM + Sentinels	SCIAMACHY, S2, S3 Losa et al. 2017
Total suspended matter, turbidity, PFT-CHL	Geostationary SEVIRI with ocean color MODIS-A	Combination of high temporally resolved but bad quality geostationary data enabled to enlarge tremendously the temporal resolution of standard ocean color products, such as SPM and turbidity. In the future with CHIME and S4 also PFT-CHL should be possible. **Beneficiary**: Intermediate users **Impact:** high impact	HCPM (CHIME) + Sentinel 4	Modis, S4 Vanhellemont et al. 2014

Co-funded by the Horizon 2020 programme of the European Union

Section 5: Analysis of the assimilation of parameters into models

Data assimilation is searching for an optimal compromise between a numerical model background and observations. Since both background and observations have uncertainties, the assimilation analysis cannot match them perfectly. In addition to that, data assimilation methods are based on basic statistical assumptions that are often violated in reality, so the use of data assimilation may at times lead to "collateral damage" or assimilation biases that would otherwise not appear without the use of data assimilation. This means that there are various reasons why the assimilation of some types of observations may be of limited efficiency or at worst left out completely. Depending on the variables, one may blame the observations, the models or the assimilation methods (or any combination of the three as the least observed processes are often the least well simulated).
In the present section, we have considered the data assimilative models used in the Copernicus services CMEMS, C3S and CLMS and reviewed their data assimilation capabilities, problems and deficiencies. Data assimilation demonstrations outside Copernicus that have been published but not yet taken up by Copernicus Services will appear in Section 4.2 below. *In situ* data are not taken into account in this review, this has been done separately in a survey from the Copernicus *In situ* initiative (cf. EEA and EuroGOOS).

5.1 Study the constraints/limitations of the parameters already being assimilated

5.1.1 Marine: Ocean, sea ice and biogeochemical models

The limitations and constraints will be discussed based on scientific literature and to the best of the authors' knowledge of the field, see Table 5. 1. References are given when available. The "Severity" colour coding is a subjective measure of the quality of assimilation, which could ideally be replaced by a signal-to-noise ratio (to be defined, for example, as the forecast error divided by the climatological variability, or any other measure able to penalize incomplete coverage in space and time), we have not come that far however. The absence of colour coding signifies that the quality of assimilation is not sufficiently documented or known to the partners to emit a judgement.

Table 5. 1: list of variables currently being assimilated, the type of analysis, the sensor and the limitations.

Assimilated Variable	Real-time / reanalysis	Sensor	Cause / Blame
Ocean			
SSH (anomaly + mean)	NRT+RAN	RA + Gravi	Obs: ice masking

Co-funded by the Horizon 2020 programme of the European Union

SST	NRT+RAN	IR	Obs: Clouds
SST	NRT+RAN	PMR	Obs: Low resolution
Sea Ice			
SIT	RAN	RA, LA	Obs: auxiliary data[2], Seasonal
SIT	RAN+NRT	PMR	Obs: Detection limit (thin ice)[3]. Seasonal
Ice Drift	RAN+NRT	PMR	Model[4]
SIC	RAN+NRT	PMR	Obs: Melt ponds[5]
Biogeochemistry			
CHL	RAN	VIS	Mixed: models, obs (clouds) & assimilation

Colour coding: Severely limited, medium level of limitation, small limitations.

5.1.2 Land models

There is to our knowledge no assimilation of satellite land data as part of the Copernicus Land nor Climate Change Services as of today (ERA5-Land appears as a free land model run[6]). The CLMS provides observation products but no forecasts and the C3S Arctic reanalyses (by DMI and MET Norway) use land remote sensing data as a surface boundary condition, which does not constitute data assimilation *sensu stricto*.

The assimilation of land remote sensing data (SMOS soil moisture and binary snow cover information from a combination of satellites) is however practiced in land models and coupled land-atmosphere models, which are not *sensu stricto* Copernicus services (the integrated forecasting system at ECMWF for example). So their potential use for CLMS and C3S is included in Section 5.2.2 below.

2 Zygmuntkowska et al. 2014

3 Kaleschke et al. 2016

4 Sakov et al. 2012

5 Ivanova et al. 2015

6 https://www.ecmwf.int/en/newsletter/159/news/first-era5-land-dataset-be-released-spring

Co-funded by the Horizon 2020 programme of the European Union

5.2 Remotely sensed variables which are not yet being assimilated

This issue can be confused with the assimilation of satellite products at lower processing levels (see section 5.3). We consider in Table 5. 2 and Table 5. 3 the satellite products that are not being assimilated, neither high nor low level of processing.

5.2.1 Marine: Ocean, sea ice and biogeochemical models

Table 5. 2: List of marine remote sensing variables which are not currently being assimilated, the type of analysis, the sensor and the limitations. *Colour coding stands for: Severely limited, medium level of limitation, small limitations.*

Non-Assimilated Variable	Real-time / reanalysis	Platform	Cause / Blame
Ocean			
SSS	NRT+RAN	PMR	Obs[7]
Sea Ice			
SIT	NRT	RA, LA	Obs: Timeliness[8], Seasonality, representativeness[9]
IST	NRT+RAN	IR	Model
Ice Type	NRT+RAN	PMR + Scat	Assimilation[10]
Ice drift	NRT+RAN	SAR	Model[11]
Ice deformation	NRT+RAN	SAR	Assimilation

7 A study is ongoing under the ESA Arctic+Salinity project.

8 The timeliness of CryoSAT2 data is being improved from 30 days to ~7 days by the CMEMS SI TAC, this will remove the "timeliness" issue, however not the seasonality nor the representativeness.

9 Zygmuntowska et al. 2014

10 There are no methods available for multivariate assimilation of categorical data like ice type.

11 Model ice drift is mostly a diagnostic variable.

Co-funded by the Horizon 2020 programme of the European Union

Roughness	NRT+RAN	SAR	Obs[12]
Melt pond fraction	NRT+RAN	VIS	Mixed[13]
Albedo	NRT+RAN	VIS/IR	
Biogeochemistry			
Chl-a	NRT	VIS	Assimilation
Phytoplankton C	NRT+RAN	LA	Obs not available[14]
Optical properties	NRT+RAN	VIS	Assimilation[15]
PFT / SCC	NRT+RAN	VIS	Assimilation[16]
Waves			
Albedo	NRT+RAN	VIS/IR	
SWH	NRT+RAN	RA	Assimilation[17]
Swell	NRT+RAN	SAR	Assimilation[18]
Other			

12 No explicit model relating sea ice state to SAR intensity.

13 Zege et al. 2015

14 Phytoplankton carbon is derived from particle backscattering measurements retrieved from lidar. Observations by Behrenfeld et al., 2016 are not publicly available. Only on demand. https://www.nature.com/articles/ngeo2861

15 The assimilation of optical properties from ocean colour data has been demonstrated by Shulman et al. 2013, Ciavatta et al (2014, PML) in other areas than the Arctic (e. g. North Sea). The tests in the Arctic remain to be done.

16 Ciavatta et al. (2018, PML), Skákala et al. (2018, PML), Pradhan et al. (2020, AWI). In the Arctic - to be done.

17 Assimilation into the CMEMS ARC MFC wave model is planned for November 2020. It is already demonstrated in global models at Meteo-France (CMEMS GLO MFC, L. Aouf) and ECMWF (J. Bidlot).

18 Same as above.

Co-funded by the Horizon 2020 programme of the European Union

Iceberg density	NRT+RAN	SAR, VIS	Scope: downstream services

5.2.2 Land models

The CLMS is neither using models nor data assimilation at present, so the table below only refers to the land models used in C3S reanalyses. Land data are used as boundary conditions for atmospheric models rather than assimilated, so the efficiency of data assimilation cannot be commented on here. The suggestions below are based on research on land models. Greenland ice sheets and glaciers (Cryosphere) are not covered by the inventory below.

Table 5. 3: List of land remote sensing variables that are not currently being assimilated, the type of analysis, the sensor and the limitations. *Colour coding stands for Severely limited, medium level of limitation, small limitations.*

Model	Non-Assimilated Variable	Real-time / reanalysis	Sensor	Cause / Blame
Hydrosphere				
Snow	fSCA	RAN	VIS	Atmospheric forcing[19]
Snow	SWE	RAN	PMR	Obs: coarse resolution, forests, terrain[20]
Land	Land surface temperature	RAN	IR	
Land	Freeze-thaw	RAN	PMR	Obs: coarse + terrain-dependent
Permafrost	Degradation[21]	RAN	InSAR	Obs: case studies only
Soil moisture	Surface soil moisture	NRT+RAN	Scat + PMR	Mixed: Obs[22] + Model

19 Aalstad et al., 2018

20 Foster, et al. 2005.

21 This is omitted from the permafrost ECV definition.

22 Difficult retrievals in most Arctic land covers (rocks/mountains/lakes). Blyverket et al., 2019.

Co-funded by the Horizon 2020 programme of the European Union

River	Water level	RAN+NRT	RA	Obs: rivers perpendicular to satellite tracks[23]
Groundwater	Mass changes	RAN	Gravi	No large-scale model?
Lake	Lake Ice Area concentration	RAN+NRT	PMR	
Lake	Water level	RAN+NRT	RA	
Lake	Lake Surface Temperature	RAN+NRT	VIS/IR	
Biosphere				
Land Cover	Classification	RAN	VIS	Classes not adequate for polar land
Vegetation	Above-ground biomass	RAN	VIS	
Fire	Burnt Area	RAN+NRT	VIS/IR	No large-scale model.
Vegetation	FAPAR / LAI	RAN	VIS	
Albedo	Albedo (4 channels)	RAN	VIS/IR	

5.3 Towards the assimilation of satellite information at lower processing levels

In this section, we explore how Services (and generally modelling and forecasting applications) would benefit from going beyond the current status-quo (assimilation of daily/weekly/monthly averaged gridded satellite products) and start assimilating individual swaths (and/or scenes) of satellite-derived product in swath projection, and even directly raw satellite data.

5.3.1 Definition of Processing Levels

Satellite data producers use the terminology of “Processing Levels” to describe the type of processing

23 ESA ArcFlux Deliverable 08 from DTU Space: Nielsen et al. 2018. EFAS from ECMWF is not using any data assimilation at present.

Co-funded by the Horizon 2020 programme of the European Union

applied to a satellite product. The Processing Levels (often just “Levels”) range from Level-0 (raw satellite data, often only accessed by the Space Agencies in the ground segments) to Level-4 (fully processed, averaged, interpolated data), see Table 5. 4. The exact definition of each processing level leaves some room for interpretation, but the general rule is that higher processing levels are further away from the raw satellite measurements. Here we reproduce a well-accepted description of Processing Levels by the World Meteorological Organization (WMO, from data to products).

Table 5. 4: Description of Data processing level

Level	Generic description of data processing levels *(to be adapted to each instrument)*	
0	**Instrument and auxiliary data reconstructed from satellite raw data after removing communication artefacts**	
1	**Instrument data extracted at full original resolution, with geolocation and calibration information** *Sub-levels named 1a, 1b, 1c for LEO data and 1.0, 1.5 for GEO data*	**1a (1.0)** - Instrument counts with geolocation and calibration information attached but not applied **1b (1.5)** - Geolocation and calibration information applied to the instrument counts **1c** - Instrument specific For example, 1b data converted to Brightness temperature (IR) or Reflectance factor (VIS) **1d** - Instrument specific For example, same as level 1c with cloud flag (for sounding data)
2	**Geophysical quantity retrieved from single instrument data in original instrument projection** Note: For example, temperature, humidity, radiative flux	

Co-funded by the Horizon 2020 programme of the European Union

3	**Geophysical quantity retrieved from single instrument data, mapped on uniform space and time grid** Note: Can be retrieved on a multi-orbital (LEO) or multi-temporal (GEO) basis.
4	**Composite multi-sensor and/or multi-satellite product or result of model analysis of lower level data**

Level-0 products are only accessed in the ground segments to prepare Level-1 products (calibrated and geo-localized satellite observations). The geo-physical processing starts from Level-1"b" and results in a Level-2 product (e.g. sea-ice concentration, sea surface temperature,...) that is still in the sensing geometry of the satellite (e.g. a single swath of the instrument). Such Level-2 files are then processed and combined in several ways to produce "Level-3" files, that are generally resampled and reprojected to a fixed Earth-referenced grid (e.g. polar stereographic, rotated lat-lon, etc…). Some communities make the difference between Level-3S products (single orbits remapped on a fixed Earth-referenced grid) and Level-3C (several orbits remapped on an Earth-referenced grid, typically 1 day worth of satellite observations). Finally, Level-4 files generally involve combining data from several satellite sensors (sometimes adding *In situ* observations), and filling remaining data gaps in the map (e.g. the polar observation hole). These are general and broadly accepted descriptions but, as noted earlier, communities have their own sub-conventions and the lines are sometimes blurred between the processing levels.

Interestingly enough, the democratization of satellite Earth Observation data as promoted by the Copernicus programme contributed to moving the lines between the Processing Levels, since satellite observations are prepared to be more easily understood and ingested by non-expert users. This typically leads to remapping the satellite data at an earlier stage than Level-3, and performing the geophysical retrieval on these remapped data. This is typically the case for Sentinel-2 (all imagery prepared on tiles) and even some Sentinel-3 (SLSTR and OLCI) products. A typical example is CIMR, that will have a Level-1C product to hold calibrated measurements of brightness temperature (thus in the accepted Level-1 sense), but remapped into an Earth-referenced grid one swath at a time (thus with traits of a Level-3S).

We also note that the definition of these Processing Levels will typically have significant programmatic implications, since different entities might be in charge of the various elements. Taking the Copernicus programme as an example, the ground segments from Level-0 to Level-2 are typically handled by Space Agencies (ESA and EUMETSAT) and/or their sub-contractors, while the higher processing levels are often taken care of in the Services (e.g. CMEMS TACs or CLMS).

In any case, the availability of several Processing Levels for a given product (e.g. sea-ice concentration at Level-2, Level-3, Level-4) means that the users can choose the most appropriate Level for their

Co-funded by the Horizon 2020 programme of the European Union

application. Such a choice often involves trade-off analysis between usability (higher processing levels are "easier" to use) and needed accuracy (higher processing levels involve compositing and smoothing that might not be adequate for the application at hand). One such application is Data Assimilation in forecast models.

5.3.2 Data Assimilation of satellite-derived products at different processing levels

At present, the vast majority of the ocean and sea-ice forecasting models access and assimilate sea-ice products at high processing levels, which is Level-3 or above. Some forecasting centers use Level-2 observations of sea surface temperature (SST) or sea-level anomalies (SLA), but all have so far been using sea-ice products at Level-3 and above. Some data producers prepare sea-ice products at Level-2 (e.g. SIC by EUMETSAT OSI SAF or the University of Bremen) but these are not yet assimilated, even at expert centers like ECMWF. Assimilation of Level-1 (satellite radiances) is in use for weather prediction, but to our knowledge not in ocean/ice forecasting.

In this section, we discuss the challenges and opportunities of assimilating satellite-derived sea-ice products (among others) at different processing levels.

Status-quo: Data Assimilation of satellite-derived products at Level-3/Level-4

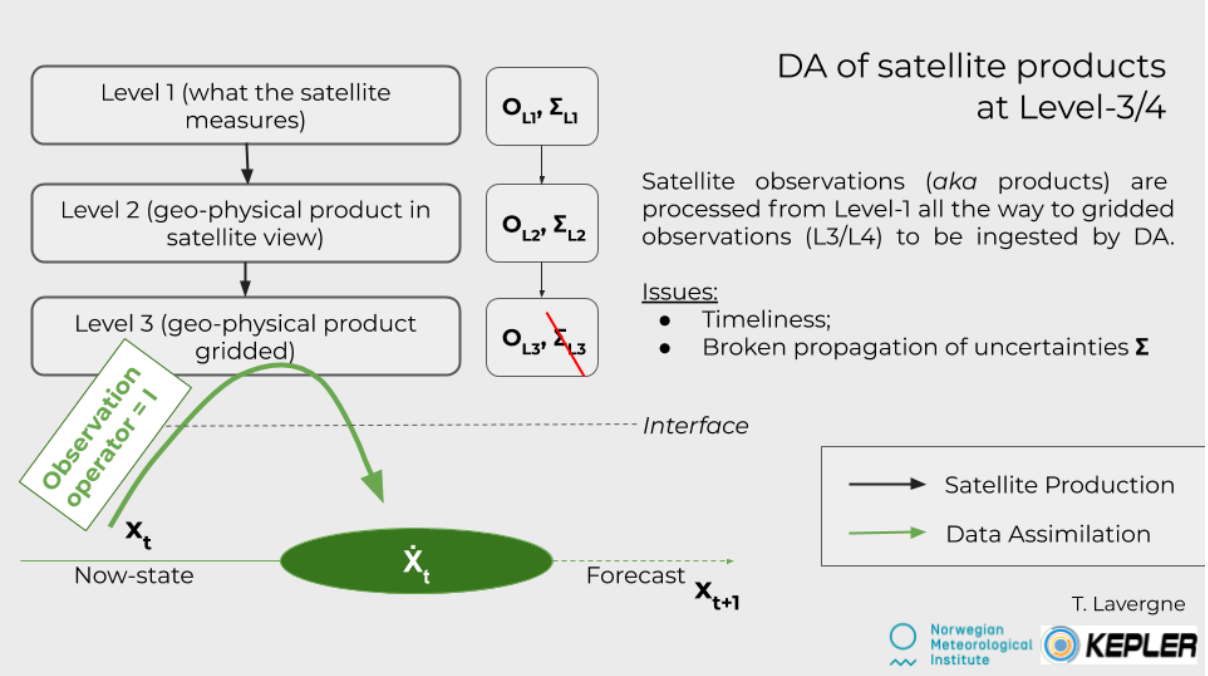

Figure 5.1: *Data Assimilation of satellite-derived products at Level-3/Level-4.*

Figure 5.1 illustrates the Data Assimilation of satellite-derived products at Level-3/Level-4. In black starting from the top-left corner is the classic satellite processing chain implemented in the ground

Co-funded by the Horizon 2020 programme of the European Union

segments or Copernicus Services and introduced earlier in this section. The raw satellite observations (Level-1) are combined through a geophysical algorithm into a Level-2 product (in satellite swath projection), which itself is further processed into a Level-3 (and/or Level-4) product. For DA purposes, it is important to note that the processing chains not only transfer observations (**O**) from Level-1 to Level-3/Level-4, but also the associated uncertainties (?).

In green at the bottom of the diagram, the forecast model and its Data Assimilation scheme produces an analyzed model state $\dot{x}_t$, from which the forecast to x_{t+1} is initialized. The DA scheme combines the now-state x_t (typically from a previous forecast) with observations. The bold green arrow is the Observation Operator and, in the case of DA at Level-3/Level-4 is identity (or a simple space/time interpolation in the model grid).

The interface between the Satellite Production (black) and the model forecast and DA "world" is symbolized with a horizontal dash line "Interface". Today, this Interface is often an interface between two distinct scientific communities: the Earth Observation experts do not know the details of the DA schemes, and the DA and modelling experts are not well known with how the satellite products are derived. The interface is also materialized physically by-product "files" (prepared by the satellite production schemes and accessed by the DA schemes) and by-product "documents" that aim at providing information on the content of the product files, the algorithms involved, known limitations, etc…

In the diagram above, which represents the status-quo for the ocean (and especially sea-ice) at time of running the KEPLER project, we note the transfer of uncertainty to Level-3 (?$_{L3}$) is striked through, indicating that the chain of uncertainties is broken, and that appropriate uncertainty is not available to users at Level-3. This interruption in the chain of uncertainties is for two main reasons: nature, and storage of the uncertainty information. The Level-3 processing step involves projecting the observations at Level-2 (in satellite swath projection) onto a fixed Earth-referenced grid. Thus, grid-cells in the Level-3 product files are assigned an observation value (e.g. an average of neighbouring Level-2 observations, weighted by the distance from the grid cell center to the position of the Level-2 observations). While computing these grid-cells values is unproblematic, the provision of associated uncertainties is a challenge as they typically include a non-negligible level of cross-correlation between neighboring grid cells, especially when the grid of the Level-3 product (or forecast model) is finer than the true resolution of the satellite observation at Level-2 (e.g. think of a satellite Field-Of-View covering several Level-3 grid cells). These covariances are by nature more difficult to compute, and - in any case- not possible to store in the Level-3 product files that are the interface between the satellite observations and the DA schemes. We note the difficulty to estimate and store Level-3 uncertainty will grow as the resolution of the forecast models increase (e.g. towards sub-km regional ocean/ice models to better serve marine operations) while the satellite observations stay at somewhat the same resolution (until new generations of satellites are available). We also note that when the spatial resolution of the satellite observation is much finer than that of the Level-3 product or model grid, there are fewer issues with storing the uncertainties (since the correlations of the uncertainties between grid cells are limited).

Co-funded by the Horizon 2020 programme of the European Union

Still in the same diagram, the second non-optimal element when assimilating Level-3/Level-4 satellite products is the poor timeliness/latency this approach allows. Since these types of products typically involve aggregating a day (sometimes 12 hours) worth of satellite data, they are made available once or twice a day, and the observations are several hours old when they reach the forecast model. This is maybe adapted when forecasts are initialized once a week or every few days, but if higher resolution ocean/ice forecast models are developed with DA in the future, they should fully benefit from the high timeliness of satellite observations in the Arctic region. This is even more so for sea-ice parameters like SIC and SIDrift that vary very rapidly (sub-daily), while ocean parameters like SST and SLA evolve more slowly in time.

In summary, the assimilation of Level-3/Level-4 sea-ice products in forecast models (status-quo) is suboptimal due to 1) the difficulty to prepare and transfer uncertainties associated to the satellite observations (especially when the forecast models evolve towards higher resolution), and 2) the limit this imposes on timeliness and access to up-to-date satellite observations.

In the next two sections, we will introduce and comment on the feasibility to assimilate satellite observations at lower processing levels (Level-2 and Level-1). Before doing so, we note that there also are good reasons for assimilating at Level-3/Level-4. Firstly, not all Data Assimilation methods can cope with Level-2 (or Level-1) data. For example, DA methods like Optimal Interpolation or nudging cannot handle well holes in space/time coverage of observations: they require complete grids of observations at all analysis times (one observation per grid cell). This is certainly one of the reasons why Level-3/Level-4 are prepared by satellite data products, and are still in wide use today. Second (and this is somewhat related), the basic DA methods cannot handle multi-variate transformations from the model state variables: only the model-state variables can be assimilated and there is no room in the formulation for Observation Operators that are not the Identity.

It must also be noted that, once having described the “theoretical” limitations of assimilating Level-3/Level-4 product files, we are not urging a change of Data Assimilation at all costs (increased software and mathematical complexity, increased data volumes, etc…). The adoption of lower-level products in Data Assimilation will be driven if and when the “theoretical” limitations imputed to the gridding process of the Level-3 files translate into sub-optimal forecasting skills.

In the next sections, we shortly describe the implications of adopting lower-level products (Level-2 and Level-1) in Data Assimilation for ocean/ice regional forecasting, as an approach to be developed in the middle term (Level-2) and long term (Level-1).

Mid-term: Data Assimilation of satellite-derived products at Level-2

Co-funded by the Horizon 2020 programme of the European Union

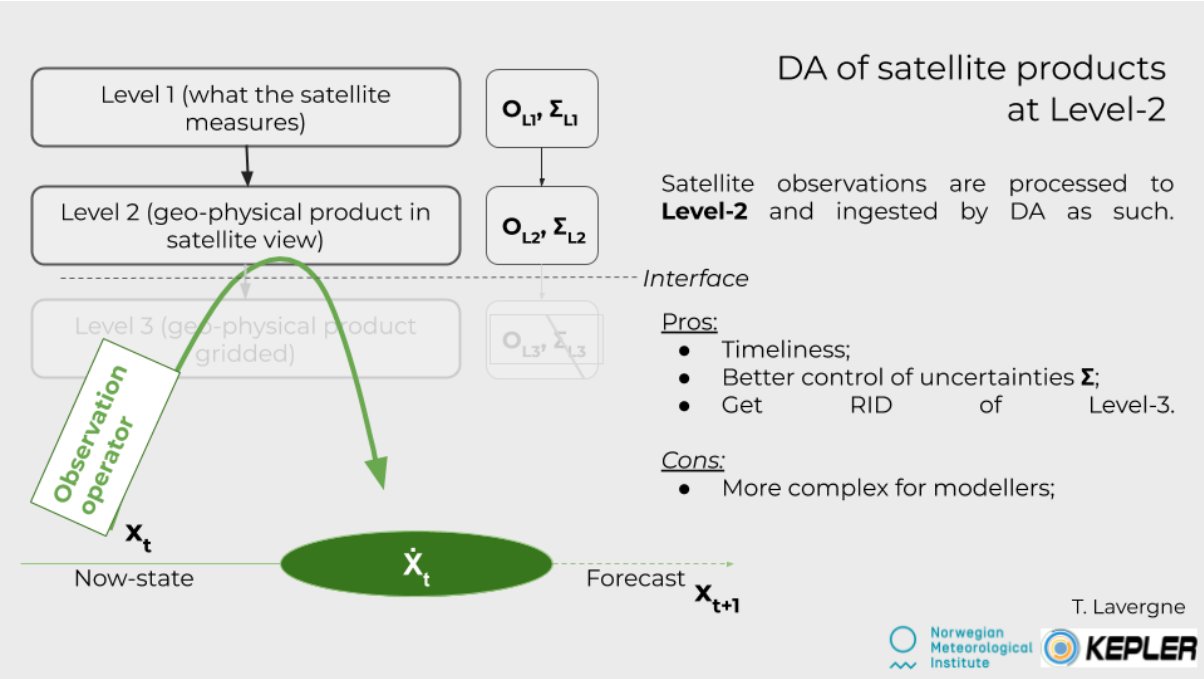

Figure 5.2 *Data Assimilation of satellite-derived products at Level-2.*

The diagram in Figure 5.2 illustrates the assimilation of satellite-derived data products at Level-2. We recall that Level-2 products are observations $\mathbf{O}_{L2}$ (and their uncertainties Σ_{L2}) of geophysical quantities (e.g. SIC) in the satellite swath projection, and thus with the geometrical characteristics of the satellite sensor (e.g. Field-Of-View).

Compared to the previous diagram, the satellite production chain is shorter (no more Level-3/Level-4 production, at least for this purpose), and the Observation Operator (green arrow) is longer and is no more "Identity". The "Interface" between the EO and modelling worlds is shifted.

The longer Observation Operator arrow symbolizes that it has to simulate more processes to link the model state variables to the (satellite) observation, than is the case for Level-3/Level-4. In the case of Level-2 products, the Observation Operator will primarily have to simulate somewhat accurately the geometry of the satellite view, and be able to reproduce satellite swath projection from the model grid. This includes the simulation of the shape, size, and orientation of the satellite Field-Of-Views, in order to simulate the "satellite view" of a model field. In the case of a satellite sensor with similar or higher spatial resolution than the model grid, the operator will only include the distortion of the model grid due to the various parameters of the view geometry (swath path, scanning principle, etc...) of the satellite sensor. When the model grid is finer (or becomes finer) than the Field-Of-View of the satellite sensor, the operator will also include the aggregation/integration of the information from several grid

Co-funded by the Horizon 2020 programme of the European Union

cells into a single satellite Field-Of-View. This aggregation is exactly the mechanism that leads to significant spatial correlation lengths in Level-3/Level-4 products, but here by including it in the observation operator, we avoid the need to express and store the correlated uncertainties in a product file. In terms of uncertainties, the Level-2 product files only store (uncorrelated) uncertainties per-FoV.

Obviously, assimilating Level-2 product files also solves the timeliness issue. Level-2 product files are typically the endpoint of the ground processing chains implemented by the Space Agencies (e.g. ESA and EUMETSAT), and are the product levels on which timeliness requirements are established (e.g. in the Mission Requirement Documents). The timeliness requirements are stringent and drive the optimization of data downlink (number of downlink stations, strategy for downlink, etc.) as well as the optimization of ground processing. Level-2 products are typically made available within 1-3 hours of satellite sensing (Near-Real-Time), and are directly ready for ingestion in a Data Assimilation cycle that can run daily or sub-daily. Being able to ingest Level-2 products would mean the most recent observations can make an impact at all times, skipping the delay of aggregating observations in Level-3/Level-4 files.

Of course, to assimilate Level-2 product files does not go without challenges. As noted earlier, not all DA methodologies can ingest observations with irregular space/time grids and data gaps like the Level-2 products are. Even when the DA methodology is advanced enough, the software for the Observation Operator will be more complex, and it has to be incorporated into the DA scheme implemented at the forecasting center. Depending on the adopted DA methodology (Variational DA, Ensemble Kalman Filter, hybrid, etc…) the Observation Operator code might have to be supplemented with its adjoint/tangent-linear model, which adds further complexity (although Automatic Differentiation techniques exist). The adoption of Level-2 products in DA systems is not straightforward, and the benefits in forecasting skills must significantly offset the additional complexity. From the experience of the Numerical Weather Prediction community, we know this path is both feasible and beneficial if sufficient R&D and implementation efforts are devoted.

We finally note that although the satellite processing chain is shorter (stopping at Level-2), there is very much need for satellite remote sensing knowledge to specify and build the Observation Operators, as these will best be developed by Earth Observation experts (in collaboration with the DA experts for the necessary trade-offs). This opens for many collaboration possibilities, and the diverse communities in and around the Copernicus Services can be the ideal framework to realize such collaborative developments.

Long-term: Data Assimilation of satellite observations at Level-1

Co-funded by the Horizon 2020 programme of the European Union

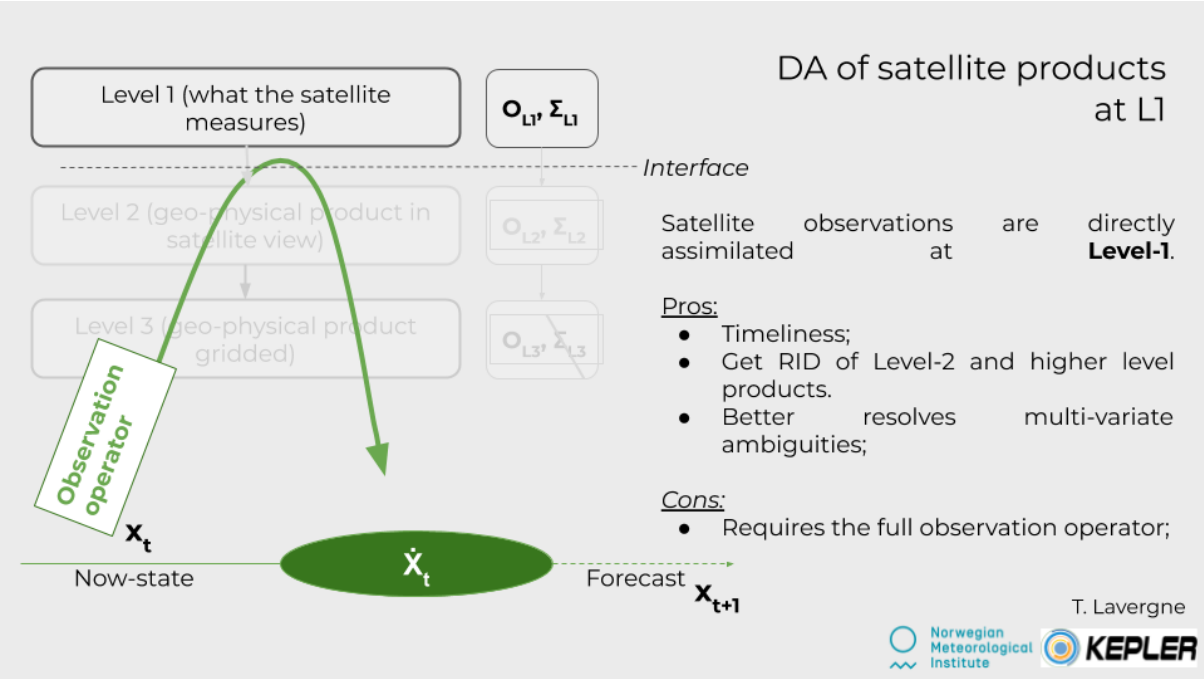

Figure 5.3: *Data Assimilation of satellite-derived products at Level-1*

The diagram in figure 5.3 illustrates the assimilation of satellite-derived data products at Level-1. We recall that Level-1 is the observations $\mathbf{O}_{L1}$ (and their uncertainties Σ_{L1}) of the "raw" (but calibrated) (e.g. brightness temperature) in the satellite swath projection, and thus with the geometrical characteristics of the satellite sensor (e.g. Field-Of-View).

The observation operator now has to handle the whole translation chain from the state variables in the model grid to the observation of radiances in the satellite view. The operator involves both the geometry aspects as in the Level-2 case, but also the simulation of the emission, reflection, scattering processes that control the interaction of electromagnetic radiation with the state variables in the model, also known as Radiative Emission and Transfer Modelling (RTM). A clear complication is when significant parts of the radiation interactions to be simulated involve processes that are not handled in the forecast model, either they involve variables that are not relevant for the forecast itself (e.g. snow grain size, surface roughness, etc… are not needed for a forecast of the sea-ice edge position but are key for radiative transfer modelling) or variables that are outside the model domain (e.g. emission and scattering in the atmosphere, that is not part of the ocean/ice model).

Both complicating aspects are the reason why there are not many experiments with such Observation Operators for sea-ice parameter retrievals. They often involve Passive Microwave Radiometer instruments and low microwave frequencies. For example, Richter et al. (2018) simulate brightness

Co-funded by the Horizon 2020 programme of the European Union

temperatures of SMOS L-band (1.4 GHz) channels and compare them to actual measurements. They observe a general agreement, controlled by the sea-ice cover and sea-ice thickness, and conclude there is a potential for direct data assimilation of Level-1 SMOS data. More recently, Burgard et al. (2020a and 2020b) investigated an Observation Operator for AMSR2 C-band (6.9 GHz) channels from the MPI-M climate model. They show good agreement between the simulations and observations (except during the summer melt season) and point at the potential for evaluating (climate) models on their simulated brightness temperatures, rather than their simulated sea-ice concentration. In these studies, L- and C-band channels are preferred because the atmosphere is mostly transparent at these frequencies, and the changes in brightness temperatures are directly linked to sea-ice surface characteristics. Both studies are relevant for preparing observation operators for the HPCM CIMR mission, but to fully exploit the improved spatial resolution of higher frequency channels (e.g. 18.7 and 36.5 GHz channels), the existing sea-ice emissivity and radiative transfer models must be further developed before the simulations can be used in a retrieval or Data Assimilation framework. Scott et al. (2012) and Scarlat et al. (2020) use an Observation Operator into an inversion framework to estimate sea-ice concentration from AMSR-E brightness temperatures (including 18.7 and 36.5 GHz channels) but in both cases, the bulk of the radiative transfer modelling is in the free-ocean surface and atmosphere (including wind speed, cloud liquid water, water vapour, etc…) while the sea-ice emissivity modelling is based on more simple parametrization.

All the examples above involve microwave radiometer data. The simulation of active microwave instruments (like SAR or altimeter) over sea-ice is not as advanced as for microwave radiometry. One can mention efforts to simulate the echo signal from radar altimeters like in Landy et al. (2019) but they are so far aiming at improving satellite retrievals of sea-ice freeboard and thickness, not the direct assimilation of altimeter raw data in forecast models.

In conclusion for this section, there is certainly a need for the development and testing of fast forward model code for sea ice emissivity as a function of sea ice model variables. We recommend the further development of these fully-fledged Observation Operators, so that they become alternatives to the assimilation of Level-2 products in the future. When supporting the development of such emission and radiative transfer models it is preferable to extend support to community, open-source models. One such model is the Snow Microwave Radiative Transfer model (SMRT, Picard, et al. 2018). It is nonetheless certain that the road is long before satellite observations will be directly assimilated in operational ocean/ice forecasts systems.

Other types of “less processed” satellite products

So far we have discussed satellite products in the widely accepted terms of processing levels (Level-1 to Level-4). This is however not the only way to think about the level of processing of satellite products.

Co-funded by the Horizon 2020 programme of the European Union

For example, in the case of sea-ice thickness from altimeter data, the concept of "less processed" product can refer both to the assimilation of along-track observations (rather than weekly or monthly aggregated maps), but also to assimilate sea-ice freeboard rather than sea-ice thickness. In the retrieval of sea-ice thickness from altimeter data, an early stage in the processing is the estimation of the "radar freeboard" (scattering horizon within the snow/ice layer), which is then transformed into a "sea ice freeboard" (scattering horizon at the snow/ice interface), and finally the so-called "freeboard to thickness" conversion (Tilling et al. 2017). All these transformations (and especially the last one) involve auxiliary information of sea-ice type, snow depth and snow density that are not derived from the altimeter missions. Because this auxiliary information about the snow cover are rather uncertain while having a large impact on the retrieval accuracy (Zygmuntowska et al. 2014), there have been attempts at direct assimilation of the altimeter freeboard observations (both radar and sea-ice freeboards). One recent example is in Kaminski et al. (2018) where the assimilation of radar freeboard, sea-ice freeboard, and sea-ice thickness are compared in a Qualitative Network Design approach.

Another aspect of using "less processed" products is illustrated in Lavergne (2017). In that case, the sea-ice concentration retrieved from satellite radiometry is not less processed per se, but rather interpreted as a less processed product by the modelling world. For example, sea-ice concentration from microwave radiometry is known to underestimate the true sea-ice concentration in the presence of thin (<20 cm) sea-ice. The forecasting models thus can "simulate" a passive microwave sea-ice concentration from their "true" sea-ice concentrations in the case of thin sea-ice. Another key example is the case of the same sea-ice concentration products during the summer melt season in the Arctic: because of the very limited penetration depth of microwave radiation in liquid water, these instruments cannot distinguish between melt pond water and open water between the floes. In the presence of melt-pond, such SIC products should thus rather be used and assimilated as net Ice Surface Fraction. This would however require the forecasting models to rely on melt-pond parametrization that also requires further developments. At this stage, and as noted earlier in this report, there is a lack of melt-pond fraction information from satellite products to calibrate other sea-ice concentration products and improve the melt-pond parameterization in forecast models. Once the products and formulation are improved, the assimilation of summer sea-ice concentration could be based on a net Ice Surface Fraction information, thus a "less processed" product.

5.3.3. Summary on DA of satellite-derived products at the lower processing level

In this section, we give an overview of the challenges and potential benefits with assimilating satellite-derived sea-ice data products at lower processing levels than is currently done in operational ocean/ice forecasting centers, including the CMEMS MFCs.

We first recall the concept of processing levels, from Level-1 (raw satellite observations), to Level-2 (geophysical products in satellite swath geometry), to Level-3 (daily aggregated geophysical products

Co-funded by the Horizon 2020 programme of the European Union

on fixed Earth-referenced grids) and finally Level-4 (multi-satellite analyses with no data gaps and that can involve *In situ* measurements). We then go through 3 stages of increasing complexity (from the Data Assimilation point of view): the status-quo where sea-ice data are assimilated as Level-3/Level-4 products, a mid-term evolution where sea-ice data are assimilated as Level-2 products, and a long-term evolution where they are assimilated as Level-1 products. We also discuss other ways of thinking about less processed products, not based on processing levels but the targeted quantity (e.g. freeboard instead of thickness, net ice surface fraction instead of sea-ice concentration).

The following recommendations are made:

1. Towards the development of higher resolution regional ocean/ice forecasting systems: test, refine, and adopt Data Assimilation of sea-ice parameters (primarily sea-ice concentration and thickness) at Level-2 (in a swath or along the track). This is a necessary preparatory step for the optimal ingestion of Level-2 data products from the HPCM CIMR, and CRISTAL. In parallel, efforts should be continued for DA of ocean and land variables at Level-2.

2. Foster the collaboration and enable further dialogue between the modelling and Earth Observation communities, so that the Data Assimilation framework of tomorrow (including their Observation Operators) are co-designed, and benefit of the expertise in both communities.

3. Continue the development of fully-fledged yet efficient microwave emission models for sea-ice and snow. Community models -such as SMRT- should be preferred, ideally coupled and reconciled with radiative transfer models for the atmosphere and ocean surface.

Co-funded by the Horizon 2020 programme of the European Union

Section 6: Conclusions and Recommendations

6.1 Conclusions and recommendations from Section 1

In **Section 1** we have reviewed the state of the art of sea ice, land, and ocean parameters acquired with current remote sensing missions. We have provided a review of the technologies used to measure each parameter, its resolution (temporal and spatial), the latency, the uncertainty of the available products, and also the validation techniques. We have also assessed the main known limitations and gaps for each parameter retrieval.

The inventoried parameters for land are the following: snow cover fraction, snow water equivalent, snowmelt, snow depth, snow avalanches, snow albedo, lake ice, permafrost and soil moisture; for sea ice: concentration, thickness, drift and deformation, ice type, ice edge position, snow on sea ice, surface albedo, characteristics of melt pond fraction, and ice surface temperature. The ocean parameters analysed are: ocean surface biogeochemical compounds and light, sea surface temperature, sea surface salinity, sea surface height, surface currents, and surface stress (winds).

Greenland and Antarctica ice sheets and glaciers are not covered in the inventory, since they are out of the scope of this project, as well as atmospheric parameters.

6.2 Conclusions and recommendations from Section 2

In **Section 2** we have provided a summary of the Copernicus products of Polar regions that are currently available. This section is therefore linked to the work carried out in WP2 'Polar Regions provision in Copernicus Services' and summarizes the main findings of WP2 as documented in its two deliverable reports (one for CMEMS (Deliverable D2.1) and one for CLMS (Deliverable 2.2). In addition, this section highlights both marine and land parameters that are observable using remote sensing techniques with acceptable accuracy (either alone or in combination with appropriate models) but not covered in the two Copernicus services (CMEMS and CLMS). The **identified parameters observable with remote sensing which are not distributed on Copernicus** services are summarized in Table 6. 1.

Co-funded by the Horizon 2020 programme of the European Union

Table 6. 1 Remote sensing parameters available which are not distributed by Copernicus nowadays.

Remote sensing products with mature R&D pre-cursors that are not distributed in Copernicus nowadays	
Sea Ice	Sea Ice Age
	Melt pond fraction
	Sea ice Albedo
	Leads fraction
Land	Lake Ice duration
	Lake ice thickness
	Snow melt
	Snow depth
	Snow avalanche monitoring
	Permafrost*
	in land water chlorophyll and turbidity
Physical Ocean and Sea state	Surface currents
	Surf. Stress (Wind)
	Wave Spectra
	Ocean Albedo

**combining models and RS.*

We recommend the inclusion of the above remotely sensed parameters in the future evolution of Copernicus services.

6.3 Conclusions and recommendations from Section 3

In Section 3, we have evaluated the parameters, which could be acquired/derived from future missions already planned or under discussion and we compiled the results in a table. This section is specially focused on the EU HPCM missions (CIMR, CRISTAL, ROSE-L, CO2M, CHIME, LSTM). The expected quality of the parameters and the advantages of the future instruments, with regards to the current missions, are summarized in this section. Besides, other missions are also assessed correspondingly, e.g. ESA FORUM

Co-funded by the Horizon 2020 programme of the European Union

The main impacts of the three polar HPCM are:

- CIMR:
  - Land: snow extent, snow water equivalent, lake extent and thickness.
  - Sea-ice: sea ice concentration, sea ice thickness for thin ice, snow-depth on ice, sea ice drift, ice surface temperature, ice type/age.
  - Ocean: sea surface temperature, sea surface salinity and surface winds.
- CRISTAL:
  - Land: land elevation and permafrost.
  - Sea-ice: thick sea ice thickness with better accuracy (>1m), snow-depth on ice, icebergs detection and height.
  - Ocean: sea level
- ROSE-L:
  - Land: snow water equivalent, snow avalanche occurrence, lake ice extent and thickness, permafrost extent and properties.
  - Sea-ice: high-resolution sea ice concentration and ice edge position, sea ice drift and deformation, iceberg occurrence and areal density, ice type.

The main conclusion is that the future HPCM missions have a great potential for improving the monitoring of the Polar Regions, especially with the three polar missions: CIMR, CRISTAL and ROSE-L.

6.4 Conclusions and recommendations from Section 4

In **Section 4** we have evaluated the **current and potential synergies** to improve the quality and resolution of remote sensing data products for the Polar Regions.

Synergies are achievable by combining data from satellite instruments operated at different frequencies/wavelengths, in passive or/and active modes, with different spatio-temporal resolutions, different penetration depths into the ground, which means to have different sensitivities to the geophysical parameters.

We have analysed the combination of the following instruments: Passive Microwave Radiometers (PMR), Radar Altimeters (RA), Infrared Radiometers (IR), Optical Radiometers and Synthetic Aperture Radars (SAR). Notice that the Lidar technology (Optical radars) has not been included since Europe does not have any satellite with this kind of technology. Each one of the future HPCM satellites is designed to use one of the above sensor technologies.

Eighteen parameter synergies that could be achieved with the current satellite data and/or with the

Co-funded by the Horizon 2020 programme of the European Union

future HPCM data once flying, are described in the text. We explain feasible instrument combinations and their advantages concerning individual measurements, all of them supported by published papers. The matrix table in **Table 6. 2** synthesizes the synergies explained in the section. The red text in the table indicates the operational synergies available by the end of Copernicus Phase 1 (2021). It evidences that many new possibilities and improvements could be achieved if more enhanced synergies are performed. Most of the future synergies are experimental nowadays and are supported by scientific literature.

Table 6. 2: Matrix of potential synergies that could be put on operation with current and future HPCM satellites. The synergies mentioned are already tested experimentally. The green boxes are synergies for land applications, light grey for ice and sea applications. Text in red means the operational product at Copernicus phase 1 (2021). Parameters with high impact for intermediate and end-users are marked with bold.

Sensors	**PMR** **(e.g. CIMR)**	**RA** **(e.g. CRISTAL)**	**IR** **(e.g.LSTM)**	**Optical** **(e.g. CHIME)**	**SAR** **(e.g. ROSE-L)**
PMR		lake ice thickness		**Soil moisture** **downscaling**	Snow Water Equivalent **Soil moisture**
RA	**SIT[1], ice type,** snow depth			Phytoplankton groups	
IR	**SIT, ice surface temperature** **sea surface temp.**	**SIT, ice type**			
Optical	**SIC, ice type**	**ice type** MPF		**Phytoplankton groups, phytoplankton dynamics**	snow extent snow wetness **snow avalanche** lake ice extent

Co-funded by the Horizon 2020 programme of the European Union

SAR	**SIC, SIDrift**	sea ice deformation evolution **iceberg properties,** snow depths on sea ice	**ice type**	**SIC, ice type**	

[1] *Requires interferometric capability.*

In addition, synergies between similar observations (i.e. similar instruments onboard on different missions) can lead to improved accuracy and increased temporal resolution, for example the Phytoplankton groups and dynamics.

Table 6. 2 **emphasizes the great potential** that the **combination of simultaneous data from different satellites** could provide to improve the monitoring of polar regions. **Synergies between future HPCM missions** (in case they fly at the same time) also have enormous potential. However, the practical implementation of these future synergies depends on the designs of the different missions regarding orbit constellations and acquisition times relative to each other.

This is a **clear recommendation to Copernicus to enable the necessary R&D and initiate the production and distribution of the resulting synergy products described in this section.**

The gap analysis of the remote sensing parameters (section 1), the analysis of new parameters derived by the potential future missions (section 3) and the feasible synergies (section 4) have allowed us to perform a list of **recommendations to improve the Copernicus services for Polar monitoring from satellite remote sensing data**. The recommendations are summarized in Table 6. 3, organized by: general, land, sea-ice and ocean applications recommendations, and by the level of effort (time) required to achieve the objective, as well as the impact to the users.

Table 6. 3: Gaps and recommendations to improve the monitoring of Polar Regions. Timeline to achieve the goal, its impact and user beneficiary.

Objectives for the improvement of RS data of Copernicus for the Polar regions		
Objectives	**Time period** **Impact** **Users**	**Enhancements needed and recommendations for achieving them**

Co-funded by the Horizon 2020 programme of the European Union

Time period: short term (<5 years, Copernicus next phase), mid-term (current and future technology <10 years, HPCM missions), long term (future technology >10 years, Sentinel-NG's) **Impact :** level of impact to achieve the challenge (high, mid and low) **Users**: marine end-users (as WP1 T1), land end users (as WP1 T2), intermediate users (as WP1 T3)		
General		
Increase *In situ* observations	mid term high impact intermediate users	*In situ* measurements in polar regions are very scarce in Copernicus and in general. This is a clear gap, since this *In situ* data is needed to improve and validate parameter retrievals and products derived from the remote sensing data. **Recommendations:** Acquisition and archiving of a more extensive *In situ* dataset, with a more active role in managing it played by the Copernicus *In situ* Component. This would allow to provide a more robust quality assessment of satellite products and improve the geophysical retrieval algorithms.
Reduce polar observation hole	mid term mid-impact intermediate users	New polar missions should consider the extent of their polar observation hole in the design phase, and reduce it as much as possible within the constraints of the mission's objectives. This is particularly important for visible/infrared imagers, for which twilight acquisition mode should be part of the core mission requirements. **Recommendations:** Carefully consider the twilight acquisition, and more generally polar data coverage, when designing future missions, e.g. the Sentinel-NG missions.
Enable low timeliness of Copernicus polar missions data flow	short term high impact intermediate and end-users	Sea ice is constantly on the move, avalanches can happen at any time, Search and Rescue operations require timely sea-ice imagery and forecasts. The requirements from the end-users for low timeliness in the access to imagery, derived products, and forecasts prompt for low latency in data downlink and processing. **Recommendations:** ensure near-real-time (<1h) or better for critical operational missions (e.g. ROSE-L, CIMR) in the Arctic region, e.g. through pass-through downlink, several receiving stations, on-site processing.

Co-funded by the Horizon 2020 programme of the European Union

Land monitoring		
Snow cover	short term high impact intermediate users	Existing snow cover services (CCI Snow, Copernicus Snow) focus all on latitudes below the Arctic circle where light conditions and favourable cloud cover allows consistent products and services using medium resolution optical radiometers (MODIS/Sentinel-3). To monitor Arctic environments considerable efforts need to be done to take into account results from alternative sensors (passive and active microwaves) and perhaps also use signals in the infrared end of the spectrum from radiometers. A complete and consistent Arctic snow cover product will probably involve using all types of data available, in addition to multi-temporal interpolation techniques. **Recommendations:** Demonstrate multi-sensor snow services for Arctic regions (above Arctic circle), and integrate them in existing PanEuropean/global services for completeness of ECV.
Snow avalanche monitoring	short term high impact land end users	Snow avalanches can be detected using SAR. This has been demonstrated in Northern Norway and for specific Arctic regions, and should be applicable for mountain areas too. Snow avalanche monitoring can be an important input to snow avalanche services, and improve the accuracy of avalanche warning. Extended activity within this field could be valuable in sparsely populated areas where limited observations are available. **Recommendations:** Extend near-real-time avalanche monitoring across, at the least, European mountains based on S1.
Soil moisture	short term mid to high impact intermediate & land end users	Current operational algorithms for soil moisture (PWR or SAR for higher resolutions) retrieval do not take properly into account freezing/thawing in Arctic regions. This parameter is used on fire risk indexes. **Recommendations:** Additional sensors or retrieved products, such as snow extent products from optical sensors (or higher-order products using SAR/PMR/models), could be used to remove erroneous detections. CIMR and ROSE-L will provide SM products.
Lake ice	short term	Lake ice products based on MODIS data exist only for a limited

Co-funded by the Horizon 2020 programme of the European Union

	mid-impact intermediate & land end users	area in Scandinavia (Copernicus) and do only cover mid-winter/ice break up periods. The freeze-up periods are not covered. Future services should be based on combinations of SAR and optical instruments to assure data also during polar night conditions. This will also allow for observations of lake ice conditions in the Arctic. **Recommendations:** Complement optical lake ice detections with SAR in Arctic regions.
Snow water equivalent/Snow depth	long term high impact intermediate & land end users	Coarse-resolution SWE products at high latitudes exist. They are not applicable in mountain areas. ROSE-L could be a potential solution for this problem using the interferometric phase. Cal/Val sites with a good characterization of snow parameters (SWE, depth, density, grain size, wetness, layering, etc.) are important to build up in the Arctic mountains to verify the proposed approach. **Recommendations:** Enhanced efforts to measure SWE in Arctic and mountain regions is highly needed. Build up of competencies alongside the development of ROSE-L.
Permafrost	long term high impact intermediate & land end users	More advanced development is needed to have a good assessment of permafrost. Only sparse *In situ* evaluations of the permafrost fraction are available, strongly complicating validation for this parameter. The quality of the active layer thickness predictions depends strongly on the quality of the prescribed ground stratigraphy. **Recommendations:** Uptake products from the ESA Permafrost CCI project, where data from RS and reanalyses are combined with the CryoGrid model to derive permafrost parameters. Additional estimates of the permafrost extent could be provided in some cases based on the detection of land surface movements. CRISTAL and ROSE-L will provide these retrievals. The new European Ground Motion service, currently being implemented as a new Copernicus Service Element, should be extended to cover the circumpolar Arctic area.
Sea-Ice monitoring		

Co-funded by the Horizon 2020 programme of the European Union

Snow depth on sea-ice	mid term high impact intermediate users	Not measured remotely with proper accuracy. This parameter is very important on its own, and to properly measure sea ice thickness from altimetry, among others. **Recommendations:** Assess possible synergies, new HPCMs (CIMR, CRISTAL and ROSE-L) will contribute to improving the retrieval of this parameter.
Near real-time high resolution ice analysis	mid term high impact intermediate & marine end-users	High resolution (sub kilometers) ice analysis is today done manually based on SAR images, and it is necessary to automatize it to handle ever-increasing volumes of data and to meet the demand for increased detail (ice rheology). Progress is also limited by the fact that radar altimetry and passive microwave radiometry satellites for sea ice thickness have a period of operation outside of summer months, which is when data of sea ice conditions are most important. **Recommendation:** Enhanced automation of high resolution (sub km) ice chart production to handle increased satellite data volumes and provide additional detail. Further research to improve sea ice parameter retrievals in summer.
Improved sea ice concentration for forecasting	mid term high impact intermediate users	Ice concentration retrievals rely on semi-operational or outdated passive microwave radiometer satellite missions (AMSR2 and SSMIS). With increased forecast model resolution, coverage and increased accuracy, SIC data is required at the ice edge and in the coastal zones. **Recommendation:** Fully operational missions with long-term continuity are needed. Synergy with SAR and/or optical must be further explored.
Multi-sensor sea-ice drift analyses.	mid term mid impact intermediate users	There is to date no satellite product (operational or research-based) that combines accurately radiometry-based and SAR-based sea-ice drift data. This would, however, fill a key observation gap (complete daily coverage, with higher spatial resolution and accuracy where SAR is available), particularly in the Antarctic where SAR coverage is sparse. The same yields for mosaicking of several SAR-based sea-ice drift products (e.g. Sentinel 1 A-B-Cs, the RCMs, etc...). Propagation of the uncertainties into the Level-4 analysed sea-ice drift product must be treated as well.

Co-funded by the Horizon 2020 programme of the European Union

		Recommendation: Develop and implement operational multi-sensor sea-ice drift analyses, e.g. in CMEMS.
Summer Sea ice concentration	medium & long term high impact intermediate users	During melting periods the accuracy of PMR-based SIC estimates considerably decrease. In the presence of melt-ponds, PMR can only sense the ice surface fraction. PMR algorithm must be refined to achieve better observation of the ice surface fraction. In parallel forecast models must be developed to ingest the Ice Surface Fraction **Recommendation:** Improve accuracy and generate melt-pond-fraction data products from visible/infrared imagers (such as OLCI-Sentinel3, Sentinel-2, MODIS, MERIS, VIIRS, ...). Investigate if modern SAR sensors (Sentinel-1) can accurately measure MPF at a basin scale. In parallel, further develop melt-pond parameterization in forecast models to exploit the ice surface fraction products routinely.
Sea ice thickness	long term high impact intermediate & marine end-users	High temporal resolution ice thickness products covering the whole range of thickness are missing. A higher spatial resolution sea ice thickness product (sub km) is also missing. Coverage for the melt season is also lacking. Snow depth measurement with enough precision is crucial for deriving SIT with good accuracy. **Recommendation:** Supplement microwave remote sensed data sources with optical satellite and *In situ* data during summer. Further research into snow retrievals over sea ice.
Ocean monitoring		
Surface ocean biogeochemical compounds (also for inland waters)	mid term high impact intermediate users	Parameters on ocean productivity, biogeochemical fluxes and radiation. The main limitations are due to the low temporal coverage, sea ice cover, unfavourable light and rough weather conditions. Higher spatial resolution (of order 10–100 m) data to retrieve parameters from bays and estuaries at the polar coasts and in inland waters are necessary. Missions providing such data are focused on land applications (e.g., Sentinel 2 or Landsat 8) which only cover the Arctic coasts below 74°N and not the Antarctic continent. Products on phytoplankton functional types are currently released but limited to S3 and need higher spatial scale which would help to improve

Co-funded by the Horizon 2020 programme of the European Union

		predictions for water quality, HABs, fishery, coastal management by themselves but also indirectly by improving the quality of Chl products. **Recommendations:** Merging satellite data can improve this tremendously. *In situ* data are sparse for validation and the implementation and further development of autonomous *In situ* bio-optical measurements needs to be promoted. Promote CHIME also for pan polar applications.
Sea surface salinity	mid term mid impact intermediate users	This parameter is provided by L-band microwave radiometers only. It is very important for the assessment of freshwater fluxes changes. Its accuracy is limited, mainly due to the sparse *In situ* data available. **Recommendations:** Promote CIMR mission since it also carries onboard an L-band radiometer. More *In situ* measurements are required to enhance satellite salinity products.
Wind speed	long term mid impact intermediate users	An improvement in the accuracy of wind speed observations over ice and ocean is needed since the wind controls the surface ocean circulation and hence freshwater transport rates and pathways. **Recommendations:** To add Doppler capability to future scatterometers, allows for simultaneous measurements of surface winds and currents and improves directional accuracy.

6.5 Conclusions and recommendations from Section 5

In this section, we have analysed the **status quo in data assimilation,** considering the data assimilation models used in the Copernicus services CMEMS, C3S and CLMS and reviewed their data assimilation capabilities, problems and deficiencies. Many observations are routinely assimilated, some with success, some with potential for improvement, and several not being assimilated at all for various reasons.

Feasible data assimilation demonstrations published but not yet taken up by Copernicus Services have also been reported. *In situ* data have not been taken into account in this review.

Nowadays, **several parameters are being assimilated into models, some of them with important constraints**. We itemize below the parameters that are assimilated organized by its level of limitations based on scientific literature and to the best of the authors' knowledge of the field:

Co-funded by the Horizon 2020 programme of the European Union

- Parameters assimilated with **severe limitations**: SST (from IR), SIT, Ice Drift, Chl.
- Parameters assimilated with a **medium** level of **limitations**: SIC.
- Parameters assimilated successfully but the efficiency **of assimilation is not sufficiently documented**: SSH, SST (from PMR).

There is to our knowledge **no assimilation of satellite land data as part of the Copernicus Land nor Climate Change Services as of today.**

The Table 6. 4 below lists some of the identified **parameters which are not yet being assimilated**, organized by the time required to achieve the goal.

The CLMS is neither using models nor data assimilation at present, so some suggestions based on research on land models are done on the corresponding section of the report. Land data are used as boundary conditions for atmospheric models rather than to be assimilated, so the efficiency of data assimilation of land parameters cannot be assessed.

Table 6. 4: Parameters that are not yet being assimilated, with the time period required to achieve the goal.

Recommendations on data assimilation		
Parameter	***Time period***	***Recommendations on DA***
Short Term		
Ocean salinity	Short term	Assimilation of sea surface salinity in near real-time.
Waves height	Short term	Optimized Arctic wave forecasts using satellite data.
Mid Term		
Sea ice drift	Mid term	Efficient data assimilation of ice drift and ice deformations.
Snow cover on land	Mid term	A yearly retrospective pan-Arctic simulation of the melt season at the hillslope scale would be useful for hydrological models.
Permafrost	Mid term	A pan-Arctic permafrost model assimilating LST and snow cover would be necessary.

Co-funded by the Horizon 2020 programme of the European Union

Ocean colour (Chl-a)	Mid term	Efficient assimilation of surface chlorophyll in a near real-time ocean biogeochemical model.
Ocean colour (Optics)	Mid term	Assimilate optical properties of water in near-real-time.
Long term		
Sea ice surface temperature	Long term	Assimilation of Ice Surface Temperature and ice albedo.
Melt Ponds	Long term	Assimilation of melt pond fraction in near real-time.
Rivers	Long term	Assimilate river levels in near real-time hydrological models.
Soil moisture	Long term	Assimilate soil moisture from L-band PMR into near-real-time land models.
Ocean colour (PFT)	Long term	Assimilate Plankton Functional Types.
High resolution (all models)	Long term	Design ways to increase model resolution on energy-limited supercomputers.

On the other hand, the **assimilation of satellite information at lower processing levels** has been investigated as well in this section. We have explored how modelling and forecasting applications would benefit from going beyond the current status-quo (assimilation of daily/weekly/monthly averaged gridded satellite products) and start assimilating individual swaths (and/or scenes) of satellite-derived products in swath projection, and even directly raw satellite data.

We have gone through 3 stages of increasing complexity: the status-quo where sea-ice data are assimilated as Level-3/Level-4 products (maps), a mid-term evolution where sea-ice data are assimilated as Level-2 products (individual swath), and a long-term evolution where they are assimilated as Level-1 products. We also have discussed other ways of thinking about less processed products, not based on processing levels but the targeted quantity (e.g. freeboard instead of thickness, net ice surface fraction instead of sea-ice concentration).

The **recommendations** to move forward on this new approach on data assimilation are resumed in Table 6. 5.

Co-funded by the Horizon 2020 programme of the European Union

Table 6. 5: Recommendations to move forward on this new approach on data assimilation

Assimilation of Level-2 satellite products	Mid term	Towards the development of **higher resolution regional ocean/ice forecasting systems**: test, refine, and adopt Data **Assimilation of sea-ice parameters** (primarily sea-ice concentration and thickness) **at Level-2** (in a swath or along-track). This is a necessary preparatory step for the optimal ingestion of Level-2 data products from the HPCM CIMR, and CRISTAL. In parallel, efforts should be continued for DA of ocean and land variables at Level-2.
Co-design of Operators	Mid Term	Foster the **collaboration** and enable further dialogue between the **modelling and Earth Observation communities**, so that the Data Assimilation framework of tomorrow (including their Observation Operators) are co-designed, and benefit of the expertise in both communities.
Towards direct **assimilation of Level-1** satellite **observations**	Long Term	Continue the **development** of fully-fledged yet efficient **microwave emission models for sea-ice and snow**. Community models -such as SMRT- should be preferred, ideally coupled and reconciled with radiative transfer models for the atmosphere and ocean surface.

Co-funded by the Horizon 2020 programme of the European Union

References

Aaboe, S., Sørensen, A., Lavergne, T., and Eastwood, S., "Sea Ice Edge and Sea Ice Type Climate Data Records Algorithm Theoretical Basis Document – v2.2", Tech. rep., *EU C3S – Copernicus Climate Change Service*, 2018. https://cds.climate.copernicus.eu.

Aaboe, S., Breivik, L.-A., and Eastwood, S., "Global Sea Ice Edge (OSI-402-c) and Type (OSI-403-c) Algorithm Theoretical Basis Document – v2.2", Tech. rep. SAF/OSI/CDOP2/MET-Norway/SCI/MA/208, *EUMETSAT OSI SAF – Ocean and Sea Ice Satellite Application Facility,* 2016. http://osisaf.met.no/docs/osisaf_cdop2_ss2_atbd_sea-ice-edge-type_v2p2.pdf.

Aalstad, K., Westermann, S., Schuler, T. V., Boike, J., & Bertino, L. "Ensemble-based assimilation of fractional snow-covered area satellite retrievals to estimate the snow distribution at Arctic sites", *The Cryosphere*, 12 (1), 2018. https://doi.org/10.5194/tc-12-247-2018.

Aalto, J., Karjalainen, O., Hjort, J. and Luoto, M., "Statistical forecasting of current and future circum-Arctic ground temperatures and active layer thickness," *Geophysical Research Letters*, 45 (10), 4889-4898, 2018.

Aiken and Moore. "Photosynthetic Available Radiation", *MERIS ATBD 2.18,* v5. 1997.

Al Bitar, A., Mialon, A., Kerr, Y. H., Cabot, F., Richaume, P., Jacquette, E., Quesney, A., Mahmoodi, A., Tarot, S., Parrens, M., Al-Yaari, A., Pellarin, T., Rodriguez-Fernandez, N., and Wigneron, J.-P.: "The global SMOS Level 3 daily soil moisture and brightness temperature maps", *Earth System Science Data,* 9, 293–315, 2017. https://doi.org/10.5194/essd-9-293-2017.

Alonso-Arroyo, A., Zavorotny, V., and Camps, A., "Sea Ice Detection Using U.K. TDS-1 GNSS-R Data", *IEEE Transactions on Geoscience and Remote Sensing*, vol. 55, no. 9, pp. 4989-5001, 2017.

Abermann, J., Eckerstorfer, M., Malnes, E. and Hansen, B.U., "A large wet snow avalanche cycle in West Greenland quantified using remote sensing and in situ observations". Natural Hazards, 97(2), pp.517-534, 2019.

Agriculture and Agri-Food Canada, "ISO 19131 RADARSAT-2 Surface Soil Moisture Mapping – Data Product Specifications. Revision A", *Technical report*, Government of Canada, Agriculture and Agri-Food Canada, 2016. Available online: http://www.agr.gc.ca/atlas/supportdocument_documentdesupport/radarsatSurfaceSoilMoisture/en/ISO_19131_RADARSAT_2_Surface_Soil_Moisture_Data_Product_Specification.pdf

Andersen, S., Tonboe, R., Kaleschke, L., Heygster, G., Pedersen,L. T., "Intercomparison of passive microwave sea ice concentration retrievals over the high-concentration Arctic sea ice", *J. Geophysical Research*, 112, 2007.

Co-funded by the Horizon 2020 programme of the European Union

Antonova, S., Duguay, C.R., Kääb, A., Heim, B., Langer, M., Westermann, S., Boike, J., "Monitoring Bedfast Ice and Ice Phenology in Lakes of the Lena River Delta Using TerraSAR-X Backscatter and Coherence Time Series", *Remote Sensing,* 8 (11), 2016. htpps://doi.org/10.3390/rs8110903.

Ardhuin et al. "Measuring currents, ice drift, and waves from space: The sea surface kinematics multiscale monitoring (SKIM) concept.", *Ocean Sci.*, 14, 337–354, 2018, https://doi.org/10.5194/os-14-337-2018.

Argo. Argo float data and metadata from global data assembly centre (argo gdac), SEANOE, 2000, http://doi.org/10.17882/42182.

Balch, W. M., Gordon, H. R., Bowler, B. C., Drapeau, D. T., and Booth, E. S. "Calcium carbonate measurements in the surface global ocean based on Moderate-Resolution Imaging Spectroradiometer data", *J. Geophys. Res*., 110, C07001, doi:10.1029/2004JC002560, 2005.

Bartsch, A., Westermann, Strozzi, T., "ESA CCI+ Permafrost Product Validation and Algorithm Selection Report (PVASR)", v1.0, 2019.

Bartsch, A., et al., "Requirements for monitoring of permafrost in polar regions - A community white paper in response to the WMO Polar Space Task Group (PSTG)", Version 4, Austrian Polar Research Institute, Vienna, Austria, 20 , 2014.

Bechor, N. B. D., Zebker, H. A., "Measuring two-dimensional movements using a single InSAR pair", *Geophys. Res. Letters*, vol. 33, L16311, 2006, DOI:10.1029/2006GL026883.

Beckers, J. F., Casey, J. A., & Haas, C.,"Retrievals of Lake Ice Thickness From Great Slave Lake and Great Bear Lake Using CryoSat-2." *IEEE Transactions on Geoscience and Remote Sensing*, *55*(7), 3708-3720, 2017.

Behrenfeld, M. J., Hu, Y., O'Malley, R. T., Boss, E. S., Hostetler, C. A., Siegel, D. A., Scarino, A. J, "Annual boom–bust cycles of polar phytoplankton biomass revealed by space-based lidar." *Nature Geoscience*, 10, 118, 2016, https://doi.org/10.1038/ngeo2861.

Belmonte Rivas,M., Otosaka, I., Stoffelen, A., and Verhoef, A.: "A scatterometer record of sea ice extents and backscatter: 1992–2016", *The Cryosphere*, 12, 2941-2953, 2018, https://doi.org/10.5194/tc-12-2941-2018.

Belmonte, R. M., and Stoffelen, A. Characterizing ERA-interim and ERA5 surface wind biases using ASCAT. Ocean Sci. Discuss. 15, 831–852. 2019. doi: 10.5194/os-15-831-2019.

Berg, A., L. E. B. Eriksson, "Investigations of a hybrid algorithm for sea ice drift measurements using synthetic aperture radar images", *IEEE Trans. Geosci. Remote Sens.*, vol. 52, no. 8, pp. 5023-5033, 2014. doi:10.1109/TGRS.2013.2286500.

Co-funded by the Horizon 2020 programme of the European Union

Bergstedt, H., Bartsch, A., Duguay, C.R., Jones, B.M. and Arp, C.D., "Influence of lake ice formation and break-up on ASCAT backscatter." *AGU Fall Meeting*, 2018.

Bianchi, F.M., Grahn, J., Eckerstorfer, M., Malnes, E., Vickers, H., "Snow avalanche segmentation in SAR images with Fully Convolutional Neural Networks." ArXiv191005411 Cs Eess Stat, 2019.

Biskaborn, B. K., Lanckman, J. P., Lantuit, H., Elger, K., Dmitry, S., William, C., and Vladimir, R., The new database of the Global Terrestrial Network for Permafrost (GTN-P), *Earth System Science Data*, 7, 245-259, 2015, doi: 10.5194/essd-7-245-2015.

Blyverket, J., Hamer, P. D., Schneider, P., Albergel, C., & Lahoz, W. A. "Monitoring soil moisture drought over northern high latitudes from space." Remote Sensing, 11 (10), 1–18, 2019. https://doi.org/10.3390/rs11101200.

Bormann, K. J., Westra, S., Evans, J. P., & McCabe, M. F., "Spatial and temporal variability in seasonal snow density" *Journal of hydrology*, 484, 63-73, 2013, https://doi.org/10.1016/j.jhydrol.2013.01.032.

Bracher, A., Vountas M.,Dinter, T., Burrows, J.P.,Ottgers, R.R, Peeken I. "Quantitative observation of cyanobacteria and diatoms from space using PhytoDOAS on SCIAMACHY data", *Biogeosciences,* 6 (6), pp.751-764, 2009 DOI: 10.5194/bg-6-751-2009

Brewin, R. J. W., Dall'olmo, G., Pardo, S., Van Dongen-Vogels, V., and Boss, E. S. "Underway spectrophotometry along the Atlantic meridional transect reveals high performance in satellite chlorophyll retrievals." *Remote Sens. Environ.* 183, 82–97, 2016.

Buckley, E. M., Farrell, S. L., Duncan, K., Connor, L. N., Kuhn, J. M., & Dominguez, R. T. "Classification of Sea Ice Summer Melt Features in High-resolution IceBridge Imagery". Journal of Geophysical Research: Oceans, 125, e2019JC015738, 2020, https://doi.org/10.1029/2019JC015738.

Burgard, C., Notz, D., Pedersen, L. T., and Tonboe, R. T. "The Arctic Ocean Observation Operator for 6.9 GHz (ARC3O) – Part 2: Development and evaluation", *The Cryosphere Discuss.*, https://doi.org/10.5194/tc-2019-318, in review, 2020.

Bühler, Y., Hafner, E.D., Zweifel, B., Zesiger, M., Heisig, H., "Where are the avalanches? Rapid mapping of a large snow avalanche period with optical satellites." The Cryosphere Discuss, 1–21, 2019,

Bühler, Y., Hüni, A., Christen, M., Meister, R., Kellenberger, T., "Automated detection and mapping of avalanche deposits using airborne optical remote sensing data.", Cold Reg. Sci. Technol. 57, 99–106, 2009. https://doi.org/10.1016/j.coldregions.2009.02.007

Casey, J. A., Howell, S. E. L., Tivy, A., Haas, C. "Separability of sea ice types from wide-swath C- and L-band synthetic aperture radar imagery acquired during the melt season", Remote Sensing of Environment 174, pp. 314-328, 2016, doi:10.1016/j.rse.2015.12.021

Cavalieri, D. J., Gloersen, P., and Campbell, W. J.," Determination of sea ice parameters with the NIMBUS 7 SMMR", J. Geophys. Res., 89 (D4), 5355– 5369, 1984, doi:10.1029/JD089iD04p05355.

Co-funded by the Horizon 2020 programme of the European Union

Chadburn, S. E., Burke, E. J., Cox, P. M., Friedlingstein, P., Hugelius, G., and Westermann, S., "An observation-based constraint on permafrost loss as a function of global warming", *Nature Climate Change,* 7(5), 340, 2017.

Chelton, D. B., M. G. Schlax, R. M. Samelson, J. T. Farrar, M. J. Molemaker, J. C. McWilliams, and J. Gula, "Prospects for future satellite estimation of small-scale variability of ocean surface velocity and vorticity." *Prog. Oceanogr.,* 173, 256–350, 2019. https:// doi.org/10.1016/j.pocean.2018.10.012.

Cheng, A., Casati, B., Tivy, A., Zagon, T., Lemieux, J.-F., and Tremblay, B., "Accuracy and Inter-Analyst Agreement of Visually Estimated Sea Ice Concentrations in Canadian Ice Service Ice Charts", *The Cryosphere Discuss*, 2019, https://doi.org/10.5194/tc-2019-190.

CHIME MRD, "Copernicus Hyperspectral Imaging Mission for the Environment - Mission Requirements Document", ESA-EOPSM-CHIM-MRD-3216, Issue 2.1, July 2019, http://esamultimedia.esa.int/docs/EarthObservation/Copernicus_CHIME_MRD_v2.1_Issued20190723.pdf

Choudhury, B. J. & Golus, R. E. "Estimating soil wetness using satellite data", International Journal of Remote Sensing, 9 (7), 1251-1257, 1988. https://doi.org/10.1080/01431168808954932.

CIMR MRD v3, "Copernicus Imaging Microwave Radiometer (CIMR) Mission Requirements Document", ESA -EOPSM-CIMR-MRD -32, Issue 3.0, September 2019, https://esamultimedia.esa.int/docs/EarthObservation/CIMR-MRD-v3.0-20190930_Issued.pdf

Clausi, D. A. "Comparison and Fusion of Co-occurrence, Gabor and MRF Texture Features for Classification of SAR Sea-Ice Imagery", Atmosphere-Ocean 39 (3), pp. 183-194, 2001, doi:10.1080/07055900.2001.9649675.

Colliander, A., T.J. Jackson, R. Bindlish, S. Chan, N. Das, S.B. Kim, M.H. Cosh, R.S. Dunbar, L. Dang, L. Pashaian, J. Asanuma, K. Aida, A. Berg, T. Rowlandson, D. Bosch, T. Caldwell, K. Caylor, D. Goodrich, H. al Jassar, E. Lopez-Baeza, J. Martínez-Fernández, A. González-Zamora, S. Livingston, H. McNairn, A. Pacheco, M. Moghaddam, C. Montzka, C. Notarnicola, G. Niedrist, T. Pellarin, J. Prueger, J. Pulliainen, K. Rautiainen, J. Ramos, M. Seyfried, P. Starks, Z. Su, Y. Zeng, R. van der Velde, M. Thibeault, W. Dorigo, M. Vreugdenhil, J.P. Walker, X. Wu, A. Monerris, P.E. O'Neill, D. Entekhabi, E.G. Njoku, S. Yueh, "Validation of SMAP surface soil moisture products with core validation sites", Remote Sensing of Environment, 191, 215-231, 2017. https://doi.org/10.1016/j.rse.2017.01.021.

Comiso, J. C., Meier, W. N., and Gersten, R., "Variability and trends in the Arctic Sea ice cover: Results from different techniques," J. Geophys. Res. Oceans, 122, 6883–6900, 2017. doi:10.1002/2017JC012768.

Co-funded by the Horizon 2020 programme of the European Union

Comiso, J. C., "Large Decadal Decline of the Arctic Multiyear Ice Cover", Journal of Climate, vol 25 (4), 2012, doi: 10.1175/JCLI-D-11-00113.1.

Comiso, J.C, Cavalieri, D.J., Parkinson, C.L., Gloersen, P., "Passive microwave algorithms for sea ice concentration: A comparison of two techniques." Remote Sens. Environ, 60, 357-384, 1997.

Comiso, J. C., "Arctic multiyear ice classification and summer ice cover using passive microwave satellite data", J. Geophys. Res., 95(C8), 13411– 13422, 1990, doi:10.1029/JC095iC08p13411

CO2M MRD, "Copernicus CO2 MonitoringMission Requirements Document", EOP-SM/3088/YM-ym, Issue 2.0, September 2019, https://esamultimedia.esa.int/docs/EarthObservation/CO2M_MRD_v2.0_Issued20190927.pdf.

Crane, R.K. "Propagation phenomena affecting satellite communication systems operating in the centimeter and millimeter wavelength bands", *Proceedings of IEEE*, 59 (2), 173–188, 1971. https://doi.org/10.1109/PROC.1971.8123.

CRISTAL MRD, "Copernicus polaR Ice and Snow Topography ALtimeter (CRISTAL) Mission Requirements Document", ESA-EOPSM-CPTM-MRD-3350 (PICE-RS-ESA-MI-0004), Issue 2.0, February 2019, http://esamultimedia.esa.int/docs/EarthObservation/Copernicus_CRISTAL_MRD_v2.0_Issued_20190228.pdf

Dammann D. O., Eriksson, L. E. B, Jones,J. M., Mahoney, A. R., Romeiser, R., Meyer, F. J., Eicken,H. , Fukamachi, Y. , "Instantaneous sea ice drift speed from TanDEM-X interferometry", *The Cryosphere*, 13, 1395-1408, 2019, https://doi.org/10.5194/tc-13-1395-2019.

Das, N.N., Entekhabi, D., Njoku, E.G., Shi, J.J.C, Johnson, J.T., & Colliander, A. "Tests of the SMAP Combined Radar and Radiometer Algorithm Using Airborne Field Campaign Observations and Simulated Data", *IEEE Transactions on Geoscience and Remote Sensing*, 52(4), 2018–2028, 2014. https://doi.org/10.1109/TGRS.2013.2257605.

Das, N., D. Entekhabi, S. Dunbar, J. Chaubell, A. Colliander, S. Yueh, T. Jagdhuber, F. Chen, W. T. Crow, P. E. O'Neill, J. Walker, A. Berg, D. Bosch, T. Caldwell, M. Cosh, C. H. Collins, E. Lopez-Baeza, and M. Thibeault, "The SMAP and Copernicus Sentinel 1A/B microwave active-passive high resolution surface soil moisture product", *Remote Sensing of Environment*. 233. 111380, 2019. https://doi.org/10.1016/j.rse.2019.111380.

Demchev D., Volkov, V., Kazakov, E., Alcantarilla, P. F., Sandven, S., Khmeleva, V., "Sea ice drift tracking from sequential SAR images using accelerated-KAZE features", *IEEE Trans. Geosc. Remote Sens.*, vol. 55, no. 9, pp. 5174-5184, 2017, doi:10.1109/TGRS.2017.2703084.

Co-funded by the Horizon 2020 programme of the European Union

Dierking, W. “Sea ice monitoring by synthetic aperture radar”, *Oceanography* 26 (2) :100–111, 2013, http://dx.doi.org/10.5670/oceanog.2013.33.

Doerffer, R. and Schiller, H., “The MERIS Case 2 Water Algorithm”, *International Journal of Remote Sensing,* 28, 517-535, 2007,doi:10.1080/01431160600821127

Donlon, C., Berruti,B., Buongiorno, A. ,Ferreira, M.-H., Féménias,P., Frerick, J. , Goryl, P., Klein, U., Laur, H. , Mavrocordatos,C. , Nieke, J., Rebhan, H., Seitz, B., Stroede, J., Sciarra, R., “The Global Monitoring for Environment and Security (GMES) Sentinel-3 mission”, *Remote Sensing of Environment*, Vol. 120, pp 37-57, 2012, https://doi.org/10.1016/j.rse.2011.07.024.

Draper, C.; Mahfouf, J.-F.; Calvet, J.-C.; Martin, E.; Wagner, W. “Assimilation of ASCAT near-surface soil moisture into the SIM hydrological model over France”, Hydrology of Earth System Sciences, 15, 3829–3841, 2011. https://doi.org/10.5194/hess-15-3829-2011.

Du, J., Kimball, J.S., Duguay, C., Kim, Y. and Watts, J.D., “Satellite microwave assessment of Northern Hemisphere lake ice phenology from 2002 to 2015.” *The Cryosphere*, 11, p.47, 2017.

Duguay, C.R., Bernier, M., Gauthier, Y. and Kouraev, A., “12 Remote sensing of lake and river ice”, *Remote Sensing of the Cryosphere*. Edited by M. Tedesco. John Wiley & Sons, Ltd. 2015.

Dybkjær, G., Eastwood, E., Luis, C. Høyer, J. “Algorithm theoretical basis document for the OSI SAF Sea and Sea Ice Surface Temperature L2 processing chain OSI-205-a and OSI-205-b”, *OSISAF report*, Version 1.4 19. February 2018.

Eastwood,S., Dybbroe, A., Scheirer, R., Håkansson, N., and Godøy, Ø., “L2 & L3 SST/IST Algorithm Theoretical Basis Document”, *EUMETSAT Report* v1.2, 2018.

Eastwood,S., Dybbroe, A., Scheirer, R., Håkansson, N., and Godøy, Ø., “OSISAF/NWC-SAF Federated activity on cloud and ice masking in polar conditions”. - OSISAF, Final Report, 2017.

Eastwood,S., Dybbroe, A., Scheirer, R., Håkansson, N., and Godøy, Ø, “Validation Report for the Atlantic High Latitude L3 Sea Surface Temperature product OSI-203 Version 1.0”, OSISAF 2011

Eckerstorfer, M., Vickers, H., Malnes, E., Grahn, J., “Near-Real Time Automatic Snow Avalanche Activity Monitoring System Using Sentinel-1 SAR Data in Norway”. Remote Sens., 11, 2863, 2019. https://doi.org/10.20944/preprints201910.0341.v1.

Eckerstorfer, M., Malnes, E., Müller, K., “A complete snow avalanche activity record from a Norwegian forecasting region using Sentinel-1 satellite-radar data.”, *Cold Reg. Sci. Technol.* 144, 39–51, 2017. http://dx.doi.org/10.1016/j.coldregions.2017.08.004.

Eckerstorfer, M., Bühler, Y., Frauenfelder, R., Malnes, E., “Remote sensing of snow avalanches: recent advances, potential, and limitations.” *Cold Reg. Sci. Technol.* 121, 126–140, 2016. https://doi.org/10.1016/j.coldregions.2015.11.001.

Co-funded by the Horizon 2020 programme of the European Union

Eckerstorfer, M., Malnes, E., "Manual detection of snow avalanche debris using high-resolution Radarsat-2 SAR images". *Cold Reg. Sci. Technol.* 120, 205–218, 2015. https://doi.org/10.1016/j.coldregions.2015.08.016.

Engram, M., D. Arp, C., Jones, B., Ajadi, O.A., Meyer, F. J. "Analyzing floating and bedfast lake ice regimes across Arctic Alaska using 25 years of space-borne SAR imagery", *Remote Sensing of Environment*, Vol. 209, pp 660-676, 2018, https://doi.org/10.1016/j.rse.2018.02.022.

Engram, M., Anthony, K.W., Meyer, F.J., Grosse, G. "Characterization of L-band synthetic aperture radar (SAR) backscatter from floating and grounded thermokarst lake ice in Arctic Alaska". *The Cryosphere* 7, pp. 1741-1752, 2013.

Entekhabi, D., R.H. Reichle, R.D. Koster, and W.T. Crow, W.T. "Performance Metrics for Soil Moisture Retrievals and Application Requirements", *Journal of Hydrometeorology*, 11, 832–840, 2010. https://doi.org/10.1175/2010JHM1223.1.

Eicken, H., Krouse, H. R., Kadko, D., and Perovich, D. K., "Tracer studies of pathways and rates of meltwater transport through Arctic summer sea ice". J. Geophys. Res., 107, 8046, 2002, doi:10.1029/2000JC000583.

EUMETSAT, "ASCAT User Guide", *Technical report,* Doc. Num. EUM/OPS-EPS/MAN/04/0028, Issue v5B, Germany, 2017. Available online: https://www.eumetsat.int/website/home/Satellites/CurrentSatellites/Metop/MetopDesign/ASCAT/index.html.

Fernandez-Moran, R., Al-Yaari, A., Mialon, A., Mahmoodi, A., Al Bitar, A., De Lannoy, G. Rodriguez-Fernandez, N., Lopez-Baeza, E., Kerr, Y., Wigneron, J.-P. "SMOS-IC: An Alternative SMOS Soil Moisture and Vegetation Optical Depth Product", *Remote Sensing*, 9 (5), 457, 2017. https://doi.org/10.3390/rs9050457.

Flett, D. G. "Operational use of SAR at the Canadian Ice Service: Present operations and a look to the future", *Proceedings of the Second Workshop on Coastal and Marine Applications of SAR*, 8-12 September 2003, Svalbard, Norway, ESA SP-565, pp. 183-198, 2004.

Foster, J. L., Sun, C., Walker, J. P., Kelly, R., Chang, A., Dong, J., and Powell, H. "Quantifying the uncertainty in passive microwave snow water equivalent observations", *Remote Sens. Environ.*, 94, 187–203, 2005. https://doi.org/10.1016/j.rse.2004.09.012.

Fournier, S., Lee, T., Tang, W., Steele, M., Olmedo, E., „Evaluation and Intercomparison of SMOS, Aquarius, and SMAP Sea Surface Salinity Products in the Arctic Ocean" Remote Sensing, 2019, 11, 3043; doi:10.3390/rs11243043

Frouin, R., and Iacobellis, S. F. "Influence of phytoplankton on the global radiation budget", *J. Geophys. Res.* 107, ACL 5-1–ACL 5-10, 2002, doi: 10.1029/2001JD000562.

Co-funded by the Horizon 2020 programme of the European Union

Furevik, B. R., Schyberg, H., Noer, G., Tveter, F., and Röhrs, J., "ASAR and ASCAT in Polar Low Situations", *J. Atm. and Ocean Techn*., 32, 783-792, 2015, doi: 10.1175/JTECH-D-14-00154.1.

Gabarro, C. , Turiel, A. , Elosegui, P. , Pla-Resina, J. A. , Portabella, M.,"New methodology to estimate Arctic sea ice concentration from SMOS combining brightness temperature differences in a maximum-likelihood estimator", *The Cryosphere*, 11, 4, 1987-2002, 2017, 10.5194/tc-11-1987-2017.

Gade, M., and Stoffelen, A. "An Introduction to Microwave Remote Sensing of the Asian Seas", *Remote Sensing of the Asian Seas*, Barale, Vittorio, Gade, Martin (Eds.), Springer, 1st ed. 2019, XXXV, 526 p., 81-101, 2019.

GCOS, Global Climate Observing System. "Implementation Plan for the Global Observing System for Climate in Support of the UNFCCC, 2010, GCOS-138", Technical report GOOS-184, GTOS-76, WMO-TD/No.1523, World Meteorological Organization (WMO), 2010. Available online: https://library.wmo.int/doc_num.php?explnum_id=3851.

GCOS-200, "The Global Observing System for Climate: Implementation Needs", GCOS 2016 Implementation Plan, WMO, 2016.

Geldsetzer, T., Arkett, M., Zagon, T., Charbonneau, F., Yackel, J. J., Scharien, R. K., "All-season compact-polarimetric C-band SAR observations of sea ice", *Can. J. Remote Sensing*, vol. 41, pp. 485-504, 2015, doi:10.1080/07038992.2015.1120661.

Girard-Ardhuin, F. and Ezraty, R. "Enhanced Arctic sea ice drift estimation merging radiometer and scatterometer data", *IEEE Trans. Geosci. Remote Sensing*, vol. 50, n. 7, pp 2639-2648, 2012, doi : 10.1109/TGRS.2012.2184124.

Gisnås, K., Westermann, S., Schuler, T. V., Litherland, T., Isaksen, K., Boike, J., and Etzelmüller, B., *A statistical approach to represent small-scale variability of permafrost temperatures due to snow cover*, *The Cryosphere*, 8, 2063-2074, 2014.

Gommenginger, C., B. Chapron, A. Martin, J. Marquez, C. Brownsword, and C. Buck, "SEASTAR: A new mission for high-resolution imaging of ocean surface current and wind vectors from space. Proc. EUSAR 2018, Aachen, Germany, IEEE, 1–6. 2018.

González-Zamora, A., Sánchez, N., Martínez-Fernández, J., Gumuzzio, A., Piles, M., Olmedo, E. "Long-term SMOS soil moisture products: A comprehensive evaluation across scales and methods in the Duero Basin (Spain)", *Physics and Chemistry of the Earth, Parts A/B/C,* 83–84, 123-136, 2015. https://doi.org/10.1016/j.pce.2015.05.009.

Graham D. Q, , Rinne E. , Passaro M., Andersen O., Dinardo S., Fleury, S., Guillot, A. , Hendricks S., Kurekin a. , Müller F , Ricker, R. , Skourup, H., Tsamados, M, "Retrieving Sea Level and Freeboard in the Arctic: A Review of Current Radar Altimetry Methodologies and Future Perspectives", *Remote Sensing*, 11, 881, 2019; doi:10.3390/rs11070881.

Co-funded by the Horizon 2020 programme of the European Union

Groom S., Sathyendranath, S., Ban, Y., Bernard S., Brewin R., Brotas V., Brockmann C., Chauhan P.h, Choi J., Chuprin A., Ciavatta S., Cipollini P., Donlon C., Franz B., He X., Hirata T., Jackson T., Kampel M., Krasemann H., Lavender S., Pardo-Martinez S., Mélin F., Platt T., Santoleri R., Skakala J., Schaeffer B., Smith M., Steinmetz F., Valente A., Wang M., "Satellite Ocean Colour: Current Status and Future Perspective. " *Frontiers in Marine Science* , 6 (486), 2019.

Gruber, A., Su, C.-H., Zwieback, S., Crow, W., Dorigo, W., Wagner, W. "Recent advances in (soil moisture) triple collocation analysis", *International Journal of Applied Earth Observation and Geoinformation*, 45, B, 200-211, 2016. https://doi.org/10.1016/j.jag.2015.09.002.

Guneriussen, T., Hogda, K. A., Johnsen, H., & Lauknes, I. "InSAR for estimation of changes in snow water equivalent of dry snow." IEEE Transactions on Geoscience and Remote Sensing, 39(10), 2101-2108, 2001.

Gupta, M., Gabarro, C., Turiel, A., Portabella, M., & Martinez, J. "On the retrieval of sea-ice thickness using SMOS polarization differences", Journal of Glaciology, 65(251), 481-493, 2019. doi:10.1017/jog.2019.26.

Han, L., D. Floricioiu, Baessler, M., Eineder, M., "An algorithm for the detection of calving glaciers frontal position from TerraSAR-X imagery". 6171-6174, 2016, 10.1109/IGARSS.2016.7730612.

He, T., S. Liang, and D.-X. Song, "Analysis of global land surface albedo climatology and spatial-temporal variation during 1981–2010 from multiple satellite products", *J. Geophys. Res. Atmos.*, 119, 10,281–10, 298, 2014, doi:10.1002/ 2014JD021667.

Henderson-Sellers, A.; Wilson, M.F., "Surface Albedo Data for Climatic Modeling". *Rev. Geophys.* 21, 1743–1778, 1983.

Hendricks, S., Gerland, S., Smedsrud, L., Haas, C., Pfaffhuber, A., & Nilsen, F. "Sea-ice thickness variability in Storfjorden, Svalbard", *Annals of Glaciology, 52* (57), 61-68. 2011.

Hendricks, S.; Paul, S.; Rinne, E. "ESA Sea Ice Climate Change Initiative (Sea_Ice_cci): Northern hemisphere sea ice thickness from the CryoSat-2 satellite on a monthly grid (L3C), v2.0.", Centre for Environmental Data Analysis, 2018, doi:10.5285/ff79d140824f42dd92b204b4f1e9 e7c2.

Hirata, T., Hardman-Mountford, N. J., Brewin, R. J. W., Aiken, J., Barlow, R., Suzuki, K., Isada, T., Howell, E., Hashioka, T., Noguchi-Aita, M., and Yamanaka, Y. "Synoptic relationships between surface Chlorophyll-*a* and diagnostic pigments specific to phytoplankton functional types", *Biogeosciences,* 8, 311–327, 2011, https://doi.org/10.5194/bg-8-311-2011.

Hollands, T., Linow, S., Dierking, W. "Reliability measures for sea ice motion retrieval from synthetic aperture radar images", IEEE J. Selected Topics in Applied Earth Observations and Remote Sensing, vol. 8, no. 1, pp. 67-75, 2015, doi: 10.1109/JSTARS.2014.2340572.

Co-funded by the Horizon 2020 programme of the European Union

Hollands, T., Dierking, W., “Performance of a multi-scale correlation algorithm for the estimation of sea ice drift from SAR images: initial results”, Annals of Glaciology 52 (57), pp. 311-317, 2011, doi:10.3189/172756411795931462.

Horstmann, J, W Koch, S Lehner, and R Tonboe. “Ocean winds from RADARSAT-1 ScanSAR”, *Can. J. Remote Sens.*, 28, 524–533, 2002.

Howell, S.E., Brown, L.C., Kang, K.K. and Duguay, C.R., “Variability in ice phenology on Great Bear Lake and Great Slave Lake, Northwest Territories, Canada, from SeaWinds/QuikSCAT: 2000–2006.”, Remote Sensing of Environment, 113(4), pp. 816-834, 2009.

Huntemann, M. , Heygster, G. , Kaleschke, L. , Krumpen, T. , Makynen, M. , Drusch, M. “Empirical sea ice thickness retrieval during the freeze up period from SMOS high incident angle observations”. The Cryosphere, 8(2), 439–451, 2014. doi: 10.5194/tc-8-439-2014.

INSITU-OCR. “International Network for Sensor Inter-comparison and Uncertainty assessment for Ocean Color Radiometry (INSITU-OCR).” http://www.ioccg.org/grou ps/INSITU-IOCCG Report 10. Atmospheric Correction for Remotely-Sensed Ocean-Colour Products, 2012.

IOCCG Report 13, “Mission Requirements for Future Ocean-Colour Sensors“, 2012.

Isern-Fontanet, J., J. Ballabrera-Poy, A. Turiel, E. García-Ladona, “Remote sensing of ocean surface currents: a review of what is being observed and what is being assimilated“. N*onlinear Processes in Geophysics,* 24 613 – 643,2017.

Istomina, L., Heygster, G., Huntemann, M., Schwarz, P., Birnbaum, G., Scharien, R., Polashenski, C., Perovich, D., Zege, E., Malinka, A., Prikhach, A., and Katsev, I., ”Melt pond fraction and spectral sea ice albedo retrieval from MERIS data – Part 1: Validation against in situ, aerial, and ship cruise data”, The Cryosphere, 9, 1551-1566, 2015a, doi:10.5194/tc-9-1551-2015.

Istomina, L., Heygster, G., Huntemann, M., Marks, H., Melsheimer, C., Zege, E., Malinka, A., Prikhach, A., and Katsev, I., ”Melt pond fraction and spectral sea ice albedo retrieval from MERIS data – Part 2: Case studies and trends of sea ice albedo and melt ponds in the Arctic for years 2002–2011”, The Cryosphere, 9, 1567-1578, 2015b, doi:10.5194/tc-9-1567-2015.

Itkin, P., Spreen, G., Cheng, B., Doble, M., Girard-Ardhuin, F., Haapala, J., Hughes, N., Kaleschke, L., Nicolaus, M., Wilkinson, J. “Thin ice and storms: Sea ice deformation from buoy arrays deployed during N-ICE2015”, J. Geophys. Res. Oceans, 122, 4661-4674, 2017, doi:10.1002/2016JC012403.

Ivanova, N., Pedersen, L. T., Tonboe, R. T., Kern, S., Heygster, G., Lavergne, T., Sørensen, A., Saldo, R., Dybkjær, G., Brucker, L., and Shokr, M., “Inter-comparison and evaluation of sea ice algorithms: towards further identification of challenges and optimal approach using passive microwave observations”, The Cryosphere, 9, 1797–1817, 2015. https://doi.org/10.5194/tc-9-1797-2015.

Co-funded by the Horizon 2020 programme of the European Union

Jackson, T., Chuprin,A. , Sathyendranath, S., Grant, M., Zuhlke,M., Dingle, J., T. Storm, M. Boettcher, N. Fomferra, "Ocean Colour Climate Change Initiative (OC-CCI) Product User Guide", v 4.1 , 2019, https://esa-oceancolour-cci.org/documents-list.

Kaleschke, L., Tian-Kunze, X., Maaß, N., Mäkynen, M. and Drusch, M., "Sea ice thickness retrieval from SMOS brightness temperatures during the Arctic freeze-up period.", Geophys. Res. Lett., 39 (5), 2012 doi: 10.1029/2012GL050916.

Kaleschke, L., Tian-Kunze, X., Maaß, N., Beitsch, A., Wernecke, A., Miernecki, M., Müller, G., Fock,B. H. , Gierisch, A. M.U., Schlünzen, K. H., Pohlmann, T. Dobrynin,M., Hendricks,S., Asseng, S., Gerdes,R., Jochmann, P. , Reimer, N., Holfort, J., Melsheimer, C. , Heygster, G., Spreen, G. , Gerland, S., King, J. , Skou, N., Schmidl Søbjærg,S., Haas,C. , Richter, F. , Casal,T., "SMOS sea ice product: Operational application and validation in the Barents Sea marginal ice zone", Remote Sensing of Environment, vol. 180, 2016. https://doi.org/10.1016/j.rse.2016.03.009.

Kaminski, T., Kauker, F., Toudal Pedersen, L., Voßbeck, M., Haak, H., Niederdrenk, L., Hendricks, S., Ricker, R., Karcher, M., Eicken, H., and Gråbak, O.:"Arctic Mission Benefit Analysis: impact of sea ice thickness, freeboard, and snow depth products on sea ice forecast performance", *The Cryosphere,* 12, 2569–2594, 2018. https://doi.org/10.5194/tc-12-2569-2018.

Kang, K.K., Duguay, C.R., Lemmetyinen, J. and Gel, Y., "Estimation of ice thickness on large northern lakes from AMSR-E brightness temperature measurements", Remote sensing of environment, 150, pp.1-19, 2014.

Karvonen, J., Vainio, J., Marnela, M., Eriksson, P., Niskanen, T., "A Comparison Between High-Resolution EO-Based and Ice Analyst-Assigned Sea Ice Concentrations", IEEE Journal of Selected Topics in Applied Earth Observations and Remote Sensing, vol. 8, no. 4, pp. 1799-1807, 2015.

Karvonen, J., "A sea ice concentration estimation algorithm utilizing radiometer and SAR data", The Cryosphere, 8, 1639–1650, 2014, https://doi.org/10.5194/tc-8-1639-2014.

Karvonen, J., "Operational SAR-based sea ice drift monitoring over the Baltic Sea", Ocean Sci. 8, pp. 473- 483, 2012, doi:10.5194/os-8-473-2012.

Kern, S., Lavergne, T., Notz, D., Pedersen, L. T., and Tonboe, R. T., "Satellite Passive Microwave Sea-Ice Concentration Data Set Intercomparison for Arctic Summer Conditions", The Cryosphere Discuss., https://doi.org/10.5194/tc-2020-35, in review, 2020.

Kern, S., Lavergne, T., Notz, D., Pedersen, L. T., Tonboe, R. T., Saldo, R., and Soerensen, A. M., "Satellite Passive Microwave Sea-Ice Concentration Data Set Intercomparison: Closed Ice and Ship-Based Observations", The Cryosphere, 13, 3261–3307, 2019, https://doi.org/10.5194/tc-13-3261-2019.

Kern, S., Rösel, A., Pedersen, L. T., Ivanova, N., Saldo, R., and Tonboe, R. T., "The impact of melt ponds on summertime microwave brightness temperatures and sea-ice concentrations", The Cryosphere, 10, 2217–2239, 2016. https://doi.org/10.5194/tc-10-2217-2016.

Co-funded by the Horizon 2020 programme of the European Union

Kern, S., and Spreen, G., "Uncertainties in Antarctic Sea-Ice Thickness Retrieval from ICESat", Ann. Glaciol., 56(69), 107–119, 2015, doi:10.3189/2015AoG69A736.

Kerr, Y. H, et al., "The SMOS Mission: New Tool for Monitoring Key Elements of the Global Water Cycle", Proceedings of the IEEE, vol. 98, no. 5, pp. 666-687, 2010, doi: 10.1109/JPROC.2010.2043032.

Kerr, Y.H., Waldteufel, P., Richaume, P., Wigneron, J.P., Ferrazzoli, P., Mahmoodi, A., Al Bitar, A., Cabot, F., Gruhier, C., Juglea, S., Leroux, D., Mialon, A., & Delwart, S. "The SMOS soil moisture retrieval algorithm", *IEEE Transactions on Geoscience and Remote Sensing*, 50(5), 1384–1403, 2012. https://doi.org/10.1109/TGRS.2012.2184548.

Key, J.R, Schweiger, A.J,"Tools for atmospheric radiative transfer: Streamer and FluxNet", Computers & Geosciences 24 (5), 443-451, 1998.

Key, J., Wang, X., Liu, Y., Dworak, R., Letterly, A., "The AVHRR Polar Pathfinder Climate Data Records", Remote Sens., 8, 167, 2016.

Khlopenkov, K. and A. P. Trishchenko, "SPARC: new cloud, clear-sky, snow/ice and cloud shadow detection scheme for historical AVHHR 1-km observations over Canada," *Journal of Atmospheric and Oceanic Technology*, vol. 24, no. 3, pp. 322–343, 2007.

Kim, E., Forman, B. A., Wang, L., Lemoigne-Stewart, J., Nag, S., Kumar, S., ... & Hofton, M., "Space-Time Coverage Scenarios for A Global Snow Satellite Constellation", In IGARSS 2019-2019 IEEE International Geoscience and Remote Sensing Symposium, pp. 5614-5616, 2019.

Kokhanovsky, A.; Lamare, M.; Danne, O.; Brockmann, C.; Dumont, M.; Picard, G.; Arnaud, L.; Favier, V.; Jourdain, B.; Le Meur, E.; Di Mauro, B.; Aoki, T.; Niwano, M.; Rozanov, V.; Korkin, S.; Kipfstuhl, S.; Freitag, J.; Hoerhold, M.; Zuhr, A.; Vladimirova, D.; Faber, A.-K.; Steen-Larsen, H.C.; Wahl, S.; Andersen, J.K.; Vandecrux, B.; van As, D.; Mankoff, K.D.; Kern, M.; Zege, E.; Box, J.E. Retrieval of Snow Properties from the Sentinel-3 Ocean and Land Colour Instrument. *Remote Sens.* 2019, *11*, 2280.

Korosov, A. A., Rampal, P., "A combination of feature tracking and pattern matching with optimal parametrization for sea ice drift retrieval from SAR data", Remote Sensing, 9, 258, 2017, doi:10.3390/rs9030258.

Kræmer, T., Johnsen, H., Brekke, C., "Emulating Sentinel-1 Doppler radial ice drift measurements using Envisat ASAR data", IEEE Trans. Geosc. Remote Sens., vol. 53, no. 12, pp. 6407-6418, 2015, doi:10.1109/TGRS.2015.2439044.

Kræmer, T., Johnsen, H., Brekke, C., Engen, G., "Comparing SAR-based short time-lag cross correlation and Doppler-derived sea ice drift velocities", IEEE Trans. Geosc. Remote Sens., vol. 56, no. 9, pp. 1898-1908, 2018, doi:10.1109/TGRS.2017.2769222.

Kummervold, P.E., Malnes, E., Eckerstorfer, M., Arntzen, I.M., Bianchi, F., "Avalanche detection in Sentinel-1 radar images using convolutional neural networks", I*nt. Snow Sci. Workshop Proc. 2018,* Innsbr. Austria 377–381, 2018.

Co-funded by the Horizon 2020 programme of the European Union

Kwiatkowska, E. J., Ruddick, K., Ramon, D., Vanhellemont, Q., Brockmann, C., Lebreton,C.,et al. "Ocean color opportunities from meteosat second and third generation geostationary platforms", *OceanSci*. 12,703–713, 2016.

Kwok, R., Cunningham, G., Markus, T., Hancock, D., Morison, J. H., Palm, S. P., Farrell, S. L., Ivanoff, A., Wimert, J., and the ICESat-2 Science Team, "ATLAS/ICESat-2 L3A Sea Ice Freeboard, Version 2", Boulder, Colorado USA. NSIDC: National Snow and Ice Data Center. 2019, doi: https://doi.org/10.5067/ATLAS/ATL10.002.

Kwok, R., "Sea ice concentration estimates from satellite passive microwave radiometry and openings from SAR ice motion", Geophys. Res. Lett., 29(9),2002. doi:10.1029/2002GL014787.

Landy, JC, Tsamados, M & Scharien, RK, "A Facet-Based Numerical Model for Simulating SAR Altimeter Echoes From Heterogeneous Sea Ice Surfaces". I*EEE Transactions on Geoscience and Remote Sensing*, vol 57., pp. 4164-4180, 2019.

Lato, M.J., Frauenfelder, R., Bühler, Y., "Automated detection of snow avalanche deposits: segmentation and classification of optical remote sensing imagery", Natural Hazards Earth System Sciences, 12, 2893–2906, 2012, https://doi.org/10.5194/nhess-12-2893-2012.

Lavergne, T., "A step back is a move forward", doi:10.6084/m9.figshare.5501536.v1, 2017.

Lavergne, T., Sørensen, A. M., Kern, S., Tonboe, R., Notz, D., Aaboe, S., Bell, L., Dybkjær, G., Eastwood, S., Gabarro, C., Heygster, G., Killie, M. A., Brandt Kreiner, M., Lavelle, J., Saldo, R., Sandven, S., and Pedersen, L. T., "Version 2 of the EUMETSAT OSI SAF and ESA CCI sea-ice concentration climate data records", The Cryosphere, 13, 49–78, 2019, https://doi.org/10.5194/tc-13-49-2019.

Lavergne, T., Eastwood, S., Teffah, Z., Schyberg, H. and Breivik, L.-A., "Sea ice motion from low resolution satellite sensors: an alternative method and its validation in the Arctic", *J. Geophys. Res.*, 115, C10032, 2010, doi:10.1029/2009JC005958.

Lavigne, H.,and Ruddick, K. "The potential use of geostationary MTG/FCI to retrieve chlorophyll-a concentration at high temporal resolution for the open oceans".*Int. J. Remote Sens.* 39, 2399–2420, 2018.

Laxon, S. W., Giles, K. A., Ridout, A. L., Wingham, D. J., Willatt, R., Cullen, R., Kwok, R., Schweiger, A.,Zhang, J., Haas, C., Hendricks, S., Krishfield, R., Kurtz, N., Farrell, S. and Davidson, M., "CryoSat-2 estimates of Arctic sea ice thickness and volume", *Geophys. Res. Lett.*, 40, 732– 737, 2013, doi:10.1002/grl.50193.

Lee, Z. P., Carder, K. L., Arnone, R. A.,"Deriving inherent optical properties from water color: a multiband quasi-analytical algorithm for optically deep waters." *Appl. Opt.* 41, 5755–5772, 2002.

Leigh, S., Wang, Z., Clausi, D. A. "Automated ice-water classification using dual polarization SAR satellite imagery", *IEEE T. Geosci. Remote*, 52(9), 5529–5539, 2014, doi:10.1109/TGRS.2013.2290231.

Co-funded by the Horizon 2020 programme of the European Union

Li, Z., Erb, A., Sun, Q., Liu, Y., Shuai, Y., Wang, Z., Boucher, P., Schaaf, C., "Preliminary assessment of 20-m surface albedo retrievals from sentinel-2A surface reflectance and MODIS/VIIRS surface anisotropy measures". *Remote Sens. Environ.,* 217, 352–365, 2018, https://doi.org/10.1016/j.rse.2018.08.025.

Lievens, H., Demuzere, M., Marshall, H. P., Reichle, R. H., Brucker, L., Brangers, I., ... & Jonas, T. "Snow depth variability in the Northern Hemisphere mountains observed from space", *Nature Communications*, *10*(1), 1-12, 2019.

Lin, W., and Portabella, M., "Towards an improved wind quality control for RapidScat," *IEEE Trans. Geosci. Rem. Sens.*, 55 (7), pp. 3922-3930, 2017, https://doi.org/10.1109/TGRS.2017.2683720.

Lin, W., Portabella, M., Foti, G., Stoffelen A., Gommenginger, C., and He, Y., "Towards the Generation of a Wind Geophysical Model Function for Space-borne GNSS-R," *IEEE Trans. Geosci. Rem. Sens.*, 57 (2), pp. 655-666, 2019 https://doi.org/10.1109/TGRS.2018.2859191.

Lindell D. B and Long, D. G., "Multiyear Arctic Sea Ice Classification Using OSCAT and QuikSCAT," in *IEEE Transactions on Geoscience and Remote Sensing*, vol. 54, no. 1, pp. 167-175, 2016. doi: 10.1109/TGRS.2015.2452215.

Lindsay, R. W., Stern, H. L., "The RADARSAR Geophysical Processor System: Quality of sea ice trajectory and deformation estimates", *J. Atmos. Ocean. Technol.*, 20, 1333-1347, 2003.

Liu, Y., Wang, Z., Sun, Q., Erb, A.M., Li, Z., Schaaf, C.B., Zhang, X., Román, M.O., Scott, R.L., Zhang, Q., Novick, K.A., Syndonia Bret-Harte, M., Petroy, S., Sanclements, M., "Evaluation of the VIIRS BRDF, albedo and NBAR products suite and an assessment of continuity with the long term MODIS record." *Remote Sens. Environ*. 2017, 256–274.

Liu. Y., Roettgers R., Ramírez-Pérez M., Dinter T., Steinmetz F., Noethig E.-M., Hellmann S., Wiegmann S., Bracher A. "Underway spectrophotometry in the Fram Strait (European Arctic Ocean): a highly resolved chlorophyll a data source for complementing satellite ocean color", Optics Express 26(14): A678-A698, 2018, doi:10.1364/OE.26.00A678.

Liu, Y., Key, J. R., Wang, X., and Tschudi, M., "Multidecadal Arctic sea ice thickness and volume derived from ice age", The Cryosphere, 14, 1325–1345, https://doi.org/10.5194/tc-14-1325-2020, 2020.

Loew, A., R. Ludwig & Mauser, W. "Derivation of surface soil moisture from ENVISAT ASAR wide swath and image mode data in agricultural areas," IEEE Transactions on Geoscience and Remote Sensing, 44 (4), 889-899, 2006. https://doi.org/10.1109/TGRS.2005.863858.

Long, D., Hadin, P.J, Whiting, P.T., "Resolution enhancement of spaceborne scatterometer data;Resolution enhancement of spaceborne scatterometer data", IEEE Trans. on Geosci. Remote Sens., 31 (3), 1993, DOI: 10.1109/36.225536.

Co-funded by the Horizon 2020 programme of the European Union

Long, D.G., Daum,D.L., “Spatial resolution enhancement of SSM/I data”, IEEE Trans. Geosci. Remote Sens., 36 (2) 1998, doi: 10.1109/36.662726.

Losa S., Soppa M. A., Dinter T., Wolanin A., Brewin R. J. W., Bricaud A., Oelker J., Peeken I., Gentili B., Rozanov. V. V., Bracher A., „Synergistic exploitation of hyper- and multispectral precursor Sentinel measurements to determine Phytoplankton Functional Types at best spatial and temporal resolution (SynSenPFT)“. Frontiers in Marine Science, 4: 203, 2017; doi: 10.3389/fmars.2017.00203

LSTM MRD, “Copernicus High Spatio-Temporal Resolution Land Surface Temperature Mission: Mission Requirements Document”, ESA-EOPSM-HSTR-MRD-3276, Issue 2.0, March 2019, http://esamultimedia.esa.int/docs/EarthObservation/Copernicus_LSTM_MRD_v2.0_Issued20190308.pdf

Ludwig, V., Spreen, G., Haas, C., Istomina, L., Kauker, F., and Murashkin, D., “The 2018 North Greenland polynya observed by a newly introduced merged optical and passive microwave sea-ice concentration dataset”, The Cryosphere, 13, 2051–2073, 2019, https://doi.org/10.5194/tc-13-2051-2019.

Maillard, P., Clausi, D. A., Deng, H., “Operational map-guided classification of SAR sea ice imagery”, IEEE Trans. Geosci. Remote Sens., vol. 43, no. 12, pp. 2940-2951, 2005, doi:10.1109/TGRS.2005.857897.

Mäkynen, M., Cheng, B., Simila, M. “On the accuracy of thin-ice thickness retrieval using MODIS thermal imagery over Arctic first-year ice”, *Annals of Glaciology,* 54(62), 87-96, 2013, DOI: 10.3189/2013AoG62A166.

Malinka, A., Zege, E., Heygster, G., Istomina, L., “Reflective properties of white sea ice and snow”, *The Cryosphere*, 10, 2541-2557, 2016, doi:10.5194/tc-10-2541-2016.

Maritorena, S., Siegel, D.A., Peterson, A.R. , “Optimization of a semianalytical ocean color model for global-scale applications”, *Applied Optics-LP,* 41, 2705-2714, 2002.

Meissner, T., and F. Wentz, “The emissivity of the ocean surface between 6 - 90 GHz over a large range of wind speeds and Earth incidence angles”. *IEEE Trans. Geosci. Rem. Sens*., 50 (8), 3004-3026, 2012, doi: 10.1109/TGRS.2011.2179662.

Meissner, T., L. Ricciardulli, and F.J. Wentz, “Capability of the SMAP Mission to Measure Ocean Surface Winds in Storms” *Bull. Amer. Meteor. Soc*., 98, 1660–1677, 2017, doi: 0.1175/BAMS-D-16-0052.1.

Merlin, O.; Walker, J.P.; Chehbouni, A.; Kerr, Y. “Towards deterministic downscaling of SMOS soil moisture using MODIS derived soil evaporative efficiency”, *Remote Sensing of Environment*. 112, 3935–3946, 2008. https://doi.org/10.1016/j.rse.2008.06.012

Co-funded by the Horizon 2020 programme of the European Union

Merlin, O.; Escorihuela, M.J.; Mayoral, M.A.; Hagolle, O.; Al Bitar, A.; Kerr, Y. "Self-calibrated evaporation-based disaggregation of SMOS soil moisture: An evaluation study at 3 km and 100 m resolution in Catalunya, Spain", Remote Sensing of Environment, 130, 25–38, 2013. https://doi.org/10.1016/j.rse.2012.11.008

Metsämäki, S., Mattila, O.P., Pulliainen, J., Niemi, K., Luojus, K. and Böttcher, K., "An optical reflectance model-based method for fractional snow cover mapping applicable to continental scale", *Remote Sensing of Environment*, 123, pp.508-521, 2012.

Mohammed, P.N., Aksoy, M., Piepmeier, J.R., Johnson, J.T. & Bringer, A. "SMAP L-Band Microwave Radiometer: RFI Mitigation Prelaunch Analysis and First Year On-Orbit Observations", *IEEE Transactions on Geoscience and Remote Sensing*, 54 (10), 6035-6047, 2016. https://doi.org/10.1109/TGRS.2016.2580459.

Moen, M.-A. N., Doulgeris, A. P., Anfinsen, S. N., Renner, A. H. H., Hughes, N., Gerland, S., Eltoft, T., "Comparison of feature based segmentation of full polarimetric SAR satellite sea ice images with manually drawn ice charts", *The Cryosphere,* 7, pp. 1693-1705, 2013, doi:10.5194/tc-7-1693-2013.

Morel, A., Huot, Y., Gentili, B., Werdell, P.J., Hooker, S.B., Franz, B. A., "Examining the consistency of products derived from various ocean color sensors in open ocean (case 1) waters in the perspective of a multi-sensor approach," Remote *Sensing of Environment,* 111, pp 69–88, 2007, doi:10.1016/j.rse.2007.03.012

Moritz, R. E., J. A. Curry, N. Untersteiner, and A. S. Thorndike, "Prospectus: Surface heat budget of the Arctic Ocean. NSF-ARCSS OAII Tech. Rep. 3," 33 pp. Available from the SHEBA Project Office, Polar Science Center, Applied Physics Laboratory, University of Washington, Seattle, WA 98105, 1993.

Mouche, A., et al., . "On the Use of Doppler Shift for Sea Surface Wind Retrieval From SAR", *IEEE Transactions on Geoscience and Remote Sensing*, 50 (7), 2901-2909, 2012. doi: 10.1109/TGRS.2011.2174998.

Muckenhuber, S., Sandven, S., "Open-source sea ice drift algorithm for Sentinel-1 SAR imagery using a combination of feature tracking and pattern matching", *The Cryosphere,* 11, 1835-1850, 2017, doi:10.5194/tc-11-1835-2017.

Muckenhuber, S., Korosov, A. A., Sandven, S., "Open source feature-tracking algorithm for sea ice drift retrieval from Sentinel-1 SAR imagery", *The Cryosphere*, vol. 10, 913-925, 2016, doi:10.5194/tc-10-913-2016.

Muñoz, J., Infante, J., Lakhankar, T., Khanbilvardi, R., Romanov, P., Krakauer, N., & Powell, A., "Synergistic use of remote sensing for snow cover and snow water equivalent estimation". British Journal of Environment & Climate Change, 3(4), 612-627, 2013.

Co-funded by the Horizon 2020 programme of the European Union

Nagler, T., Rott, H., Ripper, E., Bippus, G. and Hetzenecker, M., "Advancements for snowmelt monitoring by means of sentinel-1 SAR", *Remote Sensing*, 8(4), p.348, 2016.

Nagler, T., & Rott, H., "Retrieval of wet snow by means of multitemporal SAR data", *IEEE Transactions on Geoscience and Remote Sensing,* 38(2), 754-765, 2000.

Nakamura, K., Wakabayashi, H., Uto, S., Ushio, S., and Nishio, F., "Observation of sea-ice thickness using ENVISAT data from Lützow-Holm Bay, East Antarctica", *IEEE Geoscience and Remote Sensing Letters*, Vol. 6, No. 2, 277-281, 2009.

Niederdrenk, A.-L. and Notz, D., "Arctic Sea Ice in a 1.5 ◦C Warmer World", *Geophys. Res. Lett.*, 45, 1963–1971, 2018, https://doi.org/10.1002/2017GL076159.

Nielsen, K., Sandberg Sørensen, L., Zakharova, E., Wuite, J., "ARCFLUX – FRESHWATER FLUXES TO THE ARCTIC OCEAN Impact assessment report", Deliverable 8. 7th Feb. 2018.

Nolin, A. W. "Recent advances in remote sensing of seasonal snow", *Journal of Glaciology*, *56*(200), 1141-1150, 2010.

Obu, J., Westermann, S., Bartsch, A., Berdnikov, N., Christiansen, H., Dashtseren, D., Delaloye, R., Elberling, B., Etzelmüller, B., Kholodovh, A., Khomutov, A., Kääb, A., Leibman, M., Lewkowicz, A., Panda, S., Romanovsky, V., Way, R., Westergaard-Nielsen, A., Wu, T., Yamkin, J., and Zou, D., "Northern Hemisphere permafrost map based on TTOP modelling for 2000-2016 at 1 km2 scale", *Earth-Science Reviews*, 193, 299-316, 2019.

Ochilov, S., Clausi, D. A., "Operational SAR sea-ice image classification", *IEEE Trans. Geosci. Remote Sens.,* vol. 50, no. 11, 4397-4408, 2012, doi:10.1109/TGRS.2012.2192278.

Oliva, R., Daganzo, E., Richaume, P., Kerr, Y., Cabot, F., Soldo, Y., Anterrieu, E., Reul, N., Gutierrez, A., Barbosa, J., Lopes Barbosa, Lopes, G. "Status of Radio Frequency Interference (RFI) in the 1400–1427MHz passive band based on six years of SMOS mission", *Remote Sensing of Environment*, 180, 64-75, 2016. https://doi.org/10.1016/j.rse.2016.01.013.

Olmedo, E., Gabarró, C., González-Gambau, V., Martínez, J., Ballabrera-Poy, J., Turiel, A., Portabella, M., Fournier, S., Lee, T., "Seven Years of SMOS Sea Surface Salinity at High Latitudes: Variability in Arctic and Sub-Arctic Regions", *Remote Sensing*, 10(11), 1772, 2018, https://doi.org/10.3390/rs10111772.

Olmedo, E., Martinez, J., Turiel, A., Ballabrera-Poy, J., Portabella, M., "Debiased non-Bayesian retrieval: A novel approach to SMOS Sea Surface Salinity. Remote Sensing of the Environment", 193, 103–126, 2017, https://doi.org/10.1016/j.rse.2017.02.023.

O'Reilly, J. E., Maritorena, S., Mitchell, B. G., Siegel, D. A., Carder, K. L., Garver, S. A., et al. . "Ocean color chlorophyll algorithms for SeaWiFS." J. Geophys. Res. Oceans 103, 24937–24953, 1998.

Co-funded by the Horizon 2020 programme of the European Union

Organelli, E., Barbieux, M., Claustre, H., Schmechtig, C., Poteau, A., Bricaud, A., et al. “Two databases derived from BGC-Argo float measurements for marine biogeochemical and bio-optical applications.” Earth Syst. Sci. Data 9, 861–880, 2017.

Owe, M. & Van de Griend, A. A. “Comparison of soil moisture penetration depths for several bare soils at two microwave frequencies and implications for remote sensing”, Water Resources Research, 34 (9), 2319– 2327, 1998. https://doi.org/10.1029/98WR01469.

Painter, T. H., et al., “The Airborne Snow Observatory: Fusion of scanning lidar, imaging spectrometer, and physically-based modeling for mapping snow water equivalent and snow albedo”. Remote Sensing of Environment, 184, 139-152, 2016.

Park, J.W., Korosov, A.A., Babiker, M., Sandven, S., and Won. J., “Efficient Thermal Noise Removal for Sentinel-1 TOPSAR Cross-Polarization Channel.” *IEEE Transactions on Geoscience and Remote Sensing*, 56, 1555-1565, 2018.

Park, J., Korosov, A. A., Babiker, M., Sandven, S., and Won, J., "Efficient Thermal Noise Removal for Sentinel-1 TOPSAR Cross-Polarization Channel," in *IEEE Transactions on Geoscience and Remote Sensing*, vol. 56, no. 3, pp. 1555-1565, 2018. doi: 10.1109/TGRS.2017.2765248

Park, H., Kim, Y., & Kimball, J. S., “Widespread permafrost vulnerability and soil active layer increases over the high northern latitudes inferred from satellite remote sensing and process model assessments”, *Remote Sensing of Environment*, 175, 349-358, 2016.

Pedersen, L. T., Saldo, R., Ivanova, N., Kern, S., Heygster, G., Tonboe, R., Huntemann, M., Ozsoy, B., Ardhuin, F. and Kaleschke, L.: "Reference dataset for sea ice concentration", *Fighshare.com*, doi:10.6084/m9.figshare.6626549.v6, 2019.

Picard, G., Sandells, M., and Löwe, H.: “SMRT: an active–passive microwave radiative transfer model for snow with multiple microstructure and scattering formulations (v1.0)“, *Geosci. Model Dev.*, 11, 2763–2788, 2018. https://doi.org/10.5194/gmd-11-2763-2018.

Piles, M.; Camps, A.; Vall-llossera, M.; Corbella, I.; Panciera, R.; Rüdiger, C.; Kerr, Y.H.; Walker, J.P. “Downscaling SMOS-derived soil moisture using MODIS visible/infrared data”, IEEE Transactions on Geoscience and Remote Sensing, 49, 3156–3166, 2011. https://doi.org/10.1109/TGRS.2011.2120615.

Piles, M.; Sánchez, N.; Vall-llosera, M.; Camps, A.; Martínez, J.; Gonzalez-Gambau, V. “A downscaling approach for SMOS land observations: Evaluation of high-resolution soil moisture maps over the Iberian Peninsula”, IEEE Journal of Selected Topics in Applied Earth Observation and Remote Sensing, 7, 3845–3857, 2014. https://doi.org/10.1109/JSTARS.2014.2325398 .

Piles, M.; Petropoulos, G.; Sánchez, N.; Gonzalez-Zamora, A.; Ireland, G. “Towards improved spatio-temporal resolution soil moisture retrievals from the synergy of SMOS and MSG SEVIRI spaceborne

Co-funded by the Horizon 2020 programme of the European Union

observations", Remote Sensing of Environment, 180, 403–417, 2016. https://doi.org/10.1016/j.rse.2016.02.048.

Portabella, M., A. Stoffelen, and J. A. Johannessen, "Toward an optimal inversion method for SAR wind retrieval", *J. Geophys. Res. Oceans,* **107** (C8), https://doi.org/10.1029/2001JC000925, 2002.

Portal, G.; Vall-llossera, M.; Piles, M.; Camps, A.; Chaparro, D.; Pablos, M.; Rossato, L. "A Spatially Consistent Downscaling Approach for SMOS Using an Adaptive Moving Window", *IEEE Journal of Selected Topics in Applied Earth Observation and Remote Sensing*, 11 (6), 1883 – 1894, 2018. https://doi.org/10.1109/JSTARS.2018.2832447.

Pradhan H. K., Völker C., Losa S. N., Bracher A., Nerger L. "Global assimilation of ocean-color data of phytoplankton functional types: Impact of different datasets". *Journal of Geophysical Research Oceans*, 125, e2019JC015586. 2020. https://doi.org/ 10.1029/2019JC015586

Pulliainen, J., "Mapping of snow water equivalent and snow depth in boreal and sub-arctic zones by assimilating space-borne microwave radiometer data and ground-based observations", Remote sensing of Environment, 101.2, 257-269, 2006.

Qiao, D., Li, Z., Nianqin, W., Zhou, J., Zhang, P., & Gao, S., "Validation Of The Daily Passive Microwave Snow Depth Products Over Northern China", International Archives of the Photogrammetry, Remote Sensing & Spatial Information Sciences, 42(3), 2018.

Quartly, G.D., Rinne, E.; Passaro, M., Andersen, O.B., Dinardo, S., Fleury, S., Guillot, A., Hendricks, S., Kurekin, A.A.,Müller, F.L.; Ricker, R., Skourup, H., Tsamados, M. "Retrieving Sea Level and Freeboard in the Arctic: A Review of Current Radar Altimetry Methodologies and Future Perspectives", *Remote Sens*., 11, 881, 2019. https://doi.org/10.3390/rs11070881.

Ray, C., C. Martin-Puig, M. P. Clarizia, G. Ruffini, S. Dinardo and C. Gommenginger and J. Benveniste,"SAR altimeter backscattered waveform model". *EEE Transactions on Geoscience and Remote Sensing,* 53 911–919, 2015

Remund, Q. P., Long, D. G., and Drinkwater, M. R., "An iterative approach to multisensory sea ice classification", IEEE T. Geosci. Remote Sens., 38, 1843–1856, 2000.

Reul, N., J. Tenerelli, B. Chapron, D. Vandemark, Y. Quilfen, and Y. Kerr, "SMOS satellite L-band radiometer: A new capability for ocean surface remote sensing in hurricanes", *J. Geophys. Res*., 117, C02006, 2012, doi: 10.1029/2011JC007474.

Reul, N., Chapron, B., Zabolotskikh, E., Donlon, C., Quilfen, Y., Guimbard, S., Piolle, J.F., "A revised L-band radio-brightness sensitivity to extreme winds under Tropical Cyclones: the five year SMOS-storm database", *Remote Sensing of Environment*, Volume 180, Pages 274-291, 2016, https://doi.org/10.1016/j.rse.2016.03.011.

Co-funded by the Horizon 2020 programme of the European Union

Reverdin, G., Le Go, H., Tara Oceans Consortium and Tara Oceans Expedition, "Properties of seawater from a Sea-Bird TSG temperature and conductivity sensor mounted on the continuous surface water sampling system during campaign TARA 20090913Z of the Tara Oceans expedition 2009-2013", 2014.

Ricciardulli, L., T. Meissner, and F. Wentz, "Towards a climate data record of satellite ocean vector winds", *Proceedings of the 2012 IEEE International Geoscience and Remote Sensing Symposium*, 2067-2069, 2012.

Richter, F., Drusch, M., Kaleschke, L., Maaß, N., Tian-Kunze, X., and Mecklenburg, S.: "Arctic sea ice signatures: L-band brightness temperature sensitivity comparison using two radiation transfer models", *The Cryosphere,* 12, 921–933, 2018. https://doi.org/10.5194/tc-12-921-2018

Ricker, R., Hendricks, S., Kaleschke, L., Tian-Kunze, X., King, J., Haas, C. "A weekly Arctic sea-ice thickness data record from merged CryoSat-2 and SMOS satellite data." *The Cryosphere.* 11. 1607-1623, 2017. doi: 10.5194/tc-11-1607-2017.

Rio M.-H. and F. Hernandez, "High-frequency response of wind-driven currents measured by drifting buoys and altimetry over the world ocean". *J. Geophys. Res.*, 108, 3283, 2003

Robinson, I. S. 2004: Measuring the Oceans from Space: The principles and methods of satellite oceanography. Springer pp.669.

Rodriguez, E., Wineteer, A., Perkovic-Martin, D., Gál, T., Stiles, B. W., Niamsuwan, N., et al. "Estimating ocean vector winds and currents using a Ka-band pencil-beam Doppler scatterometer", *Remote Sens.* 10:576, 2018, doi: 10.3390/rs10040576.

Romeiser, R., H. Runge, S. Suchandt, R. Kahle, C. Rossi, and P. Bell, 2014: Quality assessment of surface cur- rent fields from TerraSAR-X and TanDEM-X along- track interferometry and Doppler centroid analysis. IEEE Trans. Geosci. Remote Sens., 52, 2759–2772,

ROSE-L MRD, "Copernicus L-band SAR Mission Requirements Document", ESA-EOPSM-CLIS-MRD-3371, Issue 2.0, October 2018, https://esamultimedia.esa.int/docs/EarthObservation/Copernicus_L-band_SAR_mission_ROSE-L_MRD_v2.0_issued.pdf.

Rösel, A., Kaleschke, L., Birnbaum, G., "Melt ponds on Arctic sea ice determined from MODIS satellite data using an artificial neural network", *The Cryosphere*, 6 (2),pp. 431-446, 2012. DOI10.5194/tc-6-431-2012.

Rott H., Yueh, S., Cline, D.W., Duguay, C., Essery, R., Haas, C., Hélière, F., Kern, M., Macelloni, G., Malnes, E., Nagler, T., Pulliainen, J., Rebhan, H., Thompson, A., "Cold Regions Hydrology High-resolution Observatory for Snow and Cold Land Processes", *IEEE Transactions on geoscience and remote sensing,* 99, 1-10,2010.

Rott, H., Nagler, T., & Scheiber, R., "Snow mass retrieval by means of SAR interferometry", *In 3rd FRINGE Workshop*, European Space Agency, Earth Observation (pp. 1-6), 2003.

Co-funded by the Horizon 2020 programme of the European Union

Sadeghi, A., Dinter, T.,Vountas, M., Taylor, B, Altenburg-Soppa, M., Bracher, A., ”Remote sensing of coccolithophore blooms in selected oceanic regions using the PhytoDOAS method applied to hyper-spectral satellite data “, Biogeosciences, 9,2127–2143, 2012.

Sakov, P., Counillon, F., Bertino, L., Lisæter, K. A., Oke, P. R., & Korablev, A., “TOPAZ4: an ocean-sea ice data assimilation system for the North Atlantic and Arctic”, Ocean Sci., 8(4), 633–656, 2012, https://doi.org/10.5194/os-8-633-2012.

Salomonson, V.V. and Appel, I., “Estimating fractional snow cover from MODIS using the normalized difference snow index”, *Remote sensing of environment,* 89(3), pp.351-360, 2004.

Scarlat, R. C., Spreen, G., Heygster, G., Huntemann, M., Patilea, C., Pedersen, L. T., & Saldo, R., “Sea ice and atmospheric parameter retrieval from satellite microwave radiometers: Synergy of AMSR2 and SMOS compared with the CIMR candidate mission“. *Journal of Geophysical Research: Oceans,* 125, e2019JC015749, 2020. https://doi.org/10.1029/2019JC015749

Scharien, R. K., Segal, R., Nasonova, S., Nandan, V., Howell, S. E. L., & Haas, C., “Winter Sentinel-1 backscatter as a predictor of spring Arctic sea ice melt pond fraction.” *Geophysical Research Letters*, 44, 12, 2017, https://doi.org/10.1002/2017GL075547.

Scheuchl, B., Flett, D., Caves, R., Cumming, I., “Potential of RADARSAT-2 data for operational sea ice monitoring”, *Can. J. Remote Sensing*, vol. 30, no. 3, pp. 448-461, 2004, doi:10.5589/m04-011.

Schubert, A., Miranda, N., Geudtner, D., Small, D., “Sentinel-1A/B combined product geolocation accuracy”, *Remote Sensing,* 9, 607, 2017, doi:10.3390/rs9060607.

Schubert, A., Jehle, M., Small, D., Meier, E., “Geometric validation of TerraSAR-X high-resolution products, Proc. 3rd TerraSAR-X Science Team Meeting”, Oberpfaffenhofen, Germany, 25-26 November 2008.

Scott, K.A., M. Buehner, A. Caya, and T. Carrieres, “Direct Assimilation of AMSR-E Brightness Temperatures for Estimating Sea Ice“, *Concentration. Mon. Wea. Rev.*, 140, 997–1013, 2012, https://doi.org/10.1175/MWR-D-11-00014.1

Sellers, P.J.; Meeson, B.W.; Hall, F.G.; Asrar, G.; Murphy, R.E.; Schier, R.A.; Bretherton, F.P.; Dickinson, R.E.;Ellingson, R.G.; Field, C.B., “Remote Sensing of the Land Surface for Studies of Global Change: Models—Algorithms—Experiments“. *Remote Sens. Environ.,* 39, 3–26, 1995.

Singha, S., Johansson, M., Hughes, N., Hvidegaard, S. M. , Skourup, H., "Arctic Sea Ice Characterization Using Spaceborne Fully Polarimetric L-, C-, and X-Band SAR With Validation by Airborne Measurements," in *IEEE Transactions on Geoscience and Remote Sensing*, vol. 56, no. 7, pp. 3715-3734, 2018, doi: 10.1109/TGRS.2018.2809504.

Sinha, S., Giffard-Roisin, S., Karbou, F., Deschatres, M., Karas, A., Eckert, N., Coléou, C., Monteleoni, C., “Can Avalanche Deposits be Effectively Detected by Deep Learning on Sentinel-1 Satellite SAR Images?”, Climate Informatics. Paris, France, 2019.

Co-funded by the Horizon 2020 programme of the European Union

Small, D., Rosich, B., Schubert, A., Meier, E., Nüesch., D., "Geometric validation of low and high-resolution ASAR imagery", *Proc. of the 2004 Envisat & ERS Symposium*, Salzburg, Austria, 6-10 September 2004, ESA SP-572, April 2005

Soh,L. K., Tsatsoulis, C., Gineris, D., Bertoia, C., "ARKTOS: An intelligent system for SAR sea ice image classification", *IEEE Trans. Geosci. Remote Sens.*, vol. 42, no. 1, pp. 229-248, 2004, doi:10.1109/TGRS.2003.817819.

Soldal, IH, Dierking, WFO, Korosov, A, Marino, A., "Automatic Detection of Small Icebergs in Fast Ice Using Satellite Wide-Swath SAR Images". *Remote Sens*, 11(7), 806. 2019; https://doi.org/10.3390/rs11070806

Stammer, D., Johanessen, J., LeTraon, P.-Y., Minnett, P., Roquet,H., and Srokosz, M. "Requirements for Ocean Observations Relevant to post-EPS", *EUMETSAT Position Paper*: AEG Ocean To-pography and Ocean Imaging, version 3, 2007.

Stoffelen, A., "Toward the true near-surface wind speed: Error modeling and calibration using triple collocation", *J. Geophys. Res*., 103(C4), 7755–7766, 1998, doi:10.1029/97JC03180.

Stramski D., Reynolds R. A., Babin M., Kaczmarek S., Lewis M. R., Röttgers R., et al., "Relationships between the surface concentration of particulate organic carbon and optical properties in the eastern South Pacific and eastern Atlantic Oceans", *Biogeosc.* 5: 171–201, 2008, doi:10.5194/bg-5-171-2008.

Supply, A., Boutin J. , Vergely, J.L., Kolodziejczyk, N. Reverdin , G. , Reul, N. Tarasenko A.,"New insights into SMOS Sea Surface Salinity retrievals in the Arctic Ocean", Remote Sensing of Enviroment. Submitted.

Tarasenko, A., Supply, A., Kusse-Tiuz, N., Ivanov, V., Makhotin, M., Tournadre, J., Chapron, B., Boutin, J. & Kolodziejczyk, N., "Surface waters properties in the Laptev and the East-Siberian Seas in summer 2018 from in situ and satellite data", *Ocean Science Discussions*, 1-27, 2019, 10.5194/os-2019-60.

Tian-Kunze, X., et al., "SMOS-derived thin sea ice thickness: algorithm baseline, product specifications and initial verification", *The Cryosphere*, 8(3), 997–1018, 2014, doi: 10.5194/tc-8-997- 2014.

Tilling, R, Ridout, A., Shepherd,A., "Estimating Arctic sea ice thickness and volume using CryoSat-2 radar altimeter data", *Advances in Space Research*, vol. 62, issue. 6, 2018, https://doi.org/10.1016/j.asr.2017.10.051.

Tikhonov, V., Khvostov, I., Romanov, A., Sharkov, E.,. Theoretical study of ice cover phenology at large freshwater lakes based on SMOS MIRAS data. The Cryosphere. 12. 2727-2740. 2018.

Tournadre, J., Whitmer, K., and Girard-Ardhuin, F., "Iceberg detection in open water by altimeter waveform analysis", J. Geophys. Res., 113, C08040, 2008, doi:10.1029/2007JC004587.

Co-funded by the Horizon 2020 programme of the European Union

Trindade, A., Portabella, M., Stoffelen, A., Lin, W., and Verhoef, A., "ERAstar: a high resolution ocean forcing product", *IEEE Trans. Geosci. Rem. Sens.*, 58 (2), pp. 1337-1347, 2020 https://doi.org /10.1109 /TGRS.2019.2946019.

Trofaier, A. M., Westermann, S., and Bartsch, A., "Progress in space-borne studies of permafrost for climate science: Towards a multi-ECV approach", *Remote Sensing of Environment,* 203, 55-70, 2017.

Tschudi M.A., Maslanik J.A., Perovich, D. K., "Derivation of melt pond coverage on Arctic sea ice using MODIS observations", *Remote Sensing of Environment* 112, 2605–2614, 2008, doi: 10.1016/j.rse.2007.12.009.

Ulaby, F. and D. Long, "Microwave radar and radiometreic remote sensing", *The University of Michigan Press,* pp 981, 2014.

Vanhellemont, Q., Neukermans, G., and Ruddick, K.,"Synergy between polar-orbiting and geostationary sensors: remote sensing of the ocean at high spatial and high temporal resolution". *Remote Sens. Environ*. 146, 49–62, 2014.

Vickers, H., Eckerstorfer, M., Malnes, E., Larsen, Y., Hindberg, H., "A method for automated snow avalanche debris detection through the use of synthetic aperture radar (SAR) imaging", *Earth Space Sci.* 18, 2016, https://doi.org/10.1002/2016E000168.

Wadhams, P., Aulicino, G., Parmiggiani, F., Persson, P. O. G., & Holt, B., "Pancake ice thickness mapping in the Beaufort Sea from wave dispersion observed in SAR imagery", *Journal of Geophysical Research: Oceans*, 123, 2213–2237, 2018, https://doi.org/10.1002/ 2017JC013003

Wagner, W., Lemoine, G., Rott, H. "A Method for Estimating Soil Moisture from ERS Scatterometer and Soil Data", Remote Sensing of Environment, 70 (2), 191-207, 1999. https://doi.org/10.1016/S0034-4257(99)00036-X.

Wakabayashi, H., Matsuoka, T., Nakamura, K., and Nishio, F., "Polarimetric characteristics of sea ice in the Sea of Okhotsk observed by airborne L-band SAR", *IEEE Trans. Geoscience and Remote Sensing*, Vol. 42, No. 11, 2412-2425, 2004.

Waldeland, A.U., Reksten, J.H., Salberg, A.-B., "Avalanche Detection in Sar Images Using Deep Learning", Presented at the IGARSS 2018 - IEEE International Geoscience and Remote Sensing Symposium, 2018, https://doi.org/10.1109/IGARSS.2018.8517536.

Wang, J., Ge, Y., Heuvelink, G. B. M., & Zhou, C. "Upscaling In Situ Soil Moisture Observations To Pixel Averages With Spatio-Temporal Geostatistics", Remote Sensing, 7(9), 11372-11388, 2015. https://doi.org/10.3390/rs70911372

Co-funded by the Horizon 2020 programme of the European Union

Wang, L., Scott, K.A, Clausi, D.A. “Improved Sea Ice Concentration Estimation Through Fusing Classified SAR Imagery and AMSR-E Data”, Canadian Journal of Remote Sensing, 42:1, 41-52, 2016, DOI: 10.1080/07038992.2016.1152547

Wang, J., Duguay, C., Clausi, D., Pinard, V. and Howell, S., “Semi-Automated Classification of Lake Ice Cover Using Dual Polarization RADARSAT-2 Imagery”, Remote Sensing, 10(11), p.1727, 2018.

Weiss, J, “Drift, Deformation, and Fracture of Sea Ice: A Perspective Across Scales, Springer Briefs in Earth Sciences”, 2013, doi:10.107/978-94-007-6202-2.

Westermann, S., Peter, M., Langer, M., Schwamborn, G., Schirrmeister, L., Etzelmüller, B., and Boike, J., “Transient modeling of the ground thermal conditions using satellite data in the Lena River delta, Siberia”, *The Cryosphere*, 11(3), 1441, 2017.

Westermann, S., Schuler, T., Gisnås, K., and Etzelmuller, B., “Transient thermal modeling of permafrost conditions in Southern Norway”, *The Cryosphere*, 7(2), 719-739, 2013.

Williamson, S. N., L. Copland, D. S. Hik, “The accuracy of satellite-derived albedo for northern alpine and glaciated land covers,“ *Polar Science*, 10-3, 262-269, 2016, doi:10.1016/j.polar.2016.06.006.

Wojtasiewicz, B.,Hardman-Mountford, N. J., Antoine, D., Dufois, F., Slawinski, D., and Trull, T. W., “Use of bio-optical profiling float data in validation of ocean color satellite products in a remote ocean region”, *Remote Sens. Environ.,* 209, 275–290, 2018.

Xiao, X., Zhang, T., Zhong, X., Shao, W., & Li, X., “Support vector regression snow-depth retrieval algorithm using passive microwave remote sensing data”, *Remote sensing of environment*, 210, 48-64, 2018.

Yu, Q. and Clausi, D. A., “SAR sea-ice image analysis based on iterative region growing using semantics”, *IEEE Trans. Geosci. Remote Sens.*, vol. 45, no. 12, pp. 3919-3931, 2007, doi:10.1109/TGRS.2004.839589.

Yueh, S. H., W. J. Wilson, S. J. Dinardo and F. K. Li, “Polarimetric microwave brightness signatures of ocean wind directions”, *IEEE Trans. Geosci. Rem. Sens.*, 37(2), 949-959, 1999, doi: 10.1109/36.752213.

Zakhvatkina, N., A. Korosov, S. Muckenhuber, S. Sandven, M. Babiker, “Operational algorithm for ice-water classification on dual-polarized RADARSAT-2 images”, *The Cryosphere,* vol. 11, pp. 33-46, 2017, doi:10.5194/tc-11-33-2017

Zavorotny, V.U., and A. G. Voronovich, “Scattering of GPS signals from the ocean with wind remote sensing application,” *IEEE Trans. Geosci. Remote Sens.*, vol. 38, no. 2, pp. 951–964, 2000.

Zege, E., Malinka, A., Katsev, I., Prikhach, A., Heygster, G., Istomina, L., Birnbaum, G., and Schwarz, P., “Algorithm to retrieve the melt pond fraction and the spectral albedo of Arctic summer ice from

Co-funded by the Horizon 2020 programme of the European Union

satellite optical data", *Remote Sens. Environ.*, 163, 153-164, 2015, doi:10.1016/j.rse.2015.03.012, 2015.

Zibordi, G.,Bailey, S., Antoine,D., Goryl, P., Kwiatkowska, E., Wang, M. , Franz, B., Johnson, C., Murakami, H., Park, Y.J., Chauhan,P., Fougnie, B. "INSITU-OCR. 2012. International Network for Sensor Inter-comparison and Uncertainty assessment for Ocean Color Radiometry (INSITU-OCR)." White Paper, http://www.ioccg.org/groups/INSITU-OCR_White-Paper.pdf, 2012.

Zwally, H. J., Yi, D., Kwok, R., Zhao, Y., "ICESat Measurements of Sea Ice Freeboard and Estimates of Sea Ice Thickness in the Weddell Sea", *Journal of Geophysical Research* 113(C2): C02S15, 2008, doi:10.1029/2007JC004284.

Zygmuntowska, M., Smedsrud, L.H., Rampal, P., "Uncertainties in Arctic sea ice thickness and volume: new estimates and implications for trends", *The Cryosphere*, 8(2), 705–720, 2014, http://doi.org/10.5194/tc-8-705-2014.

Co-funded by the Horizon 2020 programme of the European Union